CHEMICAL AND BIOCHEMICAL APPLICATIONS OF VIBRATIONAL SPECTROSCOPY

A DISSERTATION IN
CHEMISTRY
and
PHYSICS

Presented to the Faculty of the University
of Missouri-Kansas City in the partial fulfillment of
the requirement for the degree

DOCTOR OF PHILOSOPHY

By
REID ETHAN BRENNER
B.S., Physics, University of Missouri-Kansas City, 2012
M.S., Physics, University of Missouri-Kansas City, 2015

Kansas City, Missouri
2022

CHEMICAL AND BIOCHEMICAL APPLICATIONS OF VIBRATIONAL SPECTROSCOPY

Reid Ethan Brenner, Candidate for the Doctor of Philosophy Degree

University of Missouri-Kansas City, 2022

ABSTRACT

Vibrational spectroscopy is a technique that probes a molecule's vibrational modes via infrared absorption and Raman scattering, and is often used as a tool for characterization and/or functional group determination. Because infrared (IR) and Raman spectra are directly influenced by the bonds between atoms, these techniques have many other applications. Two applications of these techniques are presented herein. The current work is divided into two parts: the first half involves the chemical application of vibrational spectroscopy in determining molecular symmetry and structure, and the second part incorporates these techniques in monitoring protein-substrate binding.

To demonstrate some of the chemical applications of vibrational spectroscopy, normal coordinate and vibrational analyses were performed on two silacyclobutane derivatives: 1,1-dimethylsilacylobutane (DMSCBane) and 1,1-dimethylsilacyclobut-2-ene (DMSCBene), aided by quantum chemical calculations. Additionally, for DMSCBane, the adjusted r_0 structural parameters were determined by combining *ab initio* results with existing experimental data, whereas for DMSCBene, only predicted structural parameters have been reported. For the biochemical applications, a normal coordinate and vibrational analysis was

first performed on the substrate, phosphoenolpyruvate (PEP) in a buffer solution, using data from Fourier-transform infrared (FTIR) spectroscopy with an attenuated total reflectance (ATR) accessory. This method was then used to monitor PEP binding to rabbit muscle pyruvate kinase (rM_1-PYK) using IR difference spectroscopy. This work attempts to address deficits in previous studies of PEP/rM_1-PYK binding by: 1) using a different approach to subtracting a reference spectrum to achieve an IR difference spectrum and; 2) collecting spectral replicates to determine the statistical relevance of vibrational frequency shifting of bands from bound versus unbound PEP.

The faculty listed below, appointed by the Dean of the School of Graduate Studies have examined a dissertation titled "CHEMICAL AND BIOCHEMICAL APPLICATIONS OF VIBRATIONAL SPECTROSCOPY," presented by Reid Ethan Brenner, candidate for the Doctor of Philosophy degree, and certify that in their opinion it is worthy of acceptance.

Supervisory Committee

Kathleen V. Kilway, Ph.D., Committee Chair
Department of Chemistry

Charles J. Wurrey, Ph.D.
Department of Chemistry

Shin A. Moteki, Ph.D.
Department of Chemistry

Paul Rulis, PhD.
Department of Physics

Da-Ming Zhu, PhD.
Department of Physics

CONTENTS

ILLUSTRATIONS

Figure Page

TABLES

ACKNOWLEDGEMENTS

I would like to convey my deepest appreciation and gratitude for my advisor, Prof. Kathleen Kilway, and my research director, Prof. Charles Wurrey. Their unwavering support and mentorship have been crucial to my development as a scientist and as a professional. Their efforts and encouragement made this possible, for which I am forever thankful.

I want to thank my committee members, Profs. Shin Moteki, Paul Rulis, and Da-Ming Zhu for their support, advice, and valuable feedback. I would also like to thank our collaborator, Prof. Aron Fenton, for providing me opportunities to participate in research I never thought I would have a chance to be involved in. I also want to thank previous group members for their knowledge, advice, and support as well.

Additionally, I want to thank the late Prof. James Durig. This endeavor began when he recruited me into his lab. Though unfortunately we could not see this through together, I am forever grateful to Prof. Durig for exposing me to vibrational spectroscopy and providing me with his knowledge in the field, as well as his unique perspectives in science and research.

Lastly, I would like to thank my friends and family for their constant source of love and support through graduate school. I am sincerely thankfully for my parents, Drs. Linda and Robert Brenner, for always supporting and encouraging me to pursue my interests and follow my passion. Lastly, I want to thank my wife, Christina, for being the best partner I could ever ask for and providing me with unconditional love and support.

FUNDING

This work was supported in part by NIH grant 5R01GM115340-02. The computation for this work was performed on the high performance computing infrastructure provided by Research Computing Support Services and in part by the National Science Foundation under grant number CNS-1429294 at the University of Missouri, Columbia, MO. DOI: https://doi.org/10.32469/10355/69802

DEDICATION

To my fiercest advocate, my wife, the love of my life.

CHAPTER 1

VIBRATIONAL ANALYSIS, STRUCTURAL PARAMETERS, AND *AB INITIO* CALCULATIONS OF 1,1-DIMETHYL-1-SILACYCLOBUTANE

Introduction

The first vibrational analysis of 1,1-dimethyl-1-silacyclobutane (DMSCBane) was performed by Durig and coworkers,[1] where they recorded infrared (IR) and Raman spectra in the vapor and condensed phases. The goal of the study was to determine the ring-puckering potential function as well as barriers to internal rotation of the methyl groups. Vibrational assignments were made using group frequencies, Raman depolarization ratios in the vapor and liquid phases, and IR band contour data in the vapor phase, along with frequency correlations from previous work by Laane[2] on silacyclobutane and its derivatives. Similar to Laane's investigation, the vibrational analysis by Durig et al. was made using C_{2v} symmetry, with the assumption that the planar molecule can readily convert to the puckered form, having C_s symmetry. Initial assignments of all 48 fundamental frequencies of DMSCBane were made in the various phases of DMSCBane. Among those assignments, the two methyl torsional frequencies were assigned at 177 and 172 cm^{-1} in the Raman spectrum of the vapor, and the ring puckering mode was assigned at 112 cm^{-1} in the IR spectrum of the vapor. Using the assignments of the methyl torsional modes, a limited two-dimensional analysis of the torsional potential function estimated the methyl barrier to internal rotation to be 726 cm^{-1} (2.02 kcal/mol). No potential function for ring puckering was determined in this study due to lack of any observable overtones of the ring puckering vibrational frequency. Regarding the structure of DMSCBane, the investigators noticed the molecule appeared to follow different selection rules in the liquid versus solid state, based upon the absence/presence of

different peaks in the spectra. They speculated that the molecule was primarily planar at room temperature in the fluid phases, thus exhibiting C_{2v} symmetry selection rules, but upon cooling to the solid state, the molecule would convert to the lower energy form, resulting in a puckered ring following C_s symmetry selection rules. They concluded by speculating DMSCBane has a quasi-planar structure, or in other words, had a low barrier to planarity.

In an effort to study the Si–C bonds in strained and normal systems, Shen and coworkers conducted a structural analysis[3] of DMSCBane using gas-phase electron diffraction (ED). Using force fields obtained from a previous investigation[4] of silacyclopentane and its derivatives, Shen et al. were able to calculate amplitudes of vibrations for DMSCBane and, using a static model, were able to experimentally determine nine structural parameters. This study was the first to determine the ring was in fact puckered, with a puckering angle of 34.2º. A later study[5] by Novikov and coworkers reevaluated the original ED data[3] collected by Shen and coworkers using a dynamic model, and by treating the ring puckering as a large amplitude motion, were able to determine the structural parameters of DMSCBane and its ring puckering potential function. Additionally, Novikov et al. used force fields computed by *ab initio* calculations to fit the parameters to the electron diffraction data and were able to determine additional structural parameters of DMSCBane and improve upon the accuracy of the original data. They then calculated the puckering angle to be 29.7º. The barrier height was originally determined to be V_0 = 1.3 kcal/mol (455 cm^{-1}) with a relatively high uncertainty of ±1.2 kcal/mol (420 cm^{-1}). However, Novikov et al. obtained a much lower barrier height V_0 = 0.56 kcal/mol (196 cm^{-1}) by solving the one-dimensional Hamiltonian and fitting the 2 ← 0 ring puckering transition frequency, which they assigned to the experimental value of 112 cm^{-1}. In the same study, Novikov et al. performed a normal coordinate analysis, reanalyzed the original vibrational data by Durig et al., and updated several assignments.

However, the ring puckering frequency and the two methyl torsional assignments remained unchanged.

A more recent study[6] of DMSCBane by Hirota and coworkers used Fourier transform microwave spectroscopy (FT-MW) to understand the dynamics of the two large amplitude motions of DMSCBane, specifically the two-top internal (methyl) rotations and ring puckering as well as the coupling between the two. Hirota et al. were able to identify and assign transitions and obtain rotational constants for seven isotopomers of DMSCBane: normal, ^{29}Si, ^{30}Si, and ^{13}C at all four symmetrically unique positions within the molecule. With the aid of *ab initio* calculations, along with the rotational constants, Hirota et al. were able to determine several r_s parameters using two different sets, incorporating positive [Set I] and negative [Set II] signs for the b coordinate of the Si atom (whose rationale is discussed further in the "Structural Parameters" section), and determined the puckering angle to be either 28.6º or 30.3º. The barrier height of puckering for DMSCBane was determined to be V_0 = 395 or 347 cm^{-1} based on the splitting of the two lowest puckering states. Additionally, the barrier to internal rotation of the methyl groups was determined to be 568 cm^{-1} with the methyl groups rotating in the same direction relative to the Si atom, and 505 cm^{-1} with the methyl groups rotating in opposite directions relative to the Si atom; the coupling between the two internal rotations corresponds to torsional frequencies of 154 and 144 cm^{-1}.

Thus there are several discrepancies between previous investigations[1,3,5,6] of DMSCBane from vibrational assignments to barriers to internal rotation of the methyl groups and the ring puckering angle. Part of the complexity of this molecule is due to its unique C_s symmetry, where the σ_h symmetry plane bisects the silacyclobutane ring, resulting in two non-equivalent methyl rotors. Another layer of complexity stems from the discrepancy of the assignments of the two methyl torsional vibrational frequencies which, if incorrectly assigned, can lead to erroneous

results in the barrier to internal rotation. DMSCBane presents a unique opportunity to employ *ab initio* calculations using higher levels of theory in conjunction with a new normal coordinate analysis to more accurately determine the structural parameters and vibrational frequency assignments of DMSCBane. Additionally, the structures computed from *ab initio* calculations can be combined with isotopic data from the FT-MW study[6] to determine adjusted r_0 structural parameters, which can be compared to the existing ED data for DMSCBane.

Computational Methods

The *ab initio* calculations were performed with the Gaussian 09® program[7] by using Gaussian-type basis functions. The energy minima with respect to nuclear coordinates were obtained by the simultaneous relaxation of all geometric parameters using the gradient method of Pulay.[8] Several basis sets, as well as the corresponding ones with diffuse functions, were employed with the Møller-Plesset perturbation method[9] to the second order, MP2(full), along with the density functional theory by the B3LYP method. There are two possible structural conformations of DMSCBane: the first involves a bent (puckered) silacyclobutane ring, having C_s symmetry; the second has a planar ring, exhibiting C_{2v} symmetry. Because the ring puckering potential is directly influenced by the energy difference between these two conformations, the predicted conformational energy differences between the two forms of DMSCBane have been calculated using different basis sets and are listed in Table 1.1. The optimized geometry from the MP2(full)/6-311+G(d,p) calculation is illustrated in Fig. 1.1.

Table 1.1. Calculated energies[a] in Hartrees (H) and energy differences[b] in wavenumbers (cm^{-1}) of the two possible conformations of DMSCBane.

Basis Set		B3LYP		MP2 (full)	
		C_s	C_{2v}	C_s	C_{2v}
6-31	g(d)	1.260505	207	0.018311	604
	+g(d)	1.269133	197	0.031889	608
	g(d,p)	1.279269	205	0.118744	620
	+g(d,p)	1.287282	195	0.130791	633
6-311	g(d)	1.327864	185	0.303028	640
	+g(d)	1.329188	184	0.307592	640
	g(d,p)	1.345511	196	0.396299	721
	+g(d,p)	1.346821	196	0.400454	715
	g(2d,2p)	1.358586	205	0.479253	718
	+g(2d,2p)	1.359641	212	0.481864	731
	g(2df,2pd)	1.365987	202	0.578474	641
	+g(2df,2pd)	1.366967	203	0.580600	657
	g(3d,3p)	1.361121	204	0.527261	679
	+g(3d,3p)	1.361963	202	0.529300	667
	g(3df,3pd)	1.368730	216	0.625624	642
	+g(3df,3pd)	1.369402	215	0.627127	636
	aug-cc-pVTZ	1.372478	211	0.529258	703

[a] Energies of the C_s conformer in both columns are given as $-(E + 487)$ H.
[b] Energy differences between the C_{2v} and C_s conformers are reported in the C_{2v} columns.

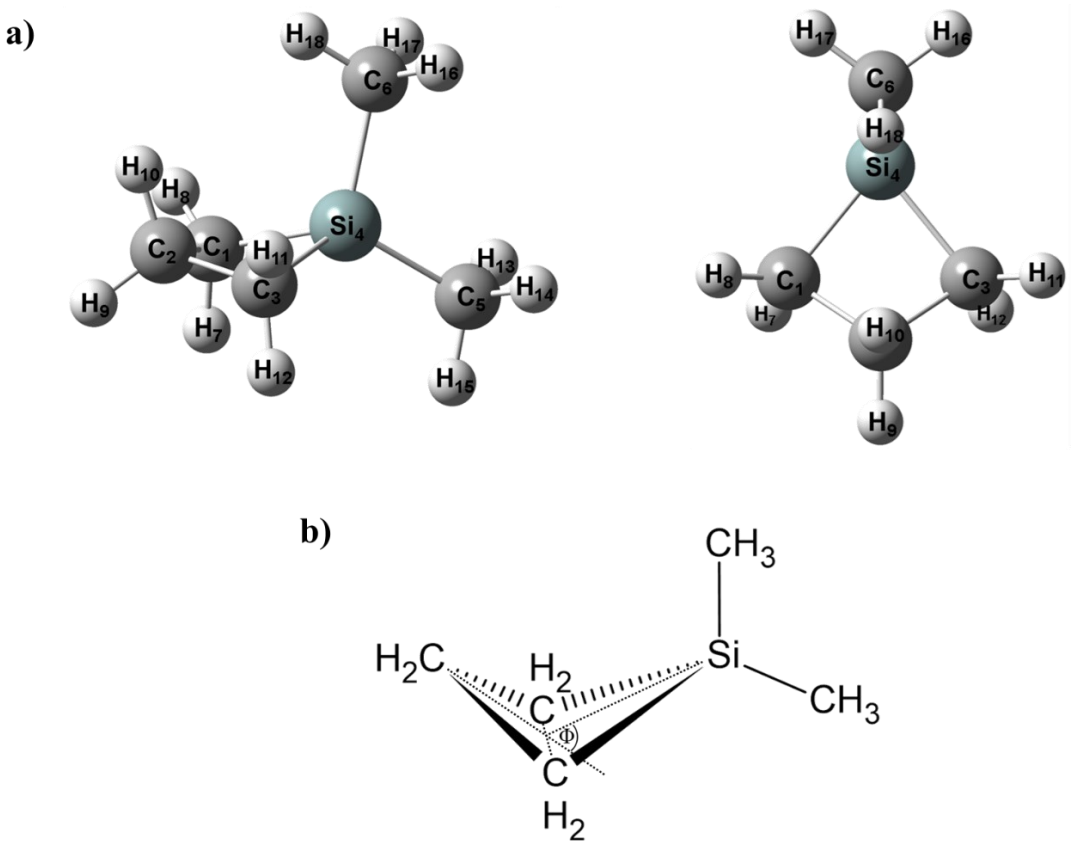

Figure 1.1. a) The C_s conformation of 1,1-dimethyl-1-silacyclobutane (DMSCBane) where the σ_h plane of symmetry bisects the ring, passing through heavy atoms $C_2Si_4C_5C_6$; both images are from two different perspectives to illustrate the molecule's symmetry. b) The puckering angle, Φ, is defined as the external angle relative to the internal angle formed between the C-C-C and C-Si-C planes.

In order to obtain a description of the molecular motions involved in the fundamental vibrational modes of DMSCBane, a normal coordinate analysis has been carried out. The force field in Cartesian coordinates was obtained with the Gaussian 09® program at the MP2(full) level with the 6-31G(d) basis set. The internal coordinates used to calculate the **G** and **B** matrices are given in Table 1.2 with the atomic numbering shown in Fig. 1.1. By using the **B** matrix,[10] the force field in Cartesian coordinates was converted to a force field in internal coordinates. Subsequently, scaling factors of 0.88 for CH stretches and CH deformations, and 0.9 for other coordinates were

applied except for the heavy atom bendings and torsions, along with the geometric average of the scaling factors for the interaction force constants, to obtain the fixed scaled force field and resultant wavenumbers. The list of symmetry coordinates provided in Table 1.2 was used to determine the corresponding potential energy distributions (P.E.D.). The evaluation of Raman activity by using the analytical gradient method has been developed,[11–14] and the activity S_j can be expressed as: $S_j = g_j(45\alpha_j^2 + 7\beta_j^2)$, where g_j is the degeneracy of the vibrational mode j, α_j is the derivative of the isotropic polarizability, and β_j is the anisotropic polarizability derivative. To obtain the Raman scattering cross sections, the polarizabilities are incorporated into S_j by multiplying S_j with $(1-\rho_j)/(1+\rho_j)$ where ρ_j is the depolarization ratio of the j^{th} normal mode. A comparison between the observed and calculated wavenumbers, along with the calculated infrared intensities, Raman activities, depolarization ratios and potential energy distributions for both conformations of DMSCBane are listed in Table 1.3.

Table 1.2. Symmetry coordinates of 1,1-dimethyl-1-silacyclobutane.

	Description	Symmetry Coordinate [a,b]
A'	α-$(CH_3)_2$ antisymmetric stretch OP–Ring	$S_1 = 2\mathbf{r}_{6,18} - \mathbf{r}_{6,17} - \mathbf{r}_{6,16} - 2\mathbf{r}_{5,15} + \mathbf{r}_{5,14} + \mathbf{r}_{5,13}$
	α-$(CH_3)_2$ antisymmetric stretch IP–Ring	$S_2 = 2\mathbf{r}_{6,18} - \mathbf{r}_{6,17} - \mathbf{r}_{6,16} + 2\mathbf{r}_{5,15} - \mathbf{r}_{5,14} - \mathbf{r}_{5,13}$
	$(CH_2)_2$ antisymmetric stretch IP	$S_3 = \mathbf{r}_{1,8} - \mathbf{r}_{1,7} - \mathbf{r}_{3,12} + \mathbf{r}_{3,11}$
	CH_2 antisymmetric stretch	$S_4 = \mathbf{r}_{2,10} - \mathbf{r}_{2,9}$
	$(CH_2)_2$ symmetric stretch IP	$S_5 = \mathbf{r}_{1,8} + \mathbf{r}_{1,7} + \mathbf{r}_{3,12} + \mathbf{r}_{3,11}$
	CH_2 symmetric stretch	$S_6 = \mathbf{r}_{2,10} + \mathbf{r}_{2,9}$
	$(CH_3)_2$ symmetric stretch IP–Ring	$S_7 = \mathbf{r}_{6,18} + \mathbf{r}_{6,17} + \mathbf{r}_{6,16} + \mathbf{r}_{5,15} + \mathbf{r}_{5,14} + \mathbf{r}_{5,13}$
	$(CH_3)_2$ symmetric stretch OP–Ring	$S_8 = \mathbf{r}_{6,18} + \mathbf{r}_{6,17} + \mathbf{r}_{6,16} - \mathbf{r}_{5,15} - \mathbf{r}_{5,14} - \mathbf{r}_{5,13}$
	CH_2 deformation	$S_9 = 4\boldsymbol{\alpha}_{10,2,9} - \boldsymbol{\phi}1_{0,2,3} - \boldsymbol{\phi}_{10,2,1} - \boldsymbol{\phi}_{9,2,3} - \boldsymbol{\phi}_{9,2,1}$
	$(CH_2)_2$ deformation IP	$S_{10} = 4\boldsymbol{\alpha}_{8,1,7} - \boldsymbol{\sigma}_{8,1,4} - \boldsymbol{\sigma}_{8,1,2} - \boldsymbol{\sigma}_{7,1,4} - \boldsymbol{\sigma}_{7,1,2} + 4\boldsymbol{\alpha}_{11,3,12} - \boldsymbol{\sigma}_{11,3,4} - \boldsymbol{\sigma}_{11,3,2} - \boldsymbol{\sigma}_{12,3,4} - \sigma_{12,3,2}$
	α-$(CH_3)_2$ antisymmetric deformation IP–Ring	$S_{11} = 2\boldsymbol{\alpha}_{16,6,17} - \boldsymbol{\alpha}_{18,6,16} - \boldsymbol{\alpha}_{18,6,17} + 2\boldsymbol{\alpha}_{14,5,13} - \boldsymbol{\alpha}_{15,5,14} - \boldsymbol{\alpha}_{15,5,13}$
	α-$(CH_3)_2$ antisymmetric deformation OP–Ring	$S_{12} = 2\boldsymbol{\alpha}_{16,6,17} - \boldsymbol{\alpha}_{18,6,16} - \boldsymbol{\alpha}_{18,6,17} - 2\boldsymbol{\alpha}_{14,5,13} + \boldsymbol{\alpha}_{15,5,13} + \boldsymbol{\alpha}_{15,5,14}$
	$(CH_3)_2$ symmetric deformation IP	$S_{13} = \boldsymbol{\alpha}_{18,6,16} + \boldsymbol{\alpha}_{18,6,17} + \boldsymbol{\alpha}_{16,6,17} + \boldsymbol{\alpha}_{15,5,14} + \boldsymbol{\alpha}_{15,5,13} + \boldsymbol{\alpha}_{14,5,13} - \boldsymbol{\theta}_{18,6,4} - \boldsymbol{\theta}_{17,6,4} - \boldsymbol{\theta}_{16,6,4} - \boldsymbol{\theta}_{15,5,4} - \boldsymbol{\theta}_{14,5,4} - \boldsymbol{\theta}_{13,5,4}$
	$(CH_3)_2$ symmetric deformation OP	$S_{14} = \boldsymbol{\alpha}_{18,6,16} + \boldsymbol{\alpha}_{18,6,17} + \boldsymbol{\alpha}_{16,6,17} - \boldsymbol{\alpha}_{15,5,14} - \boldsymbol{\alpha}_{15,5,13} - \boldsymbol{\alpha}_{14,5,13} - \boldsymbol{\theta}_{18,6,4} - \boldsymbol{\theta}_{17,6,4} - \boldsymbol{\theta}_{16,6,4} + \boldsymbol{\theta}_{15,5,4} + \boldsymbol{\theta}_{14,5,4} + \boldsymbol{\theta}_{13,5,4}$
	$(CH_2)_2$ twist IP	$S_{15} = \boldsymbol{\sigma}_{8,1,2} - \boldsymbol{\sigma}_{8,1,4} - \boldsymbol{\sigma}_{7,1,2} + \boldsymbol{\sigma}_{7,1,4} \boldsymbol{\sigma}_{11,3,2} - \boldsymbol{\sigma}_{11,3,4} - \boldsymbol{\sigma}_{12,3,2} + \boldsymbol{\sigma}_{12,3,4}$
	$(CH_2)_2$ wag IP	$S_{16} = \boldsymbol{\sigma}_{8,1,2} - \boldsymbol{\sigma}_{8,1,4} + \boldsymbol{\sigma}_{7,1,2} - \boldsymbol{\sigma}_{7,1,4} \boldsymbol{\sigma}_{11,3,2} - \boldsymbol{\sigma}_{11,3,4} + \boldsymbol{\sigma}_{12,3,2} - \boldsymbol{\sigma}_{12,3,4}$
	$(CH_2)_2$ rock IP	$S_{17} = \boldsymbol{\sigma}_{8,1,2} + \boldsymbol{\sigma}_{8,1,4} - \boldsymbol{\sigma}_{7,1,2} - \boldsymbol{\sigma}_{7,1,4} \boldsymbol{\sigma}_{11,3,2} + \boldsymbol{\sigma}_{11,3,4} - \boldsymbol{\sigma}_{12,3,2} - \boldsymbol{\sigma}_{12,3,4}$
	Ring C–C symmetric stretch	$S_{18} = \mathbf{R}_{2,1} + \mathbf{R}_{2,3}$
	$(CH_3)_2$ rock IP	$S_{19} = 2\boldsymbol{\theta}_{18,6,4} - \boldsymbol{\theta}_{17,6,4} - \boldsymbol{\theta}_{16,6,4} + 2\boldsymbol{\theta}_{15,5,4} - \boldsymbol{\theta}_{14,5,4} - \boldsymbol{\theta}_{13,5,4}$
	CH_2 rock	$S_{20} = \boldsymbol{\phi}_{10,2,1} + \boldsymbol{\phi}_{10,2,3} - \boldsymbol{\phi}_{9,2,1} - \boldsymbol{\phi}_{9,2,3}$
	$(CH_3)_2$ rock OP	$S_{21} = 2\boldsymbol{\theta}_{18,6,4} - \boldsymbol{\theta}_{17,6,4} - \boldsymbol{\theta}_{16,6,4} - 2\boldsymbol{\theta}_{15,5,4} + \boldsymbol{\theta}_{14,5,4} + \boldsymbol{\theta}_{13,5,4}$
	Ring Si–C symmetric stretch	$S_{22} = \mathbf{R}_{4,1} + \mathbf{R}_{4,3}$
	Si–C antisymmetric stretch	$S_{23} = \mathbf{R}_{4,6} - \mathbf{R}_{4,5}$
	Si–C symmetric stretch	$S_{24} = \mathbf{R}_{4,6} + \mathbf{R}_{4,5}$
	Ring deformation	$S_{25} = \boldsymbol{\Delta}_{1,2,3} + \boldsymbol{\Delta}_{1,4,3} - \boldsymbol{\Delta}_{2,1,4} - \boldsymbol{\Delta}_{2,3,4}$
	Ring puckering	$S_{26} = \boldsymbol{\tau}_{4,1,2,3} - \boldsymbol{\tau}_{2,1,4,3} - \boldsymbol{\tau}_{1,2,3,4} + \boldsymbol{\tau}_{2,3,4,1}$
	Si–$(CH_3)_2$ deformation	$S_{27} = 4\boldsymbol{\lambda}_{6,4,5} - \boldsymbol{\lambda}_{1,4,6} - \boldsymbol{\lambda}_{1,4,5} - \lambda_{3,4,6} - \boldsymbol{\lambda}_{3,4,5}$
	Si–$(CH_3)_2$ rock	$S_{28} = \boldsymbol{\lambda}_{1,4,6} - \boldsymbol{\lambda}_{1,4,5} + \boldsymbol{\lambda}_{3,4,6} - \boldsymbol{\lambda}_{3,4,5}$
A''	β-$(CH_3)_2$ antisymmetric stretch IP–Ring	$S_{29} = \mathbf{r}_{6,16} - \mathbf{r}_{6,17} + \mathbf{r}_{5,14} - \mathbf{r}_{5,13}$
	$(CH_2)_2$ antisymmetric stretch OP	$S_{30} = \mathbf{r}_{1,8} - \mathbf{r}_{1,7} + \mathbf{r}_{3,12} - \mathbf{r}_{3,11}$
	β-$(CH_3)_2$ antisymmetric stretch OP–Ring	$S_{31} = \mathbf{r}_{6,16} - \mathbf{r}_{6,17} - \mathbf{r}_{5,14} + \mathbf{r}_{5,13}$
	$(CH_2)_2$ symmetric stretch OP	$S_{32} = \mathbf{r}_{1,8} + \mathbf{r}_{1,7} - \mathbf{r}_{3,12} - \mathbf{r}_{3,11}$
	β-$(CH_3)_2$ antisymmetric deformation IP–Ring	$S_{33} = \boldsymbol{\alpha}_{18,6,16} - \boldsymbol{\alpha}_{18,6,17} - \boldsymbol{\alpha}_{15,5,13} + \boldsymbol{\alpha}_{15,5,14}$
	β-$(CH_3)_2$ antisymmetric deformation OP–Ring	$S_{34} = \boldsymbol{\alpha}_{18,6,16} - \boldsymbol{\alpha}_{18,6,17} + \boldsymbol{\alpha}_{15,5,13} - \boldsymbol{\alpha}_{15,5,14}$
	$(CH_2)_2$ deformation OP	$S_{35} = 4\boldsymbol{\alpha}_{8,1,7} - \boldsymbol{\sigma}_{8,1,4} - \boldsymbol{\sigma}_{8,1,2} - \boldsymbol{\sigma}_{7,1,4} - \boldsymbol{\sigma}_{7,1,2} - 4\boldsymbol{\alpha}_{11,3,12} + \boldsymbol{\sigma}_{11,3,4} + 4\boldsymbol{\sigma}_{11,3,2} + \boldsymbol{\sigma}_{12,3,4} + \boldsymbol{\sigma}_{12,3,2}$
	CH_2 wag	$S_{36} = \boldsymbol{\phi}_{10,2,1} - \boldsymbol{\phi}_{10,2,3} + \boldsymbol{\phi}_{9,2,1} - \boldsymbol{\phi}_{9,2,3}$
	CH_2 twist	$S_{37} = \boldsymbol{\phi}_{10,2,1} - \boldsymbol{\phi}_{10,2,3} - \boldsymbol{\phi}_{9,2,1} + \boldsymbol{\phi}_{9,2,3}$
	$(CH_2)_2$ wag OP	$S_{38} = \boldsymbol{\sigma}_{8,1,2} - \boldsymbol{\sigma}_{8,1,4} + \boldsymbol{\sigma}_{7,1,2} - \boldsymbol{\sigma}_{7,1,4} - \boldsymbol{\sigma}_{11,3,2} + \boldsymbol{\sigma}_{11,3,4} - \boldsymbol{\sigma}_{12,3,2} + \boldsymbol{\sigma}_{12,3,4}$
	Ring C–C antisymmetric stretch	$S_{39} = \mathbf{R}_{2,1} - \mathbf{R}_{2,3}$
	$(CH_2)_2$ twist OP	$S_{40} = \boldsymbol{\sigma}_{8,1,2} - \boldsymbol{\sigma}_{8,1,4} - \boldsymbol{\sigma}_{7,1,2} + \boldsymbol{\sigma}_{7,1,4} - \boldsymbol{\sigma}_{11,3,2} + \boldsymbol{\sigma}_{11,3,4} + \boldsymbol{\sigma}_{12,3,2} - \boldsymbol{\sigma}_{12,3,4}$
	$(CH_3)_2$ wag IP-Ring	$S_{41} = \boldsymbol{\theta}_{16,6,4} - \boldsymbol{\theta}_{17,6,4} + \boldsymbol{\theta}_{14,5,4} - \boldsymbol{\theta}_{13,5,4}$
	$(CH_3)_2$ wag OP-Ring	$S_{42} = \boldsymbol{\theta}_{16,6,4} - \boldsymbol{\theta}_{17,6,4} - \boldsymbol{\theta}_{14,5,4} + \boldsymbol{\theta}_{13,5,4}$
	Ring Si–C antisymmetric stretch	$S_{43} = \mathbf{R}_{4,1} - \mathbf{R}_{4,3}$
	$(CH_2)_2$ rock OP	$S_{44} = \boldsymbol{\sigma}_{8,1,2} + \boldsymbol{\sigma}_{8,1,4} - \boldsymbol{\sigma}_{7,1,2} - \boldsymbol{\sigma}_{7,1,4} - \boldsymbol{\sigma}_{11,3,2} - \boldsymbol{\sigma}_{11,3,4} + \boldsymbol{\sigma}_{12,3,2} + \boldsymbol{\sigma}_{12,3,4}$
	Si–$(CH_3)_2$ wag	$S_{45} = \boldsymbol{\lambda}_{1,4,6} + \boldsymbol{\lambda}_{1,4,5} - \boldsymbol{\lambda}_{3,4,6} - \boldsymbol{\lambda}_{3,4,5}$
	Si–$(CH_3)_2$ twist	$S_{46} = \boldsymbol{\lambda}_{1,4,6} - \boldsymbol{\lambda}_{1,4,5} - \boldsymbol{\lambda}_{3,4,6} + \boldsymbol{\lambda}_{3,4,5}$
	CH_3 Torsion IP-Ring	$S_{47} = \boldsymbol{\tau}_{5,4,6,18} - \boldsymbol{\tau}_{6,4,5,15}$
	CH_3 Torsion OP-Ring	$S_{48} = \boldsymbol{\tau}_{5,4,6,18} + \boldsymbol{\tau}_{6,4,5,15}$

[a]Not normalized.

[b]The subscripted numbers of the internal coordinates correspond to the atom numbering in Fig.1 of DMSCBane.

Table 1.3. Observed[a] and calculated[b] frequencies (cm^{-1}) for the C_s conformation of 1,1-dimethyl-1-silacyclobutane.

	Vib. No.	Approximate Descriptions [c]	ab initio	fixed scaled[d]	IR int.	Raman act.	dp ratio	IR		Raman			P.E.D.[e]	Band Contours [f]		
								Gas	Solid	Gas	Liquid	Solid		A	B	C
A'	ν_1	α-$(CH_3)_2$ antisymmetric stretch OP-Ring	3198	3000	10.8	73.7	0.75	2972	2975	2974	–	2973	52 S_1, 48 S_2	29	71	0
	ν_2	α-$(CH_3)_2$ antisymmetric stretch IP-Ring	3196	2998	11.5	63.5	0.75	2972	2975	2974	–	2973	52 S_2, 46 S_1	78	22	0
	ν_3	$(CH_2)_2$ antisymmetric stretch IP	3191	2993	21.0	72.0	0.57	2972	2975	2974	–	2973	86 S_3	0	100	0
	ν_4	CH_2 antisymmetric stretch	3156	2961	23.2	79.7	0.46	2962	2960	2966	2962	2961	90 S_4	50	51	0
	ν_5	$(CH_2)_2$ symmetric stretch IP	3117	2924	5.2	178.8	0.13	2924	2927	2921	2927	2926	87 S_5	5	95	0
	ν_6	CH_2 symmetric stretch	3102	2910	41.1	146.1	0.16	–	2916	2911	2916	2912	95 S_6	88	13	0
	ν_7	$(CH_3)_2$ symmetric stretch IP-Ring	3099	2907	5.3	89.6	0.01	–	2900	–	2901	2901	57 S_7, 40 S_8	81	19	0
	ν_8	$(CH_3)_2$ symmetric stretch OP-Ring	3098	2906	3.6	80.5	0.00	–	2900	–	2901	2901	59 S_8, 40 S_7	72	28	0
	ν_9	CH_2 deformation	1565	1472	1.2	9.6	0.57	–	–	–	–	–	92 S_9	28	72	0
	ν_{10}	$(CH_2)_2$ deformation IP	1526	1436	8.3	18.8	0.73	1453	1451	–	1454	1452	85 S_{10}	25	76	0
	ν_{11}	α-$(CH_3)_2$ antisymmetric deformation IP-Ring	1526	1432	1.8	28.7	0.75	1453	1451	–	1454	1452	92 S_{11}	100	0	0
	ν_{12}	α-$(CH_3)_2$ antisymmetric deformation OP-Ring	1517	1424	1.3	1.1	0.70	1420	1423	1425	–	1424	85 S_{12}	16	85	0
	ν_{13}	$(CH_3)_2$ symmetric deformation IP	1366	1289	19.1	0.8	0.66	–	1294	–	–	–	98 S_{13}	83	18	0
	ν_{14}	$(CH_3)_2$ symmetric deformation OP	1361	1283	44.4	2.4	0.75	–	1290	–	–	–	96 S_{14}	11	90	0
	ν_{15}	$(CH_2)_2$ twist IP	1261	1198	2.9	5.6	0.69	1186	1187	1189	1186	1187	47 S_{15}, 23 S_{20}, 16 S_{17}, 10 S_{16}	13	87	0
	ν_{16}	$(CH_2)_2$ wag IP	1209	1153	33.9	1.3	0.54	1125	1117	1127	1122	1118	67 S_{16}, 12 S_{18}	99	1	0
	ν_{17}	$(CH_2)_2$ rock IP	966	922	58.5	7.2	0.27	926	924	–	927	928	26 S_{18}, 19 S_{20}, 14 S_{15}, 13 S_{17}	24	76	0
	ν_{18}	Ring C-C symmetric stretch	950	907	62.0	6.0	0.10	907	904	908	906	906	37 S_{18}, 18 S_{19}, 11 S_{15}, 10 S_{22}	37	63	0
	ν_{19}	$(CH_3)_2$ rock IP	906	867	64.9	3.0	0.42	884	889	886	887	894	49 S_{19}, 19 S_{18}	97	3	0
	ν_{20}	CH_2 rock	868	833	18.2	4.4	0.19	–	813	813	811	815	25 S_{25}, 23 S_{20}, 17 S_{17}, 16 S_{22}	78	23	0
	ν_{21}	$(CH_3)_2$ rock OP	768	732	25.0	2.0	0.52	731	728	729	728	728	32 S_{21}, 28 S_{23}, 13 S_{15}, 11 S_{20}	7	93	0
	ν_{22}	Ring Si-C symmetric stretch	741	706	31.7	4.1	0.68	707	706	708	703	708	39 S_{24}, 25 S_{22}, 12 S_{17}, 10 S_{19}	95	5	0
	ν_{23}	Si-C antisymmetric stretch	719	682	7.0	5.6	0.74	–	680	–	685	686	54 S_{23}, 44 S_{21}	17	83	0
	ν_{24}	Si-C symmetric stretch	628	601	3.0	12.9	0.03	609	608	610	612	608	37 S_{24}, 20 S_{17}, 14 S_{25}, 10 S_{22}	75	25	0
	ν_{25}	Ring deformation	459	447	5.8	12.6	0.14	445	446	445	446	446	44 S_{25}, 26 S_{22}, 18 S_{24}	89	12	0
	ν_{26}	Ring puckering	256	253	2.2	0.6	0.45	–	254	–	–	255	45 S_{26}, 32 S_{28}, 14 S_{17}	14	87	0
	ν_{27}	Si-$(CH_3)_2$ deformation	200	199	0.6	1.6	0.68	197	190	–	–	197	89 S_{27}	98	2	0
	ν_{28}	Si-$(CH_3)_2$ rock	134	134	0.5	0.4	0.69	–	–	–	–	131	55 S_{28}, 43 S_{26}	0	100	0

Table 1.3. --Continued.

	Vib. No.	Approximate Descriptions[c]	ab initio	fixed scaled[d]	IR int.	Raman act.	dp ratio	IR		Raman			P.E.D.[e]	Band Contours [f]		
								Gas	Solid	Gas	Liquid	Solid		A	B	C
A"	ν_{29}	β-$(CH_3)_2$ antisymmetric stretch IP-Ring	3192	2995	14.4	104.0	0.75	2972	2975	2974	–	2973	75 S_{29}, 25 S_{31}	0	0	100
	ν_{30}	$(CH_2)_2$ antisymmetric stretch OP	3190	2992	4.0	87.4	0.75	2972	2975	2974	–	2973	65 S_{30}, 20 S_{31}	0	0	100
	ν_{31}	β-$(CH_3)_2$ antisymmetric stretch OP-Ring	3190	2992	13.4	25.7	0.75	2972	2975	2974	–	2973	55 S_{31}, 27 S_{30}, 16 S_{29}	0	0	100
	ν_{32}	$(CH_2)_2$ symmetric stretch OP	3116	2923	17.7	11.7	0.75	2924	2927	2921	2927	2926	92 S_{32}	0	0	100
	ν_{33}	β-$(CH_3)_2$ antisymmetric deformation IP-Ring	1530	1436	4.8	0.2	0.75	1453	1451	–	1454	1452	93 S_{33}	0	0	100
	ν_{34}	β-$(CH_3)_2$ antisymmetric deformation OP-Ring	1515	1422	0.5	29.2	0.75	1420	1423	1425	–	1424	93 S_{34}	0	0	100
	ν_{35}	$(CH_2)_2$ deformation OP	1506	1418	8.3	4.8	0.75	1410	1410	1418	1415	1416	93 S_{35}	0	0	100
	ν_{36}	CH_2 wag	1335	1267	0.9	2.4	0.75	1258	1260	1260	1252	1260	79 S_{36}	0	0	100
	ν_{37}	CH_2 twist	1283	1218	1.2	8.8	0.75	1215	1210	–	1213	1213	60 S_{37}, 19 S_{38}	0	0	100
	ν_{38}	$(CH_2)_2$ wag OP	1125	1068	1.1	4.2	0.75	–	1046	–	–	1041	72 S_{38}	0	0	100
	ν_{39}	Ring C-C antisymmetric stretch	1002	958	9.8	5.8	0.75	–	–	–	–	952	75 S_{39}, 10 S_{36}	0	0	100
	ν_{40}	$(CH_2)_2$ twist OP	994	946	3.2	1.0	0.75	–	–	–	–	945	59 S_{40}, 23 S_{37}	0	0	100
	ν_{41}	$(CH_3)_2$ wag IP-Ring	885	845	77.0	0.3	0.75	841	836	840	840	841	67 S_{41}, 12 S_{45}	0	0	100
	ν_{42}	$(CH_3)_2$ wag OP-Ring	806	767	1.0	2.5	0.75	–	778	781	782	–	70 S_{42}, 15 S_{44}	0	0	100
	ν_{43}	Ring Si-C antisymmetric stretch	684	652	10.1	4.9	0.75	648	646	650	646	651	42 S_{43}, 27 S_{44}, 13 S_{41}	0	0	100
	ν_{44}	$(CH_2)_2$ rock OP	648	619	4.1	1.9	0.75	613	614	–	–	613	41 S_{43}, 37 S_{44}, 12 S_{42}	0	0	100
	ν_{45}	Si-$(CH_3)_2$ wag	228	227	1.1	0.5	0.75	226	–	228	–	–	77 S_{45}, 10 S_{47}	0	0	100
	ν_{46}	Si-$(CH_3)_2$ twist	177	177	0.0	0.8	0.75	–	–	177	–	–	83 S_{46}	0	0	100
	ν_{47}	CH_3 torsion IP-Ring	167	167	0.0	0.0	0.75	–	–	172	–	–	83 S_{47}	0	0	100
	ν_{48}	CH_3 torsion OP-Ring	148	148	0.0	0.2	0.75	–	148	–	–	141	84 S_{48}	0	0	100

[a] Experimental data used in table is taken from Ref. [1].

[b] MP2(full)/6-31G(d) *ab initio* calculations, scaled frequencies, infrared intensities (km/mol), Raman activities (Å^4/amu), depolarization ratios and potential energy distributions (P.E.D.).

[c] IP and OP are modes which are in/out of phase with respect to the σ_h symmetry plane for the C_s form. IP-Ring and OP-Ring are modes which are in/out of phase with respect to the plane of four-membered ring in planar form pertaining to the C_{2v} point group.

[d] MP2(full)/6-31G(d) fixed scaled frequencies with factors of 0.88 for CH stretches and CH_2 deformations, 1.0 for heavy atom bends, and 0.90 for all other modes.

[e] Contributions less than 10% are omitted.

[f] A, B and C values in the last three columns are percentage infrared band contours.

Vibrational Analysis

The original vibrational analysis[1] of DMSCBane contained assignments made from infrared and Raman spectra, with the sample in various phases (vapor, liquid, and solid). The investigators assumed the structure to be of C_{2v} symmetry with a planar silacyclobutane ring, assigning and sorting the 48 vibrational modes according to their respective depolarization values and band contour data of the symmetry species: $15A_1 + 9A_2 + 11B_1 + 13B_2$. Group frequencies and frequency correlations from previous work on silacyclobutane derivatives were also utilized as an aid in assignments. Using the available data, Durig et al. were able to initially assign all the fundamental transitions of the 48 possible normal modes of vibration, between the various phases in the infrared and Raman spectra. The investigators noted that the molecule appeared to follow different selection rules in the liquid versus solid state, suggesting the existence of a quasi-planar (C_{2v}) conformer at ambient temperatures, which shifted toward the puckered form (C_s) at lower temperatures. Durig and coworkers concluded the study by suggesting additional analysis was needed to identify the correct configuration of the molecule. It was not until two decades later that an electron diffraction study[5] revisited the vibrational data of DMSCBane. Novikov et al. performed the first normal coordinate analysis on the molecule, using *ab initio* results from HF/6-311G(d,p) calculations. While several assignments were updated, many were in agreement with the initial assignments, including some of the larger-amplitude vibrational modes: the asymmetric torsional mode at 177 cm^{-1}, symmetric torsional mode at 172 cm^{-1}, and ring puckering at 112 cm^{-1}. In a more recent microwave study,[6] however, Hirota et al. determined the two torsional vibrational frequencies were at 154 and 144 cm^{-1} instead.

Because DMSCBane is a relatively small molecule (< 25 atoms), one would expect the vibrational analysis to be relatively straight forward, however, this has not been the case thus far.

The depolarization values from Durig et al., specifically the number of polarized bands in the Raman spectra of the vapor and liquid phases, suggests the molecule still favors the C_s form, even at ambient temperatures. Additionally, a newer vibrational analysis[15] was performed on silacyclobutane and its derivatives, where many assignments were updated from their original ones, which Durig et al. had used previously to aid in DMSCBane's assignments. Furthermore, the microwave study by Hirota et al. conflicts with previous vibrational assignments of the two methyl torsional frequencies. Because all three studies were interested in determining the barrier(s) to internal rotation of the methyl groups and/or the ring-puckering potential function, it is imperative to have an accurate assignment for all three of these vibrational modes. With all of this in consideration, a new vibrational analysis of DMSCBane has been performed in the current work in an attempt to establish, with reasonable certainty, accurate vibrational assignments using the original vibrational spectroscopic data.

As previously indicated in the "Computational Methods" section, the MP2(full)/6-31G(d) calculation was used to determine the predicted vibrational frequencies for both the C_s and C_{2v} conformations of DSMCBane. The C_s form was predicted (see Table 1.1) to be more stable than C_{2v} by approximately 200 – 700 cm^{-1}, and the C_{2v} frequency calculation produced an imaginary (negative) frequency, which suggests the C_{2v} form is a transition state and not a stable conformation; for these reasons, only the vibrational data for the C_s form is given (Table 1.3). The 48 vibrational modes for the C_s form can be sorted into two symmetry blocks which contain the following symmetry species: 28A' + 20A''. The A' vibrational modes consist of A/B hybrid gas phase IR band contours and are predicted to have depolarization ratios up to 0.75. The A'' vibrational modes, however, are all predicted to exhibit C-type band contours and with bands in the Raman spectrum that are depolarized.

The descriptions, or labels, for the 48 vibrational modes differs from the two previous vibrational analyses[1,5] of DMSCBane in an attempt to simplify and clarify their meanings. Durig and coworkers opted to use "α" and "β" for modes that correspond to the ring carbons in the α and β positions relative to the Si atom. Novikov and coworkers opted to use "β" and "γ" instead. In the current work, the two ring methylene groups in the α position, relative to the Si atom, are labeled as $(CH_2)_2$, whereas the β methylene group is labeled CH_2. The two methyl groups are simply labeled as $(CH_3)_2$. Certain descriptions contain the terms "IP" (in-phase) and "OP" (out-of-phase), which correspond to modes which are symmetric or antisymmetric with respect to the σ_h plane of symmetry in the molecule; these terms are synonymous with "synphase" and "asynphase" used by Novikov et al. Additionally, some modes contain "IP-Ring" or "OP-Ring" to connect vibrational assignments between the C_{2v} and C_s symmetry species. These two terms are meant to distinguish modes that would be symmetric (IP), or antisymmetric (OP) with respect to a planar silacyclobutane ring (C_{2v} symmetry). An illustrative definition of IP/OP-Ring is given in Fig. 1.2 below. To further distinguish between the different antisymmetric stretching and antisymmetric deformation modes, the Greek letters "α" and "β" are used in this work; the exact definitions for these modes can be determined from the symmetry coordinates given in Table 1.2. A comparison of the updated vibrational assignments and the two previous assignments for DMSCBane is given in Table 1.4.

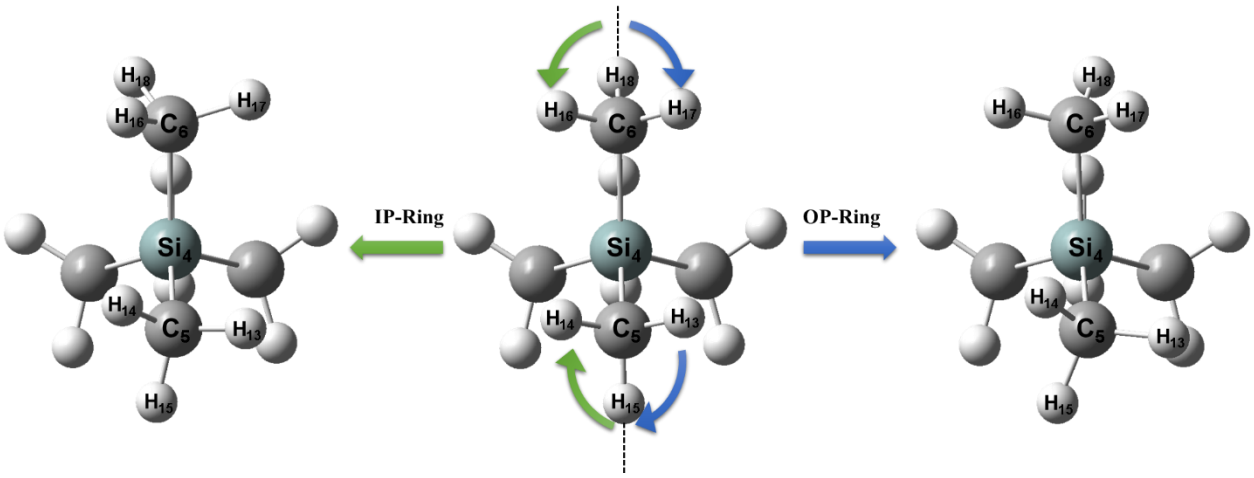

Figure 1.2. Illustration of the "IP-Ring" and "OP-Ring" nomenclature of vibrational modes. The example above uses the two CH_3 torsional modes and the local symmetry of each relative to the C-Si-C plane. The IP-Ring CH_3 torsion (left) starts from the equilibrium structure (middle) with the top methyl group rotating counterclockwise and the bottom methyl group rotating clockwise. The OP-Ring CH_3 torsion (right) shows both methyl groups rotating clockwise in the same direction. Alternatively, other authors may use "gear" and "anti-gear" instead of "IP-Ring" and "OP-Ring".

Table 1.4. Comparison of Vibrational Assignments[a] for DMSCBane.

Vib. Freq.	From Ref. [1]	Vib. Freq.	From Ref. [5]	Vib. Freq.	Current Work[b]
				2972	α-$(CH_3)_2$ antisymmetric stretch OP-Ring α-$(CH_3)_2$ antisymmetric stretch IP-Ring β-$(CH_3)_2$ antisymmetric stretch IP-Ring $(CH_2)_2$ antisymmetric stretch IP $(CH_2)_2$ antisymmetric stretch OP β-$(CH_3)_2$ antisymmetric stretch OP-Ring
2972	β-CH_2 antisymmetric stretch α-CH_2 in-plane antisymmetric stretch	2972	β-CH_2 antisymmetric stretch		
2966	CH_3 antisymmetric stretch CH_3 antisymmetric stretch CH_3 antisymmetric stretch	2966	CH_3 synphase stretch CH_3 asynphase stretch β-CH_2 asymmetric stretch	2966	CH_2 antisymmetric stretch
2962	CH_3 antisymmetric stretch	2962	β-CH_2 symmetric stretch		
2952	α-CH_2 out-of-plane antisymmetric stretch	2952	CH_3 asymmetric stretch asynphase		
2944	β-CH_2 symmetric stretch	2944	γ-CH_2 antisymmetric stretch		
2921	CH_3 symmetric stretch	2921	γ-CH_2 symmetric stretch	2921	$(CH_2)_2$ symmetric stretch IP $(CH_2)_2$ symmetric stretch OP
2911	CH_3 symmetric stretch	2911	β-CH_2 symmetric stretch	2911	CH_2 symmetric stretch
2901	α-CH_2 in-plane symmetric stretch	2901	CH_3 symmetric stretch synphase CH_3 symmetric stretch asynphase	*2900	$(CH_3)_2$ symmetric stretch IP-Ring $(CH_3)_2$ symmetric stretch OP-Ring
2887	α-CH_2 out-of-plane symmetric stretch	2887	CH_3 asymmetric stretch synphase		
				–	CH_2 deformation
1453	α-CH_2 in-plane deformation	1453	γ-CH_2 deformation	1453	$(CH_2)_2$ deformation IP β-$(CH_3)_2$ antisymmetric deformation IP-Ring α-$(CH_3)_2$ antisymmetric deformation IP-Ring
1425	β-CH_2 deformation	1425	β-CH_2 deformation	1425	α-$(CH_3)_2$ antisymmetric deformation OP-Ring β-$(CH_3)_2$ antisymmetric deformation OP-Ring
1418	CH_3 antisymmetric deformation	1418	CH_3 twist synphase	1418	$(CH_2)_2$ deformation OP
1410	CH_3 antisymmetric deformation	1410	CH_3 symmetric scissoring		
1399	α-CH_2 out-of-plane deformation	1399	CH_3 twist asynphase		
1390	CH_3 antisymmetric deformation	1390	CH_3 antisymmetric scissoring		
1364	CH_3 antisymmetric deformation	1364	β-CH_2 deformation		
1352	α-CH_2 out-of-plane wag				
				*1294	$(CH_3)_2$ symmetric deformation IP
				*1290	$(CH_3)_2$ symmetric deformation OP
1258	CH_3 symmetric deformation	1258	CH_3 wag synphase		
1254	CH_3 symmetric deformation	1254	CH_3 wag asynphase		
1246	α-CH_2 out-of-plane twist	1246	γ-CH_2 wag	1246	CH_2 wag
1215	β-CH_2 wag	1215	γ-CH_2 twist	1215	CH_2 twist
1189	α-CH_2 in-plane twist	1189	β-CH_2 twist	1189	$(CH_2)_2$ twist IP
1150	β-CH_2 twist	1150	β-CH_2 wag		
1127	α-CH_2 in-plane wag	1127	β-CH_2 wag	1127	$(CH_2)_2$ wag IP
				*1041	$(CH_2)_2$ wag OP

Table 1.4. --Continued.

Vib. Freq.	From Ref. [1]	Vib. Freq.	From Ref. [5]	Vib. Freq.	Current Work[b]
				*952	Ring C–C antisymmetric stretch
				*945	$(CH_2)_2$ twist OP
926	Ring C–C antisymmetric stretch	926	β-CH_2 twist	926	$(CH_2)_2$ rock IP
908	Ring C–C symmetric stretch	908	C–C stretch	908	Ring C–C symmetric stretch
886	Si-ring C symmetric stretch	886	Si–C stretch	886	$(CH_3)_2$ rock IP
877	CH_3 out-of-plane antisymmetric rock	877	C–C stretch		
841	CH_3 antisymmetric rock	841	CH_2 rock synphase	841	$(CH_3)_2$ wag IP-Ring
				813	CH_2 rock
807	α-CH_2 in-plane rock	807	Si–C–H symmetric scissoring		
781	CH_3 symmetric rock	781	γ-CH_2 rock	781	$(CH_3)_2$ wag OP-Ring
728	α-CH_2 out-of-plane rock	728	CH_2 rock asynphase	729	$(CH_3)_2$ rock OP
707	Si–C_2 antisymmetric stretch	707	Si–C_m asymmetric stretch	707	Ring Si–C symmetric stretch
701	CH_3 symmetric rock	701	Si–C_m symmetric stretch		
685	β-CH_2 rock	685	Si–C–H asymmetric scissoring	*686	Si–C antisymmetric stretch
648	Si-ring C antisymmetric stretch	648	Si–C stretch	648	Ring Si–C antisymmetric stretch
				*614	$(CH_2)_2$ rock OP
610	Si–C_2 symmetric stretch	610	β-CH_2 rock Si–C_m symmetric stretch	610	Si–C symmetric stretch
		–	β-CH_2 rock		
445	Ring deformation	445	Ring deformation	445	Ring deformation
255	Si–C_2 wag	255	Si–C_2 wag	*255	Ring puckering
229	Si–C_2 rock	229	Si–C_2 rock	228	Si–$(CH_3)_2$ wag
205	Si–C_2 deformation	205	Si–C_2 deformation		
				197	Si–$(CH_3)_2$ deformation
186	Si–C_2 twist	186	Si–C_2 twist		
177	CH_3 torsion	177	Asymmetric torsion	177	Si–$(CH_3)_2$ twist
172	CH_3 torsion	172	Symmetric torsion	172	CH_3 torsion IP-Ring
				*141	CH_3 torsion OP-Ring
				*131	Si–$(CH_3)_2$ rock
112	Ring puckering	112	Ring puckering		

[a] Listed assignments are primarily from the Raman and IR vapor-phase spectra.
[b] Frequencies with an asterisk indicate assignments are from the Raman or IR solid-phase spectra.

CH_2 & CH_3 Stretching Modes

There are 12 C–H stretching vibrations, which were predicted to occur within the 3000 – 2900 cm^{-1} region. The *ab initio* results indicate all vibrations have nonzero IR intensities and Raman activities. The 12 modes can be separated by species type: 8A' + 4A''. Because the C–H stretching frequencies are in close proximity to one another, there is significant band overlap in this region, which makes assignments for each C–H stretching vibration difficult, or not at all possible. In the occurrence of band overlap, with frequencies in too close proximity such that individual bands are not resolvable, then one or more vibrational modes were assigned to that particular vibrational band and frequency.

Comparing this work to the two previous vibrational analyses by Durig and Novikov (Table 1.4), there are many differences in assignments within the C–H stretching region. Therefore discussion about the comparison of each analysis will be limited to certain vibrational modes. However, all three analyses have assigned all six antisymmetric stretching modes at 2944 cm^{-1} and to fall between 3000 – 2992 cm^{-1}. The observed frequencies in the IR and Raman spectra of the gas, however, show only one resolvable band in this region at 2972 and 2974 cm^{-1} in the IR and Raman spectra of the gas, respectively. The peak is assigned primarily to the ν_3 mode, $(CH_2)_2$ antisymmetric stretch IP, based on predicted polarization and intensity/activity values, but because no other resolvable bands were observed in this region, all six modes (ν_1-ν_3 and ν_{29}-ν_{31}) were assigned to the same band. Conversely, the frequency at 2966 cm^{-1} was assigned to the CH_2 antisymmetric stretch (ν_4).

The five remaining symmetric C–H stretching vibrations were all observed between 2921 – 2900 cm^{-1} in the gas-phase Raman spectrum. The two $(CH_2)_2$ symmetric stretches (ν_5 and ν_{32}) were predicted to be within 1 cm^{-1} of one another, therefore both were assigned at 2921 cm^{-1}; however, the in-phase $(CH_2)_2$ symmetric stretching mode is primarily responsible for the observed band due a significantly higher predicted Raman activity, compared to the out-of-phase mode. While the CH_2 symmetric stretch (ν_6) was expected to have the highest IR intensity in this region, no band was observed near 2910 cm^{-1} in the gas-phase IR spectrum, but was observed and assigned at a higher frequency of 2916 cm^{-1} in both solid-phase spectra; additionally, this assignment was further confirmed in the gas-phase Raman spectra, which exhibited a strong polarized band at 2911 cm^{-1}. Similar to the two $(CH_2)_2$ symmetric modes, both $(CH_3)_2$ symmetric mode frequencies (ν_7 and ν_8) were predicted within 1 cm^{-1} of another. Because they have similar IR intensities and

Raman activities, both were assigned to a single band at 2901 cm^{-1} in the solid-phase Raman spectrum.

Additional bands of varying intensities below 2900 cm^{-1} were observed in multiple phases in the IR and Raman spectra, but were not attributed to fundamental frequencies of DMSCBane in this work. While overtones and combination bands may be responsible for the observed bands in this region, evidence of many unassigned bands in the 1750 – 1550 cm^{-1} and 1400 – 1300 cm^{-1} regions in the IR spectrum of the solid suggests the presence of one or more possible impurities. It is possible the impurities may not have been removed during purification, or the sample may have degraded over time. In any event, the presence of these bands may lead to incorrect assignments without additional assistance from a normal coordinate analysis and/or previous vibrational assignments of related molecules.

CH_2 & CH_3 Bending Modes

There are nine C–H deformation modes (6A' + 3A") pertaining to the CH_2 and CH_3 groups, which are predicted to appear in the 1475 – 1275 cm^{-1} region for DMSCBane. The CH_2 deformation (ν_9) was the highest predicted frequency at 1472 cm^{-1} for the C–H deformation modes, but was not observed in any IR or Raman spectrum, and is the only unassigned vibrational mode for DMSCBane. A medium intensity peak at 1453 cm^{-1} in the IR spectrum of the gas was assigned primarily to the α-$(CH_3)_2$ antisymmetric deformation IP-Ring (ν_{11}) mode. However, the $(CH_2)_2$ deformation IP (ν_{10}) and β-$(CH_3)_2$ antisymmetric deformation IP-Ring (ν_{33}) were also assigned to the same peak, as they both likely contribute to the intensity based on their predicted values at 1436 cm^{-1}. The α-$(CH_3)_2$ antisymmetric deformation OP-Ring (ν_{12}) and β-$(CH_3)_2$ antisymmetric deformation OP-Ring (ν_{34}) modes were both assigned to a single shoulder peak at 1420 cm^{-1} in the IR gas-phase spectrum and a very weak polarized band at 1425 cm^{-1} in the Raman gas-phase

spectrum, also observed in the IR gas phase spectrum. Because their predicted IR intensities were considerably low, this suggests both modes are present in the IR spectrum and were assigned to the same band, even though the ν_{34} mode primarily contributes to the intensity in the Raman spectra. A very weak band was observed at 1418 cm^{-1} for which the intensity data and polarization matches closely with the $(CH_2)_2$ deformation OP (ν_{35}) mode. The two remaining IP (ν_{13}) and OP (ν_{14}) symmetric $(CH_3)_2$ deformations were only observed in the IR spectrum of the solid at 1294 and 1290 cm^{-1}, respectively.

CH_2 & CH_3 Twisting, Wagging, and Rocking Modes

There are 6A' + 7A" modes corresponding to the twisting, wagging, and rocking vibrations of these two types of "C–H" groups, although the "twisting" motion of a methyl group is formally called its "torsion," and the two methyl torsional modes are discussed in a subsequent section. All six A' modes are predicted to have polarized Raman bands, whereas the seven A" modes are depolarized. It is also worth mentioning that both rocking and wagging vibrational modes have the same motion, but the directions are perpendicular to one another. Generally, the motion of the rocking modes is in the plane of symmetry (symmetric) and the wagging modes involve motion out of the symmetry plane (antisymmetric). The *ab initio* results predict all 13 modes excluding the torsions within the broad region of 1275 – 600 cm^{-1}. Additionally, all 13 modes are predicted to have non-zero IR intensities and Raman activities.

There are three CH_2 twisting modes consisting of A' + 2A" symmetry species. The CH_2 twist (ν_{37}) mode was assigned to a C-type band with medium intensity at 1215 cm^{-1} and is in agreement with the assignment made by Novikov et al. Similarly, the $(CH_2)_2$ twist IP mode (ν_{15}) was assigned to the band observed at 1189 cm^{-1} which is in agreement with both Durig and

Novikov. Lastly, the $(CH_2)_2$ twist OP (ν_{40}) mode was only observed as a very weak peak at 945 cm^{-1} in the IR spectrum of the solid.

There are five C–H wagging modes, pertaining to the CH_2 and CH_3 groups, sorted into the following: A' + 4A". The CH_2 wag (ν_{36}) mode was assigned to a very weak depolarized band at 1246 cm^{-1} in the gas-phase Raman spectrum due to its predicted frequency of 1267 cm^{-1} and being the only vibrational mode in this region. In a previous vibrational analysis of silacyclobutane derivatives,[2] the investigators noted that several silacyclobutanes have a band of moderate intensity in their IR spectra near 1130 cm^{-1} that corresponds to the $(CH_2)_2$ in-phase wagging mode. For DMSCBane, this characteristic frequency was observed as an A-type band at 1125 cm^{-1} in the gas-phase IR spectrum, and was assigned to the in-phase $(CH_2)_2$ wag (ν_{16}), which is also in agreement with the assignments made by Durig and Novikov. The out-of-phase $(CH_2)_2$ wag (ν_{38}) was only visible in the IR and Raman spectrum of the solid at 1046 and 1041 cm^{-1}, respectively. Durig et al. observed a very strong C-type band at 841 cm^{-1} which corresponds to the $(CH_3)_2$ wag IP-Ring mode (ν_{41}), and further confirmed by the very weak polarized line in the Raman spectrum. Similarly, the $(CH_3)_2$ wag OP-Ring (ν_{42}) vibration was assigned at 781 cm^{-1}.

There are five C–H rocking modes arising from the CH_2 and CH_3 groups, containing species: 4A' + A". The $(CH_2)_2$ rock IP (ν_{17}) mode was assigned at 926 cm^{-1} and was initially indicated as a C-type band; however, the IR gas-phase spectrum reveals the peak is next to a highly convoluted region and therefore the band contour may not be easily ascertained. The observed band of very strong intensity at 884 cm^{-1} in the IR spectrum was assigned to the $(CH_3)_2$ rock IP (ν_{18}) mode and is further verified by the polarized band at 886 cm^{-1} in the Raman spectrum. The CH_2 rock (ν_{20}) mode was observed and assigned to a very weak polarized band at 813 cm^{-1}. The shoulder observed at 731 cm^{-1} was assigned to the out-of-phase $(CH_3)_2$ rock (ν_{21}) mode. Lastly,

the $(CH_2)_2$ rock OP (ν_{44}) mode was only observed in the IR gas-phase spectrum at 613 cm^{-1} which was not assigned in previous studies.

Heavy-Atom Stretching Modes

There are six heavy atom (C–C or Si–C) stretching modes between 1000 – 600 cm^{-1} which can be sorted into: 4A' + 2A". Four of these modes correspond to the heavy atoms comprising the four-membered ring, and the remaining two modes to the methyl groups attached to the ring. The highest frequency ring mode, the ring C–C antisymmetric stretch (ν_{39}) was only observed at 952 cm^{-1} in the Raman spectrum of the solid, which had been unassigned in previous studies. The ring C–C symmetric stretch (ν_{18}), however, was observed in all phases and spectra and assigned to the band at 908 cm^{-1} in the Raman spectrum of the gas. Durig and Novikov originally assigned the band at 886 cm^{-1} to the (methyl) antisymmetric Si–C_2 stretch; however, this assignment has been updated to the ring Si–C symmetric stretch (ν_{22}), which was also observed in all phases in the IR and Raman spectra. The Si–C antisymmetric stretch (ν_{23}) was only observed in the condensed phases, and is assigned to the 686 cm^{-1} band in the Raman spectrum of the solid. The original assignment for the ring Si–C antisymmetric stretch at 648 cm^{-1} remained unchanged for the same ν_{43} mode in this study. Last, but not least, the Si–C symmetric stretch (ν_{24}) was assigned at 610 cm^{-1} and it also remained unchanged from its previous assignments.

Other Low-Frequency Modes

The remaining eight vibrational modes involve two ring bending modes, two methyl torsions, and four Si–$(CH_3)_2$ angle bending modes (twist, wag, rock, and deformation). The original assignment for the ring deformation (ν_{25}) at 445 cm^{-1} has remained unchanged from the initial investigation. The ring puckering mode, however, was predicted at, and reassigned to, a much higher frequency of 254 cm^{-1} in the IR spectrum of the solid, compared to the original

assignment of 112 cm^{-1}. This change in assignment of the ring puckering vibrational mode, assuming the assignment is in fact the correct one, would consequently impact the ring puckering potential function and perhaps the electron diffraction studies carried out by Novikov. The Si–$(CH_3)_2$ wagging (ν_{45}) was originally assigned at 255 cm^{-1}; however, normal coordinate analysis in this study indicated the ν_{45} mode should be reassigned to 228 cm^{-1} instead. Likewise, the Si–$(CH_3)_2$ deformation (ν_{27}) mode was updated and assigned to a lower (and previously unassigned) frequency of 197 cm^{-1}, compared to the original assignment of 205 cm^{-1}. The Si–$(CH_3)_2$ twist (ν_{46}) vibration was originally assigned at a higher frequency of 186 cm^{-1}; however, the predicted frequencies indicate the band at 177 cm^{-1} is in fact the ν_{45} mode, and not one of the methyl torsional modes, as was previously assigned to it. In order to determine the barrier(s) to internal rotation of the methyl groups, it is important to have correct assignments for the two torsional fundamental transitions. The previous vibrational studies on DMSCBane assigned the two torsional modes at 177 and 172 cm^{-1} respectively. The CH_3 torsion IP-Ring (ν_{47}) mode was moved to a slightly lower assignment of 172 cm^{-1}, compared to the previous assignment at 177 cm^{-1}. The CH_3 torsion OP-Ring (ν_{48}) mode was previously assigned at 172 cm^{-1}, and has been reassigned in this work to a band in the solid phase spectrum at 141 cm^{-1}. This assignment for the ν_{48} mode appears to be the correct assignment as determined from the microwave study[6] of DMSCBane. Lastly, the lowest predicted vibrational frequency was, in fact, the Si–$(CH_3)_2$ rock (ν_{28}) mode, predicted at 134 cm^{-1}, and assigned to a band observed at 131 cm^{-1} in the Raman spectrum of the solid phase, compared to the original assignment at 229 cm^{-1}.

Structural Parameters

One of the first structural studies[3] of DMSCBane was carried out using gas-phase electron diffraction (ED), where Shen et al. determined the first experimental structural parameters using a "static model" approach, while utilizing valence force fields from a vibrational study on silacyclopentanes.[4] This model, however, provided limited information as it did not take into account the large-amplitude ring-puckering vibrational mode, but did indicate that the ring was puckered and not planar. A more recent ED study[5] determined the structural parameters of DMSCBane using a "dynamic model" approach, which accounted for the large-amplitude ring-puckering vibrational mode. With the aid of *ab initio* calculations, Novikov et al. reanalyzed the original ED data collected by Shen and coworkers, obtaining more accurate values with lower uncertainties. Several years later, structural parameters were determined in a microwave (MW) study[6] of DMSCBane, where Hirota and coworkers were able to determine seven r_s values for the following heavy-atom parameters: three bond distances, three bond angles, and the ring puckering angle. In their study, Hirota et al. provided two sets of structural parameters using different assumptions for the b coordinate of the Si atom, since its position lies close to the a-inertial axis: Set I assumed the sign of the b coordinate was negative, whereas Set II assumed a positive value. The two sets yielded slightly different results, but are still consistent with the ED results by Novikov and coworkers. The lack of robust structural information obtained from spectroscopic methods makes for a compelling rationale to perform an updated structural study on DMSCBane and to compare it to existing structural data.

Good structural parameters have been found for hydrocarbons, and many substituted ones, which can be determined by adjusting the structural parameters obtained from the *ab initio* MP2(full)/6-311+G(d,p) calculation to fit the rotational constants obtained from microwave

experimental data using a computer program "A&M" (*Ab initio* and Microwave) developed[16] in our laboratory. In order to reduce the number of independent variables, the structural parameters are separated into sets according to their types, where bond distances/angles in the same set keep their relative ratio difference in Angstroms or degrees. This assumption is based on the fact that errors from *ab initio* calculations are systematic. It has also been shown[17] for more than fifty carbon-hydrogen distances, that the *ab initio* MP2(full)/6-311+G(d,p) calculations predict the r_0 structural parameters to better than 0.002 Å, compared to the experimentally determined values from isolated C–H stretching frequencies, which were compared[18] to previously determined values from earlier microwave studies. Therefore, all of the carbon-hydrogen distances, r(C–H), have been taken from the MP2(full)/6-311+G(d,p) calculated values for DMSCBane.

The main advantages adjusted r_0 structural parameters have over other methods, such as ED and MW, is the symmetry restrictions (or lack thereof) which can be imposed and the number of parameters which can be determined. In the present work, it was assumed DMSCBane has C_s symmetry with the σ_H plane extending from the opposite vertex of the ring and passing through both methyl groups. Therefore, identical bond distances and angles, with respect to the σ_H plane, were placed into the same set in the A&M program as described above. While the dihedral angles of the methyl groups, as well as CH parameters determined from the MP2(full)/6-311+G(d,p) calculation were held constant, no other symmetry restrictions or assumptions were imposed on the molecule including: keeping all r(C–H) and ∠(H–C–H) values equivalent, assuming C_{3v} symmetry for the methyl groups, or that the axial and equatorial methyl groups have identical parameters.

The parameters of DMSCBane were separated into sets according to bond types, angles, and symmetry elements. Nine unique sets of bonds/angles were used to adjust the predicted *ab*

initio values to fit the 21 experimental rotational constants[6] corresponding to the seven isotopomers of DMSCBane. The experimental rotational constants used in the fitting include: the normal species, ^{29}Si, ^{30}Si, and ^{13}C at all four non-equivalent positions (with respect to C_s symmetry). The results of the adjusted r_0 structural parameters, predicted *ab initio* values, and the experimental structural parameters determined from ED[5] and MW[6] studies are provided in Table 1.5. It is believed that the C–C and C–Si bond distances should be accurate to ±0.003 Å, the C–H bond distances to 0.002 Å, and bond angles to 0.5°. The fit of the 21 experimentally determined rotational constants has very little variation, with differences of 0.917 MHz or less between the experimental and fitted rotational constants shown in Table 1.6. Therefore, it is believed that the adjusted r_0 structural parameters of DMSCBane are as accurate as similar methods, mainly MW and ED, which are used to obtain structural information in the gaseous phase.

Table 1.5. Structural parameters (Å and º), rotational constants (MHz) and dipole moments (Debye) for DMSCBane.

Parameter	Label	ED[a]	MW[b]		This Work	
		r_a, $\angle_\alpha$	r_s (set I)	r_s (set II)	*Ab Initio*[c]	Adjusted r_0
$r(C_1C_2)$	C–C	1.563(4)	1.560	1.560	1.561	1.574(3)
$r(C_1Si_4)$	C–Si	1.885(2)	1.877	1.882	1.893	1.887(3)
$r(Si_4C_5)$	Si–C_{eq}	1.872(2)	1.871	1.865	1.875	1.866(3)
$r(Si_4C_6)$	Si–C_{ax}	1.872(2)	1.871	1.865	1.876	1.874(3)
$r(C_1H_7)$	C–H_{ax}	1.115(3)			1.096	1.096(2)
$r(C_1H_8)$	C–H_{eq}	1.115(3)			1.092	1.092(2)
$r(C_2H_9)$	C–H_{eq}	1.115(3)			1.095	1.095(2)
$r(C_2H_{10})$	C–H_{ax}	1.115(3)			1.095	1.095(2)
$r(C_5H_{13})$	C_{eq}–H	1.115(3)			1.095	1.095(2)
$r(C_5H_{15})$	C_{eq}–H	1.115(3)			1.094	1.094(2)
$r(C_6H_{16})$	C_{ax}–H	1.115(3)			1.095	1.095(2)
$r(C_6H_{18})$	C_{ax}–H	1.115(3)			1.094	1.094(2)
$\angle(C_1Si_4C_3)$	C–Si–C	79.2(11)	79.2	79.9	78.2	79.3(5)
$\angle(C_2C_1Si_4)$	C–C–Si	86.8(6)			86.4	86.2(5)
$\angle(C_1C_2C_3)$	C–C–C	99.9(14)	100.1	100.1	99.9	99.8(5)
$\angle(C_1Si_4C_5)$	C–Si–C_{eq}	119.0			120.2	119.2(5)
$\angle(C_1Si_4C_6)$	C–Si–C_{ax}	113.6			112.5	113.4(5)
$\angle(C_5Si_4C_6)$	C_{eq}–Si–C_{ax}	109.9(47)	109.8	110.3	110.0	109.7(5)
$\angle(C_2C_1H_7)$	C–C–H_{ax}	107.2(32)			110.1	109.5(5)
$\angle(C_2C_1H_8)$	C–C–H_{eq}	112.1(32)			116.0	116.7(5)
$\angle(Si_4C_1H_7)$	Si–C–H_{ax}	108.6(32)			111.3	111.3(5)
$\angle(Si_4C_1H_8)$	Si–C–H_{eq}	118.2(32)			122.5	122.4(5)
$\angle(C_1C_2H_9)$	C–C–H_{eq}	114.6			114.8	115.0(5)
$\angle(C_1C_2H_{10})$	C–C–H_{ax}	109.9			109.8	109.6(5)
$\angle(Si_4C_5H_{13})$	Si–C_{eq}–H	113.9(17)			110.9	110.9(5)
$\angle(Si_4C_5H_{15})$	Si–C_{eq}–H	113.9(17)			111.2	111.2(5)
$\angle(Si_4C_6H_{16})$	Si–C_{ax}–H	113.9(17)			111.1	111.1(5)
$\angle(Si_4C_6H_{18})$	Si–C_{ax}–H	113.9(17)			111.1	111.1(5)
$\angle(H_7C_1H_8)$	H_{eq}–C–H_{ax}	118.8(32)			108.8	108.8(5)
$\angle(H_9C_2H_{10})$	H_{eq}–C–H_{ax}	107.6			107.6	107.6(5)
$\angle(H_{13}C_5H_{14})$	H–C_{eq}–H				107.7	107.7(5)
$\angle(H_{13}C_5H_{15})$	H–C_{eq}–H				108.0	107.0(5)
$\angle(H_{16}C_6H_{17})$	H–C_{ax}–H				107.7	107.7(5)
$\angle(H_{16}C_6H_{18})$	H–C_{ax}–H				107.9	107.9(5)
$\tau(C_1C_2C_3Si_4)$	C–C–C–Si				24.9	23.8(5)
$\tau(C_6Si_4C_5H_{15})$	C_{ax}–Si–C_{eq}–H				180.0	180.0
$\tau(C_5Si_4C_6H_{18})$	C_{eq}–Si–C_{ax}–H				180.0	180.0
Φ	Pucker. Angle	29.7(45)	28.6	30.3	32.7	31.5(5)
A			3776.907(15)		3789.792	3777.070
B			2297.3971(11)		2292.517	2297.472
C			2010.9084(11)		1999.476	2010.929
$\lvert\mu_a\rvert$					0.391	
$\lvert\mu_b\rvert$					0.000	
$\lvert\mu_c\rvert$					0.119	
$\lvert\mu_t\rvert$					0.409	

[a] Taken from Ref. [5]. The reported error is given as three times the standard deviation.
[b] Taken from Ref. [6].
[c] Calculated using MP2(full)/6-311+G(d,p).

Table 1.6. Comparison of Observed and Adjusted r_0 Rotational Constants (MHz).

Species		Observed[a]	Adjusted r_0	$\|\Delta\|$
Normal	*A*	3776.907	3777.070	0.163
	B	2297.397	2297.472	0.075
	C	2010.908	2010.929	0.021
^{29}Si	*A*	3776.762	3777.058	0.296
	B	2295.570	2295.623	0.053
	C	2009.512	2009.509	0.003
^{30}Si	*A*	3776.837	3777.047	0.210
	B	2293.780	2293.817	0.037
	C	2008.143	2008.122	0.021
$^{13}C_1$	*A*	3735.817	3734.900	0.917
	B	2272.322	2272.281	0.041
	C	2002.247	2002.153	0.094
$^{13}C_2$	*A*	3776.860	3776.941	0.081
	B	2258.583	2258.623	0.040
	C	1981.028	1981.068	0.040
$^{13}C_5$	*A*	3736.910	3737.389	0.479
	B	2261.883	2261.833	0.050
	C	1972.509	1972.574	0.065
$^{13}C_6$	*A*	3695.698	3695.459	0.239
	B	2285.188	2285.141	0.048
	C	1978.411	1978.324	0.087

[a] Data from Ref. [6].

Predicted values from the MP2(full)/6-311+G(d,p) calculation provided in Table 1.5 were reasonably accurate, compared to the adjusted r_0 parameters. In terms of adjustments in bond distances, differences between the *ab initio* and adjusted parameters were observed to be 0.013 Å or lower. The C–C bond had the largest change of 0.013 Å, followed by the exocyclic Si–C_{eq} bond change of 0.009 Å. Bond distances for other heavy atoms, such as the endocyclic C–Si bond and exocyclic Si–C_{ax} bond changed by 0.006 Å and 0.002 Å, respectively. The Si–C_{eq} and Si–C_{ax} bonds were put into different sets and thus were allowed to adjust independently of one another. The result was a change from 0.001 Å between the two bonds in the *ab initio* values to 0.008 Å for the adjusted parameters. For bond angles, the differences between the *ab initio* and adjusted r_0 parameters were 1.2° or lower. Because all the heavy atom bond distances/angles (which heavily influence the rotational constants of DMSCBane) were allowed to change, it was expected that the

largest differences (~1°) between the *ab initio* and the adjusted structural parameters were a result of modifications in heavy atom bonds/angles. Additionally, the predicted rotational constants for the normal species were modified only slightly with resulting changes between 5.0 – 12.7 MHz.

To test the accuracy of adjusted r_0 structural parameters, it is desirable to compare the values obtained in this method to the available structural data from DMSCBane. Based on the reported parameters, the discussion will be primarily limited to heavy atom bond distances/angles, so comparisons to the ED and MW results can be readily made. Table 1.5 indicates the adjusted r_0 structural parameters are in reasonable agreement with the existing experimental data.[5,6] One exception to this, however, is the C–C bond distance which was determined to be 1.574 Å compared to the experimental values of 1.563 Å and 1.560 Å. Additionally, the C–H bond distances are quite a bit different based on assumptions, or symmetry restrictions, investigators made in the ED study. For the methyl groups, the average exocyclic Si–C distance from the ED and MW studies was 1.872 Å and 1.871 Å respectively, whereas the adjusted parameters for Si–C_{eq} and Si–C_{ax} were 1.866 and 1.874 Å. Upon further inspection, the average of these two adjusted parameters is ~1.870 Å, which is in good agreement with the existing experimental data. The heavy atom angles between the experimental and adjusted r_0 structural parameters are in excellent agreement with one another, including the puckering angle of 31.5° in the silacyclobutane ring. Although the adjusted puckering angle is the largest value, compared to its value reported in other methods in Table 1.5, it falls within the range of 29.7° (± 4.5°) for the ED data. In conclusion, fitting the parameters from *ab initio* calculations to the experimental rotational constants has proven to be reasonably accurate, with many parameters on par with ED methods, but also informative because of the number of larger parameters presented in this work.

Conclusion

Quantum chemical calculations were performed on the C_s and C_{2v} conformations of DMSCBane using a number of basis sets via both DFT (B3LYP) and MP2 methods. The *ab initio* calculations indicate the C_s conformer is the only stable conformation of DMSCBane. With the aid of quantum chemical calculations, the vibrational assignments have been updated. Only one of the 48 possible vibrational modes was not observed in the vibrational spectra of this compound. Of particular importance, in the present work, are the updated assignments for the ring puckering mode and both methyl torsional modes. Previous mono-substituted[19–21] and di-substituted[22,23] silacylobutane vibrational studies by the Durig group predicted and assigned one or both ring puckering modes (of the two possible conformations) between 255 – 235 cm^{-1}; therefore, it is believed the assignment of the ring puckering mode at 254 cm^{-1} for DMSCBane is correct. The predicted structural parameters and previously determined experimental rotational constants were used to obtain adjusted r_0 structural parameters. The vibrational assignments and structural parameters, both predicted and adjusted, confirm the ring structure of DMSCBane is puckered with C_s symmetry

Future Work

It appears prudent to re-collect the vibrational spectra using modern instrumentation with a sample free of possible impurities, considering that the original data was reported over four decades ago. It is expected that using updated instrumentation would yield improved resolution and reveal more detail in otherwise convoluted regions in both the mid-IR and Raman spectra. Using the information provided in this work, others can update or confirm existing assignments in the spectra. Additionally, it would be of interest to conduct a variable temperature IR study on DMSCBane dissolved in a rare-gas solution to: 1) determine if the C_{2v} conformer is present in the

spectra; 2) and if so, then determine the enthalpy difference between the C_s and C_{2v} forms. Lastly, it would be of interest to conduct a far-IR study on DMSCBane to: 1) correctly identify the ring puckering mode, the two methyl torsional modes, and, possibly, their associated overtones; and 2) Use the information obtained from the vibrational overtones to determine the potential function governing the ring puckering as well as the barrier to internal rotation of the methyl groups.

CHAPTER 2

VIBRATIONAL ANALYSIS AND *AB INITIO* CALCULATIONS OF 1,1-DIMETHYL-1-SILACYCLOBUT-2-ENE

Introduction

1,1-Dimethyl-1-silacyclobut-2-ene (DMSCBene), an analog of DMSCBane (Chapter 1), has received little attention in the spectroscopic community. In fact, only one published study[24] exists which contains vibrational spectroscopic data, whereas no other information exists, computationally or experimentally, on the structure of DMSCBene. In this particular study, Korolev and coworkers attempted to trap 1,1-dimethyl-1-sila-1,3-butadiene from the vacuum pyrolysis of two different reactants: dimethyldiallylsilane and DMSCBene. In the study, Korolev et al. reported the infrared spectrum of DMSCBene in an argon (Ar-IR) matrix at 10 K. While a few preliminary assignments were reported, a vast number of frequencies were left unassigned. Therefore, in order to continue on with the vibrational and structural analysis of some analogs of silacyclobutane, the very first normal coordinate analysis was conducted on this cycloalkene molecule to assign as many transitions as possible in the reported Ar-IR spectrum[24] and the IR spectrum of the gas-phase molecule obtained using an infrared instrument coupled to a gas chromatograph (GC-IR) in a previous work[25] on gas-phase thermolysis reactions of organosilanes. Additionally, this study will be the first to report predicted structural parameters using *ab initio* calculations.

Computational Methods

The *ab initio* calculations for DMSCBene were performed in a similar manner to those for DMSCBane (Chapter 1), using the Gaussian 09® program.[7] The optimized geometry from the

MP2(full)/6-311+G(d,p) calculation is provided in Fig 2.1. Based on the normal coordinate analysis of cyclobutene[26] and a theoretical study of silacyclobutene,[27] both of which indicate a planar four-membered ring, quantum chemical calculations were performed for DMSCBene assuming C_s point group symmetry with a planar ring. Because no other stable conformations are expected to exist for DMSCBene, only two calculations were performed: MP2(full)/6-31G(d), for the normal coordinate analysis; and MP2(full)/6-311+G(d,p) for predicted structural parameters. The method of obtaining descriptions of the molecular motions for the normal coordinate analysis for DMSCBene was previously described in Chapter 1 under "Computational Methods" for 1,1-dimethyl-1-silacyclobutane (DMSCBane). Additionally, the same scaling factors from DMSCBane were also used for DMSCBene. A comparison between the observed and calculated wavenumbers, along with the calculated infrared intensities, Raman activities, depolarization ratios and potential energy distributions for DMSCBene are listed in Table 2.1.

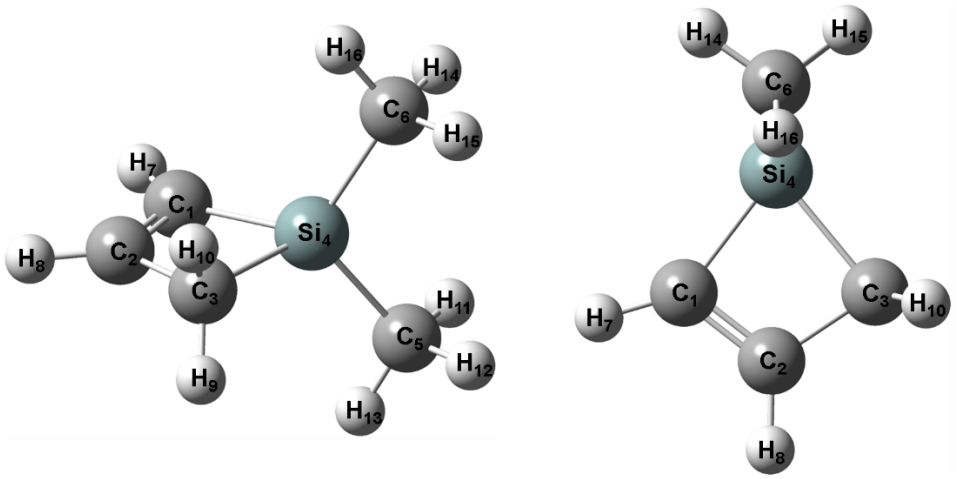

Figure 2.1. The C_s conformation of 1,1-dimethyl-1-silacyclobut-2-ene (DMSCBene) where the σ_h plane of symmetry passes through the ring including heavy atoms $C_1C_2C_3Si_4$. Note the images are of DMSCBene from two different perspectives to illustrate its symmetry.

Table 2.1. Observed and calculated frequencies (cm^{-1}) for 1,1-dimethyl-1-silacyclobut-2-ene (DSMCBene).

	Vib. No.	Approximate Descriptions[a]	*ab initio*[b]	Fixed Scaled[c]	IR Int.	Raman act.	dp Ratio	IR		P.E.D.[f]	Band Contours[g]		
								GC[d]	Ar[e]		A	B	C
A'	ν_1	=C–H symmetric stretcH	3257	3055	12.8	136.8	0.28	3065	3062	62 S_1, 38 S_4	37	0	63
	ν_2	α-$(CH_3)_2$ antisymmetric stretch IP	3201	3003	11.4	94.4	0.75	2961	2978	100 S_2	100	0	0
	ν_3	β-$(CH_3)_2$ antisymmetric stretch IP	3191	2994	16.4	132.1	0.75	2961	2978	100 S_3	0	0	100
	ν_4	=C–H antisymmetric stretch	3161	2966	44.8	200.2	0.32	2961	2969	62 S_4, 37 S_1	100	0	0
	ν_5	CH_2 symmetric stretch	3113	2920	15.2	110.4	0.21	2912	2921	99 S_5	1	0	99
	ν_6	$(CH_3)_2$ symmetric stretch IP	3099	2907	3.7	208.0	0.00	2912	2910	100 S_6	100	0	1
	ν_7	C=C stretch	1591	1522	7.4	5.1	0.11	1511	1518	81 S_7	24	0	76
	ν_8	β-$(CH_3)_2$ antisymmetric deformation IP	1530	1437	4.8	6.3	0.69	1404	1428	78 S_8, 11 S_{10}	12	0	88
	ν_9	α-$(CH_3)_2$ antisymmetric deformation IP	1526	1432	3.8	28.5	0.75	1404	1428	82 S_9, 11 S_8	57	0	43
	ν_{10}	CH_2 deformation	1513	1425	7.7	12.7	0.59	1404	1403	82 S_{10}	10	0	90
	ν_{11}	$(CH_3)_2$ symmetric deformation IP	1366	1289	17.5	0.7	0.72	–	1300	98 S_{11}	100	0	0
	ν_{12}	=C–H in-plane bend (wag)	1339	1275	15.8	1.6	0.57	1255	1248	77 S_{12}	94	0	6
	ν_{13}	CH_2 Wag	1197	1139	27.2	3.0	0.23	1122	1131	58 S_{13}, 15 S_{14}, 13 S_{15}	100	0	0
	ν_{14}	=C–H in-plane bend (scissor)	1082	1027	2.0	13.1	0.63	–	1028	68 S_{14}, 21 S_{13}	1	0	99
	ν_{15}	C–C stretch (ring)	992	946	31.1	8.9	0.17	931	936	63 S_{15}, 12 S_{21}	79	0	21
	ν_{16}	$(CH_3)_2$ rock IP	917	877	103.1	1.9	0.65	–	886	65 S_{16}, 10 S_{23}	97	0	4
	ν_{17}	$(CH_3)_2$ wag IP	876	837	59.8	0.4	0.47	838	835	66 S_{17}, 12 S_{22}	0	0	100
	ν_{18}	Ring deformation	828	799	1.3	3.9	0.27	–	789	32 S_{18}, 31 S_{21}	61	0	39
	ν_{19}	Si-$(CH_3)_2$ symmetric stretch	712	683	38.7	8.5	0.18	684	686	59 S_{19}, 27 S_{18}	99	0	1
	ν_{20}	Si-C_2 antisymmetric stretch (ring)	670	642	12.1	7.1	0.75	–	644	80 S_{20}, 11 S_{17}	1	0	99
	ν_{21}	Si-C_2 symmetric stretch (ring)	496	479	5.7	17.3	0.09	483	486	38 S_{21}, 31 S_{19}, 29 S_{18}	100	0	0
	ν_{22}	Si–$(CH_3)_2$ wag	232	230	0.8	0.6	0.75	–	–	75 S_{22}, 12 S_{24}	7	0	93
	ν_{23}	Si–$(CH_3)_2$ deformation	201	200	0.8	1.9	0.67	–	–	88 S_{23}	99	0	1
	ν_{24}	CH_3 torsion IP	171	171	0.0	0.0	0.75	–	–	88 S_{24}, 11 S_{22}	17	0	83

Table 2.1. --Continued.

	Vib. No.	Approximate Descriptions[a]	*ab initio*[b]	Fixed Scaled[c]	IR Int.	Raman act.	dp Ratio	IR		P.E.D.[f]	Band Contours[g]		
								GC[d]	Ar[e]		A	B	C
A"	ν_{25}	α-$(CH_3)_2$ antisymmetric stretch OP	3201	3002	5.2	41.0	0.75	2961	3021	100 S_{25}	0	100	0
	ν_{26}	β-$(CH_3)_2$ antisymmetric stretch OP	3190	2992	0.0	10.2	0.75	–	2978	100 S_{26}	0	100	0
	ν_{27}	CH_2 antisymmetric stretch	3168	2972	9.5	79.8	0.75	2961	2969	100 S_{27}	0	100	0
	ν_{28}	$(CH_3)_2$ symmetric stretch OP	3099	2907	1.9	0.4	0.75	2912	2910	100 S_{28}	0	100	0
	ν_{29}	α-$(CH_3)_2$ antisymmetric deformation OP	1518	1424	2.9	2.5	0.75	1404	1403	88 S_{29}	0	100	0
	ν_{30}	β-$(CH_3)_2$ antisymmetric deformation OP	1515	1421	0.1	23.1	0.75	–	1403	88 S_{30}	0	100	0
	ν_{31}	$(CH_3)_2$ symmetric deformation OP	1360	1283	42.5	1.7	0.75	1255	1254	97 S_{31}	0	100	0
	ν_{32}	CH_2 twist	1130	1082	15.8	1.5	0.75	1072	1074	62 S_{32}, 18 S_{38}	0	100	0
	ν_{33}	=C–H out-of-plane bend (twist)	981	976	0.3	1.2	0.75	–	–	91 S_{33}	0	100	0
	ν_{34}	CH_2 rock	892	868	22.5	3.4	0.75	838	846	18 S_{34}, 23 S_{32}, 17 S_{38}	0	100	0
	ν_{35}	$(CH_3)_2$ rock OP	820	790	113.1	2.7	0.75	768	769	31 S_{35}, 25 S_{34}, 17 S_{37}, 15 S_{36}	0	100	0
	ν_{36}	$(CH_3)_2$ wag OP	764	732	11.8	5.9	0.75	768	707	72 S_{36}, 16 S_{34}	0	100	0
	ν_{37}	Si–$(CH_3)_2$ antisymmetric stretch	718	681	11.1	7.0	0.75	684	686	59 S_{37}, 38 S_{35}	0	100	0
	ν_{38}	=C–H out-of-plane bend (rock)	648	628	23.2	1.6	0.75	632	618	45 S_{38}, 28 S_{34}, 11 S_{37}, 10 S_{35}	0	100	0
	ν_{39}	Ring puckering	347	345	3.8	1.4	0.75	–	–	49 S_{39}, 29 S_{42}, 12 S_{38}	0	100	0
	ν_{40}	Si–$(CH_3)_2$ twist	191	190	0.1	3.1	0.75	–	–	79 S_{40}, 11 S_{41}	0	100	0
	ν_{41}	CH_3 torsion OP	154	154	0.0	0.6	0.75	–	–	88 S_{41}	0	100	0
	ν_{42}	Si–$(CH_3)_2$ rock	116	116	0.0	3.8	0.75	–	–	58 S_{42}, 38 S_{39}	0	100	0

[a] IP & OP refer to vibrational modes that are "in-phase" and "out-of-phase" with respect to the σ_h plane.
[b] MP2(full)/6-31G(d) *ab initio* calculations, scaled frequencies, infrared intensities (km/mol), Raman activities (Å^4/amu), depolarization ratios and potential energy distributions (P.E.D.s).
[c] MP2(full)/6-31G(d) fixed scaled frequencies with scaling factors of 0.88 for CH stretches and CH deformations, 1.0 for torsions and heavy atom bends, and 0.90 for all other modes.
[d] Assignments are made for the GC-IR spectrum, which was provided by K. V. Kalasinsky and K. G. Whitehead from their previous work in Ref. [25].
[e] Assignments taken from Ref. [24] with DMSCBene trapped in an argon matrix at 10 K.
[f] Contributions less than 10% are omitted.
[g] A, B and C values in the last three columns are percentage infrared band contours.

The predicted scaled frequencies from the MP2(full)/6-31G(d) calculations were used together with a Lorentzian function to obtain a simulated IR spectrum of DMSCBene. IR intensities were obtained based on the derivatives of the dipole moment components with respect to Cartesian coordinates. These derivatives were transformed with respect to normal coordinates by $(\partial\mu_u/\partial Q_i) = \sum_j (\partial\mu_u/\partial X_j)L_{ij}$, where Q_i is the i^{th} normal coordinate, X_j is the j^{th} Cartesian displacement coordinate, and L_{ij} is the transformation matrix between the Cartesian displacement coordinates and the normal coordinates. The infrared intensities were then calculated by $[(N\pi)/(3c^2)]\ [(\partial\mu_x/\partial Q_i)^2 + (\partial\mu_y/\partial Q_i)^2 + (\partial\mu_z/\partial Q_i)^2]$. A comparison of experimental and simulated infrared spectra of DMSCBene is shown in Fig 2.2. The predicted spectrum is in good agreement with the experimental spectrum, which shows the utility of the scaled predicted frequencies and predicted intensities for supporting the vibrational assignment. While a Raman spectrum has yet to be collected for DMSCBene, a simulated Raman spectrum (Fig 2.3) has been provided for future studies. The Raman scattering cross sections and calculated wavenumbers obtained from the Gaussian 09® program were used together with a Lorentzian function to obtain the simulated Raman spectrum.

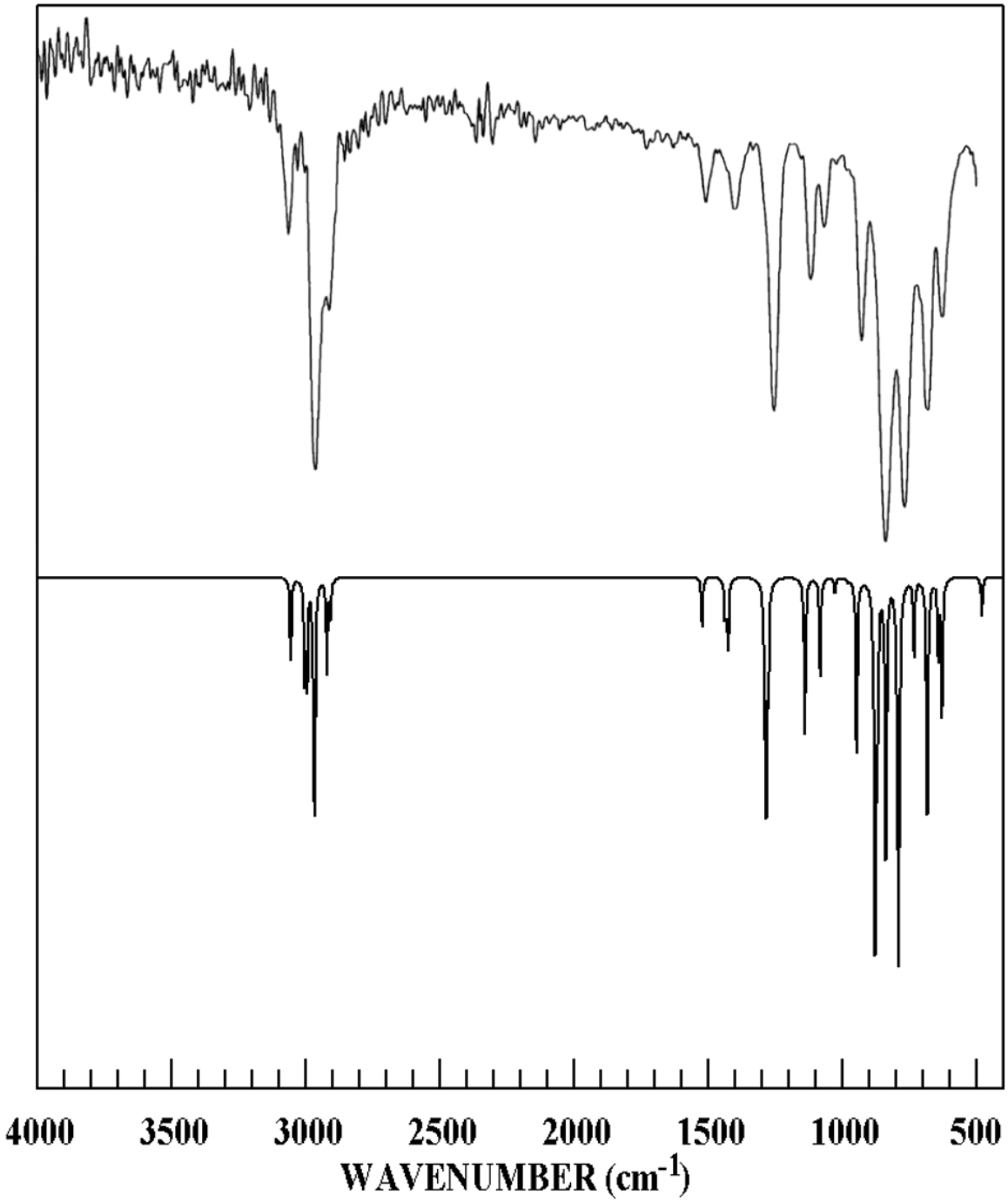

Figure 2.2. Comparison of experimental (top) and predicted (bottom) infrared spectra for DMSCBene.

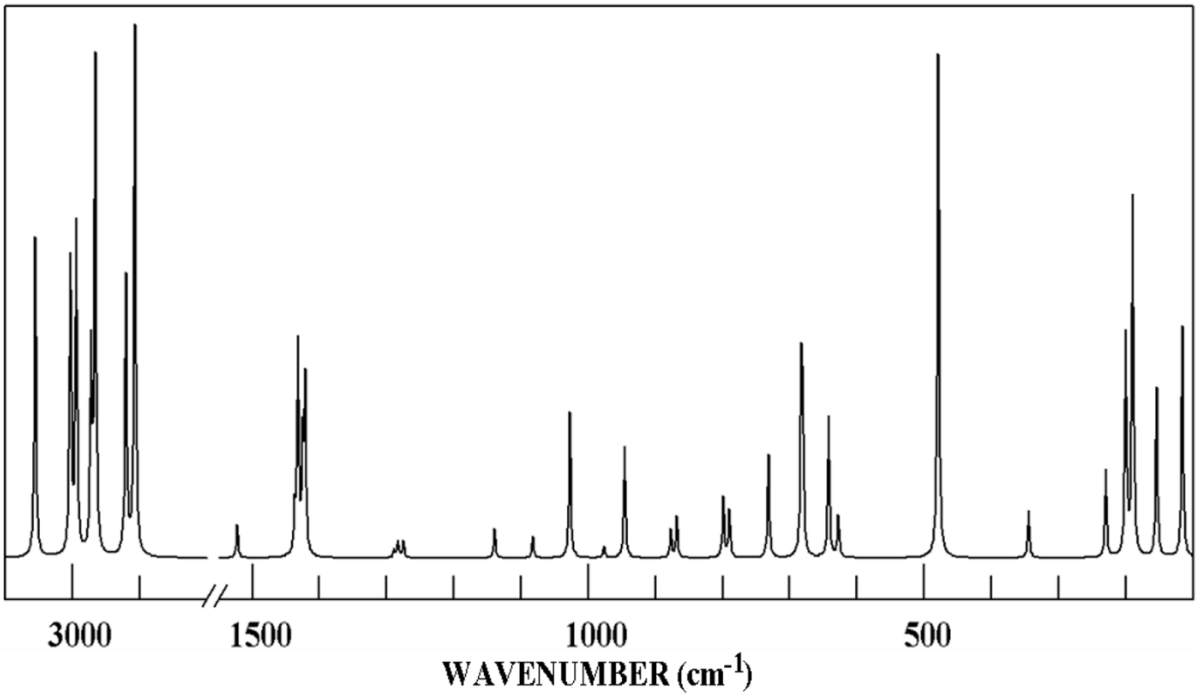

Figure 2.3. Predicted Raman spectrum of DMSCBene.

Vibrational Analysis

DMSCBene has 42 vibrational modes, which can be sorted into the following symmetry species: 24 A' + 18 A". In the Raman spectrum, the *ab initio* results indicate the A' species vibrational modes exhibit depolarization values between 0 and 0.75, whereas all modes in the A" species have values of 0.75. In the IR spectrum of DMSCBene in the vapor phase, the A' vibrations are predicted to exhibit A/C hybrid IR band contours, and the A" species only B-type band contours. Because the reported GC-IR spectrum (4000 – 450 cm^{-1}) in this work is of low resolution (8 cm^{-1}), no band contour information could be obtained experimentally to aid in assigning the spectrum. Therefore, assignments will rely exclusively on the normal coordinate analysis using predicted fixed scaled frequencies and IR intensities (See Table 2.2). The updated assignments

from this work have been compared in Table 2.2 to the original mid-IR (3100 – 450 cm^{-1}) assignments[24] by Korolev et al. with the compound trapped in a solid argon matrix (IR-Ar) at 10 – 15 K.

Similar to 1,1-dimethyl-1-silacyclobutane (DMSCBane), there were situations where more than one vibrational mode was assigned to a single band when the predicted frequencies for vibrational modes were in close proximity and the bands were unresolvable in the IR spectra. For purposes of clarification, some methyl group, $(CH_3)_2$, vibrational mode descriptions contain "IP" or "OP". The IP/OP terms indicate normal modes of vibration that are in-phase (symmetric) or out-of-phase (antisymmetric) with the σ_H plane passing through the ring atoms (see Fig 2.1 for molecular structure). To further distinguish between the different antisymmetric $(CH_3)_2$ stretching and antisymmetric deformation modes, the Greek letters "α" and "β" are used in this work; the exact definitions for these modes can be determined from the symmetry coordinates provided in Table 2.3. All assignments discussed henceforth refer to the Ar-IR spectrum, unless otherwise specified.

Table 2.2. Updated DMSCBene vibrational assignments from original argon-matrix IR data.[a]

Vib. No.[a]	Updated Assignments	Vib. Freq. (cm^{-1})	Previous Assignments[b]
ν_1	=C–H symmetric stretch	3062	=C–H stretches
ν_{25}	α-$(CH_3)_2$ antisymmetric stretch OP	3021	
ν_2	α-$(CH_3)_2$ antisymmetric stretch IP	2978	CH_2 & CH_3 stretches
ν_3	β-$(CH_3)_2$ antisymmetric stretch IP		
ν_{26}	β-$(CH_3)_2$ antisymmetric stretch OP		
ν_{27}	CH_2 antisymmetric stretch	2969	
ν_4	=C–H antisymmetric stretch		
		2955	
ν_5	CH_2 symmetric stretch	2921	
ν_6	$(CH_3)_2$ symmetric stretch IP	2910	
ν_{28}	$(CH_3)_2$ symmetric stretch OP		
ν_7	C=C stretch	1518	C=C stretch
ν_8	β-$(CH_3)_2$ antisymmetric deformation IP	1428	CH_2 & CH_3 bends
ν_9	α-$(CH_3)_2$ antisymmetric deformation IP		
ν_{10}	CH_2 deformation	1403	
ν_{29}	α-$(CH_3)_2$ antisymmetric deformation OP		
ν_{30}	β-$(CH_3)_2$ antisymmetric deformation OP		
ν_{11}	$(CH_3)_2$ symmetric deformation IP	1300-1270	=C–H bend
ν_{31}	$(CH_3)_2$ symmetric deformation OP	1254	CH_3 & Si–$(CH_3)_2$ bends
ν_{12}	=C–H in-plane bend (wag)	1248	
ν_{13}	CH_2 wag	1131	CH_2 twist & wag
		1123	
		1118	C–C stretch
ν_{32}	CH_2 twist	1074	CH_2 rock
ν_{14}	=C–H in-plane bend (scissor)	1028	
ν_{15}	C–C stretch (ring)	936	Si–$(CH_3)_2$ bend
ν_{16}	$(CH_3)_2$ rock IP	886	
ν_{34}	CH_2 rock	846	
ν_{17}	$(CH_3)_2$ wag IP	835	
ν_{18}	Ring deformation	789	
ν_{35}	$(CH_3)_2$ rock OP	769	
ν_{36}	$(CH_3)_2$ wag OP	707	Si–C stretches
ν_{37}	Si–$(CH_3)_2$ antisymmetric stretch	686	
ν_{19}	Si-$(CH_3)_2$ symmetric stretch		
ν_{20}	Si-C_2 antisymmetric stretch (ring)	644	C=C–H rock
ν_{38}	=C–H out-of-plane bend (rock)	618	
ν_{21}	Si-C_2 symmetric stretch (ring)	486	

[a] Modes are listed in descending order according to the fixed scaled frequencies from Table 2.1.
[b] Frequencies and assignments taken from Ref. [24].

Table 2.3. Symmetry coordinates of 1,1-dimethyl-1-silacyclobut-2-ene (DSMCBene).

	Description	Symmetry Coordinate[a,b]
A′	=C–H symmetric stretch	$\mathbf{S}_1 = \mathbf{r}_{1,7} + \mathbf{r}_{2,8}$
	α-$(CH_3)_2$ antisymmetric stretch IP	$\mathbf{S}_2 = 2\mathbf{r}_{6,16} - \mathbf{r}_{6,15} - \mathbf{r}_{6,14} + 2\mathbf{r}_{5,13} - \mathbf{r}_{5,11} - \mathbf{r}_{5,12}$
	β-$(CH_3)_2$ antisymmetric stretch IP	$\mathbf{S}_3 = \mathbf{r}_{6,15} - \mathbf{r}_{6,14} - \mathbf{r}_{5,11} + \mathbf{r}_{5,12}$
	=C–H antisymmetric stretch	$\mathbf{S}_4 = \mathbf{r}_{1,7} - \mathbf{r}_{2,8}$
	CH_2 symmetric stretch	$\mathbf{S}_5 = \mathbf{r}_{3,9} + \mathbf{r}_{3,10}$
	$(CH_3)_2$ symmetric stretch IP	$\mathbf{S}_6 = \mathbf{r}_{6,15} + \mathbf{r}_{6,14} + \mathbf{r}_{6,16} + \mathbf{r}_{5,11} + \mathbf{r}_{5,12} + \mathbf{r}_{5,13}$
	C=C stretch	$\mathbf{S}_7 = \mathbf{R}_{1,2}$
	β-$(CH_3)_2$ antisymmetric deformation IP	$\mathbf{S}_8 = \boldsymbol{\alpha}_{15,6,16} - \boldsymbol{\alpha}_{14,6,16} - \boldsymbol{\alpha}_{11,5,13} + \boldsymbol{\alpha}_{12,5,13}$
	α-$(CH_3)_2$ antisymmetric deformation IP	$\mathbf{S}_9 = 2\boldsymbol{\alpha}_{15,6,14} - \boldsymbol{\alpha}_{15,6,16} - \boldsymbol{\alpha}_{14,6,16} + 2\boldsymbol{\alpha}_{11,5,12} - \boldsymbol{\alpha}_{11,5,13} - \boldsymbol{\alpha}_{12,5,13}$
	CH_2 deformation	$\mathbf{S}_{10} = 4\boldsymbol{\alpha}_{9,3,10} - \boldsymbol{\phi}_{4,3,9} - \boldsymbol{\phi}_{4,3,10} - \boldsymbol{\phi}_{2,3,9} - \boldsymbol{\phi}_{2,3,10}$
	$(CH_3)_2$ symmetric deformation IP	$\mathbf{S}_{11} = \boldsymbol{\alpha}_{15,6,14} + \boldsymbol{\alpha}_{15,6,16} + \boldsymbol{\alpha}_{14,6,16} + \boldsymbol{\alpha}_{11,5,12} + \boldsymbol{\alpha}_{11,5,13} + \boldsymbol{\alpha}_{12,5,13} - \boldsymbol{\theta}_{4,6,15} - \boldsymbol{\theta}_{4,6,14} - \boldsymbol{\theta}_{4,6,16} - \boldsymbol{\theta}_{4,5,11} - \boldsymbol{\theta}_{4,5,12} - \boldsymbol{\theta}_{4,5,13}$
	=C–H in-plane bend (wag)	$\mathbf{S}_{12} = \boldsymbol{\sigma}_{4,1,7} - \boldsymbol{\sigma}_{2,1,7} - \boldsymbol{\sigma}_{3,2,8} + \boldsymbol{\sigma}_{1,2,8}$
	CH_2 wag	$\mathbf{S}_{13} = \boldsymbol{\phi}_{4,3,9} + \boldsymbol{\phi}_{4,3,10} - \boldsymbol{\phi}_{2,3,9} - \boldsymbol{\phi}_{2,3,10}$
	=C–H in-plane bend (scissor)	$\mathbf{S}_{14} = \boldsymbol{\sigma}_{4,1,7} - \boldsymbol{\sigma}_{2,1,7} + \boldsymbol{\sigma}_{3,2,8} - \boldsymbol{\sigma}_{1,2,8}$
	C–C stretch (ring)	$\mathbf{S}_{15} = \mathbf{R}_{2,3}$
	$(CH_3)_2$ rock IP	$\mathbf{S}_{16} = 2\boldsymbol{\theta}_{4,6,16} - \boldsymbol{\theta}_{4,6,15} - \boldsymbol{\theta}_{4,6,14} + 2\boldsymbol{\theta}_{4,5,13} - \boldsymbol{\theta}_{4,5,11} - \boldsymbol{\theta}_{4,5,12}$
	$(CH_3)_2$ wag IP	$\mathbf{S}_{17} = \boldsymbol{\theta}_{4,6,15} - \boldsymbol{\theta}_{4,6,14} - \boldsymbol{\theta}_{4,5,11} + \boldsymbol{\theta}_{4,5,12}$
	Ring deformation	$\mathbf{S}_{18} = \boldsymbol{\Delta}_{3,4,1} - \boldsymbol{\Delta}_{4,3,2} - \boldsymbol{\Delta}_{4,1,2} + \boldsymbol{\Delta}_{3,2,1}$
	Si-$(CH_3)_2$ symmetric stretch	$\mathbf{S}_{19} = \mathbf{R}_{4,6} + \mathbf{R}_{4,5}$
	Si-C_2 antisymmetric stretch (ring)	$\mathbf{S}_{20} = \mathbf{R}_{4,3} - \mathbf{R}_{4,1}$
	Si-C_2 symmetric stretch (ring)	$\mathbf{S}_{21} = \mathbf{R}_{4,3} + \mathbf{R}_{4,1}$
	Si–$(CH_3)_2$ wag	$\mathbf{S}_{22} = \boldsymbol{\lambda}_{6,4,1} - \boldsymbol{\lambda}_{6,4,3} + \boldsymbol{\lambda}_{5,4,1} - \boldsymbol{\lambda}_{5,4,3}$
	Si–$(CH_3)_2$ deformation	$\mathbf{S}_{23} = 4\boldsymbol{\lambda}_{6,4,5} - \boldsymbol{\lambda}_{6,4,1} - \boldsymbol{\lambda}_{6,4,3} - \boldsymbol{\lambda}_{5,4,1} - \boldsymbol{\lambda}_{5,4,3}$
	CH_3 torsion IP	$\mathbf{S}_{24} = \boldsymbol{\tau}_{16,6,4,5} - \boldsymbol{\tau}_{13,5,4,6}$
A″	α-$(CH_3)_2$ antisymmetric stretch OP	$\mathbf{S}_{25} = 2\mathbf{r}_{6,16} - \mathbf{r}_{6,15} - \mathbf{r}_{6,14} - 2\mathbf{r}_{5,13} + \mathbf{r}_{5,11} + \mathbf{r}_{5,12}$
	β-$(CH_3)_2$ antisymmetric stretch OP	$\mathbf{S}_{26} = \mathbf{r}_{6,15} - \mathbf{r}_{6,14} + \mathbf{r}_{5,11} - \mathbf{r}_{5,12}$
	CH_2 antisymmetric stretch	$\mathbf{S}_{27} = \mathbf{r}_{3,9} - \mathbf{r}_{3,10}$
	$(CH_3)_2$ symmetric stretch OP	$\mathbf{S}_{28} = \mathbf{r}_{6,15} + \mathbf{r}_{6,14} + \mathbf{r}_{6,16} - \mathbf{r}_{5,11} - \mathbf{r}_{5,12} - \mathbf{r}_{5,13}$
	α-$(CH_3)_2$ antisymmetric deformation OP	$\mathbf{S}_{29} = 2\boldsymbol{\alpha}_{15,6,14} - \boldsymbol{\alpha}_{15,6,16} - \boldsymbol{\alpha}_{14,6,16} - 2\boldsymbol{\alpha}_{11,5,12} + \boldsymbol{\alpha}_{11,5,13} + \boldsymbol{\alpha}_{12,5,13}$
	β-$(CH_3)_2$ antisymmetric deformation OP	$\mathbf{S}_{30} = \boldsymbol{\alpha}_{15,6,16} - \boldsymbol{\alpha}_{14,6,16} + \boldsymbol{\alpha}_{11,5,13} - \boldsymbol{\alpha}_{12,5,13}$
	$(CH_3)_2$ symmetric deformation OP	$\mathbf{S}_{31} = \boldsymbol{\alpha}_{15,6,14} + \boldsymbol{\alpha}_{15,6,16} + \boldsymbol{\alpha}_{14,6,16} - \boldsymbol{\alpha}_{11,5,12} - \boldsymbol{\alpha}_{11,5,13} - \boldsymbol{\alpha}_{12,5,13} - \boldsymbol{\theta}_{4,6,15} - \boldsymbol{\theta}_{4,6,14} - \boldsymbol{\theta}_{4,6,16} + \boldsymbol{\theta}_{4,5,11} + \boldsymbol{\theta}_{4,5,12} + \boldsymbol{\theta}_{4,5,13}$
	CH_2 twist	$\mathbf{S}_{32} = \boldsymbol{\phi}_{4,3,9} - \boldsymbol{\phi}_{4,3,10} - \boldsymbol{\phi}_{2,3,9} + \boldsymbol{\phi}_{2,3,10}$
	=C–H out-of-plane bend (twist)	$\mathbf{S}_{33} = \boldsymbol{\tau}_{7,1,2,8}$
	CH_2 rock	$\mathbf{S}_{34} = \boldsymbol{\phi}_{4,3,9} - \boldsymbol{\phi}_{4,3,10} + \boldsymbol{\phi}_{2,3,9} - \boldsymbol{\phi}_{2,3,10}$
	$(CH_3)_2$ rock OP	$\mathbf{S}_{35} = 2\boldsymbol{\theta}_{4,6,16} - \boldsymbol{\theta}_{4,6,15} - \boldsymbol{\theta}_{4,6,14} - 2\boldsymbol{\theta}_{4,5,13} + \boldsymbol{\theta}_{4,5,11} + \boldsymbol{\theta}_{4,5,12}$
	$(CH_3)_2$ wag OP	$\mathbf{S}_{36} = \boldsymbol{\theta}_{4,6,15} - \boldsymbol{\theta}_{4,6,14} + \boldsymbol{\theta}_{4,5,11} - \boldsymbol{\theta}_{4,5,12}$
	Si–$(CH_3)_2$ antisymmetric stretch	$\mathbf{S}_{37} = \mathbf{R}_{4,6} - \mathbf{R}_{4,5}$
	=C–H out-of-plane bend (rock)	$\mathbf{S}_{38} = \boldsymbol{\tau}_{8,2,1,4} - \boldsymbol{\tau}_{7,1,2,3}$
	Ring puckering	$\mathbf{S}_{39} = \boldsymbol{\tau}_{3,2,1,4} - \boldsymbol{\tau}_{2,1,4,3}$
	Si–$(CH_3)_2$ twist	$\mathbf{S}_{40} = \boldsymbol{\lambda}_{6,4,1} - \boldsymbol{\lambda}_{6,4,3} - \boldsymbol{\lambda}_{5,4,1} + \boldsymbol{\lambda}_{5,4,3}$
	CH_3 torsion OP	$\mathbf{S}_{41} = \boldsymbol{\tau}_{16,6,4,5} + \boldsymbol{\tau}_{13,5,4,6}$
	Si–$(CH_3)_2$ rock	$\mathbf{S}_{42} = \boldsymbol{\lambda}_{6,4,1} + \boldsymbol{\lambda}_{6,4,3} - \boldsymbol{\lambda}_{5,4,1} - \boldsymbol{\lambda}_{5,4,3}$

[a] Not normalized.

[b] The subscripted numbers of the internal coordinates correspond to the atom numbering in Fig.1 of DMSCBene.

=C–H, CH_2, & CH_3 Stretching Modes

There are 10 vibrational "C–H" stretching modes, the majority of which were assigned between 3100 – 2900 cm^{-1}. The 10 modes are assorted into the following groups (and symmetry species): =C–H (2A'), CH_2 (A' + A"), and CH_3 (3A' + 3A"). The GC-IR spectrum has limited resolution near ~3000 cm^{-1}, but there are two bands at 3063 and 2961 cm^{-1} and a shoulder band at

approximately 2912 cm^{-1}. The highest frequency vibrational mode, the =C–H symmetric stretch (ν_1), is assigned at the isolated peak of medium-weak intensity at 3065 cm^{-1} in the GC-IR spectra and is supported by the assignment at 3062 cm^{-1} in the Ar-IR spectrum. The band at 2961 cm^{-1} was assigned to five modes: ν_2-ν_4, ν_{25}, and ν_{27}, with the main assignment attributed to the =C–H antisymmetric Stretch (ν_4), since it has the highest predicted IR intensity of all the modes in this particular region. The Ar-IR data, however, reveals two strong peaks in the region with the ν_2,ν_3, and ν_{25} modes assigned to 2978 cm^{-1}, and the ν_4 and ν_{27} modes assigned to 2969 cm^{-1}. The CH_2 symmetric stretch (ν_5), $(CH_3)_2$ symmetric stretch IP (ν_6), and $(CH_3)_2$ antisymmetric stretch OP (ν_{28}) modes were all assigned to the shoulder band in the GC-IR spectrum at 2912 cm^{-1}. In the Ar-IR spectrum, the bands were split, with the ν_5 mode assigned to a single medium intensity band at 2921 cm^{-1}, and the ν_6 and ν_{28} modes both assigned to a separate medium intensity band at 2910 cm^{-1}. The only unassigned mode in this region was the β-$(CH_3)_2$ antisymmetric stretch OP (ν_{26}) mode as it was predicted to have zero intensity and thus was not assigned to any observable peaks in either IR spectra.

CH, CH_2, & CH_3 Bending Modes

There are 11 vibrational "C–H" deformation modes, typically assigned within the 1450 – 850 cm^{-1} range. These 11 deformation modes are assorted by the following groups (and symmetry species): CH (2A'+2A"), CH_2 (A'), and CH_3 (3A' + 3A"). In the GC-IR spectrum, the band at 1404 cm^{-1} has been assigned to five vibrational modes (ν_8-ν_{10}, ν_{29}, and ν_{30}) due to insufficient resolution in this region, and because all five modes are predicted to have weak or very weak intensities. The Ar-IR spectrum, however, resolves this region into a weak band at 1428 cm^{-1} and a medium band at 1403 cm^{-1}. The β (ν_8) and α (ν_9) in-phase $(CH_3)_2$ antisymmetric deformation modes were both assigned at 1428 cm^{-1}. The CH_2 wag (ν_{13}), as well as the α (ν_{29}) and β (ν_{30}) out-of-phase $(CH_3)_2$

antisymmetric deformations, were all assigned at 1403 cm^{-1}. The in-phase $(CH_3)_2$ symmetric deformation (ν_{11}) mode was assigned at approximately 1300 cm^{-1}, whereas the out-of-phase $(CH_3)_2$ symmetric deformation (ν_{31}) was assigned to a strong peak at 1254 cm^{-1}, as it corresponds to the highest predicted intensity within this region (1400 – 1200 cm^{-1}). The wagging =C–H in-plane bend (ν_{12}) was assigned to a strong band at 1248 cm^{-1}. Both the ν_{12} and ν_{31} modes were not individually resolvable in the GC-IR spectrum and thus were assigned to a single strong intensity peak at 1255 cm^{-1}. The scissoring (deformation) =C–H in-plane bend (ν_{14}) band was assigned as a weak peak at 1028 cm^{-1} consistent with the *ab initio* intensity predictions. No band was observed for the twisting =C–H out-of-plane bend (ν_{33}) mode in either spectrum, which is consistent with its predicted near-zero intensity. The rocking =C–H out-of-plane bend (ν_{38}) mode was observed and assigned to a strong band at 618 cm^{-1} in the Ar-IR spectrum, as it is the highest predicted intensity mode near 600 cm^{-1}.

CH_2 and CH_3 Rocking, Twisting, and Wagging Modes

For the CH_2 group, there are three vibrational modes (A'+2A") that correspond to rocking, twisting, and wagging modes occurring between 1130 – 615 cm^{-1}. The CH_2 wag (ν_{13}) mode was assigned to a strong intensity peak at 1131 cm^{-1} in the Ar-IR spectrum and a medium intensity peak at 1122 cm^{-1} in the GC-IR spectrum. This assignment is in good agreement with previous studies on silacyclobutane derivatives,[15] including DMSCBane (see Chapter 1). Al-Saadi et al. noted a band of moderate intensity at ~1123 cm^{-1}, corresponding to the CH_2 wagging frequency, which is considered a characteristic band for silacyclobutane and its derivatives. The CH_2 twist (ν_{32}) mode was observed as a medium-weak band in the GC-IR spectrum and a strong intensity band in the Ar-IR spectrum at 1072 and 1074 cm^{-1}, respectively. A very strong band at 846 cm^{-1} was assigned to the CH_2 rock (ν_{34}) mode in the Ar-IR spectrum.

For the $(CH_3)_2$ group(s), excluding the two torsional modes, there are four vibrational modes (2A' + 2A") with two types of rocking and wagging modes (with respect to the symmetry plane) that are expected to occur between 1150 – 600 cm^{-1}. The in-phase $(CH_3)_2$ rock (ν_{16}) and wag (ν_{17}) modes were not individually resolvable in the GC-IR spectrum; however, they were observed in the Ar-IR spectrum at 886 and 835 cm^{-1}, respectively. The out-of-phase $(CH_3)_2$ rock (ν_{35}) and wag (ν_{36}) modes were both assigned to the same 768 cm^{-1} band in the GC-IR spectrum, but primarily assigned to the ν_{35} vibration based on its very strong predicted intensity. This assumption is validated in the Ar-IR spectrum as the out-of-phase $(CH_3)_2$ rock (ν_{35}) mode is assigned to a very strong band at 769 cm^{-1}, whereas the out-of-phase $(CH_3)_2$ wag (ν_{36}) mode was assigned to a strong intensity peak at 707 cm^{-1}.

Heavy-Atom Stretching and Other Modes

There are six heavy atom stretches observed in the 1550 – 475 cm^{-1} region, sorted according to the symmetry species: 5A' + A". The highest observed frequency corresponds to the C=C stretch (ν_7) mode, observed as a single peak in both the GC-IR and Ar-IR at 1511 and 1518 cm^{-1} respectively. The next highest mode is the C–C stretch (ν_{15}), which was also observed as individual bands in both IR spectra as a medium (GC-IR) and strong (GC-IR) band at 931 and 936 cm^{-1}, respectively. The remaining four modes correspond to the symmetric and antisymmetric Si–C stretching modes for the ring ($Si–C_2$) and the methyl groups ($Si–(CH_3)_2$). The ring $Si–C_2$ symmetric stretch (ν_{19}) and $Si–(CH_3)_2$ antisymmetric stretch (ν_{37}) modes were both assigned to the strong intensity peak at 684 cm^{-1} in the GC-IR spectrum; this assignment is further evidenced with the same two modes assigned at 686 cm^{-1} in the Ar-IR spectrum, and closely matches the original assignments by Korolev et al. Conversely, the $Si–C_2$ antisymmetric stretch (ν_{20}) mode was assigned to a single strong intensity band at 644 cm^{-1} in the Ar-IR spectrum. The lowest stretching

frequency, the Si-C_2 symmetric stretch (ν_{21}), was observed at 486 and 483 cm^{-1} in the Ar-IR and GC-IR spectra, respectively. The only other heavy-atom mode observed for DMSCBene was the ring deformation (ν_{18}) at 789 cm^{-1}; This assignment, however, is questionable and would need to be validated by assignments via a Raman spectrum, as the assigned band is of medium intensity, whereas the *ab initio* results indicate a weak IR intensity. All other modes (below 450 cm^{-1}) fall below the range of mid-IR detection and thus were not assigned in the experimental spectra.

Structural Parameters

The predicted DMSCBene structure was determined at the 6-311+G(d,p) level of theory, and is provided in Table 2.4. Unfortunately, no experimental structural data exists for DMSCBene for which to compare the predicted parameters. Therefore, structural data from other closely related molecules must be used for comparison. Predicted structural parameters for heavy atom bond distances and angles using the HF/3-21G(d) calculation were determined for silacyclobutene[27] and provided in Table 2.3. Because Boatz and Gordon used a different method, and a lower basis set, relative to this study, the provided parameters are given only for the purpose of comparison and no further discussion is given. Furthermore, by removing the C_2–C_3 bond in the silacyclobutane ring of DMSCBene (and adding a hydrogen atom to each carbon), one opens the four-membered ring to obtain vinyltrimethylsilane (VTMS), for which there is gas-phase ED data[28] collected by Page et al. that can be used to compare with the predicted values in the current study, and is provided in Table 2.3. Because VTMS is a branched organosilane, its bond angles are not directly comparable to DMSCBene's, thus comparisons will primarily be limited to bond distances only.

The predicted heavy-atom bond distances for DMSCBene are in excellent agreement with ED data for VTMS. Of the three directly comparable bond distances, the r(Si–C_m) parameter had

the largest difference of 0.003 Å between the theoretical and experimental values of DMSCBene and VTMS. The other predicted distances for DMSCBene, r(C=C) and r(C–Si), only differed from the experimental values of VTMS by 0.001 Å. Unsurprisingly, the r(C–H) values differ by as much as 0.017 Å due to the fact that Page et al. assumed all C–H bonds to be equivalent in the structure refinement to reduce the number of unique solutions. As previously stated, because the two molecules have different heavy-atom frameworks (branched versus cyclic), the three reported angles by Page and coworkers are, not surprisingly, significantly different from DMSCBene with differences between 3 – 34º. Nonetheless, based on the experimental data from VTMS, it is expected that the *ab initio* results should reasonably match DMSCBene's experimental structural data.

Table 2.4. Structural parameters (Å and º), rotational constants (MHz) and dipole moments (Debye) for DMSCBene.

Parameter	Bonding[a]	DMSCBene	SCB	VTMS
		Calc[b]	Calc[c]	ED[d]
$r(C_1C_2)$	C=C	1.360	1.338	1.359(10)
$r(C_2C_3)$	C–C	1.526	1.549	
$r(C_1Si_4)$	C–Si	1.866	1.867	1.867(3)
$r(C_3Si_4)$	C–Si	1.907	1.909	
$r(Si_4C_5)$	Si–C_m	1.874		1.877(3)
$r(C_1H_7)$	C–H	1.086		1.076(8)
$r(C_2H_8)$	C–H	1.093		1.076(8)
$r(C_3H_9)$	C–H	1.095		1.076(8)
$r(C_5H_{11})$	C_m–H	1.095		1.076(8)
$r(C_5H_{13})$	C_m–H	1.094		1.076(8)
$\angle(C_1C_2C_3)$	C=C–C	108.5	108.0	
$\angle(C_2C_1Si_4)$	C=C–Si	90.5	91.6	124.6(1.8)
$\angle(C_2C_3Si_4)$	C–C–Si	84.1	83.9	
$\angle(C_1Si_4C_3)$	C–Si–C	76.8	76.5	112.6(0.8)
$\angle(C_1Si_4C_5)$	C–Si–C_m	117.2		
$\angle(C_3Si_4C_5)$	C–Si–C_m	116.3		
$\angle(C_5Si_4C_6)$	C–Si–C_m	109.9		
$\angle(C_2C_1H_7)$	C–C–H	125.8		
$\angle(Si_4C_1H_7)$	Si–C–H	143.7		
$\angle(C_1C_2H_8)$	C=C–H	127.0		
$\angle(C_3C_2H_8)$	C–C–H	124.5		
$\angle(C_2C_3H_{10})$	C–C–H	113.6		
$\angle(Si_4C_5H_{11})$	Si–C_m–H	111.1		114.2(1.4)
$\angle(Si_4C_5H_{13})$	Si–C_m–H	110.8		114.2(1.4)
$\angle(H_9C_3H_{10})$	H–C–H	108.6		
$\angle(H_{11}C_5H_{12})$	H–C_m–H	107.7		
$\angle(H_{11}C_5H_{13})$	H–C_m–H	108.0		
$\angle(C_1C_2C_3Si_4)$	C=C–C–Si	0.0		
$\angle(H_7C_1C_2H_8)$	H–C=C–H	0.0		
$\angle(C_5Si_4C_6H_{16})$	C_m–Si–C_m–H	–178.7		
$\angle(C_6Si_4C_5H_{13})$	C_m–Si–C_m–H	178.7		
A		3960.621		
B		2404.424		
C		2085.574		
$\lvert\mu_a\rvert$		0.463		
$\lvert\mu_b\rvert$		0.000		
$\lvert\mu_c\rvert$		0.146		
$\lvert\mu_t\rvert$		0.486		

[a] The methyl carbons (C_5 & C_6) are labeled as C_m.
[b] Calculated using MP2(full)/6-311+G(d,p) level of theory.
[c] Calculated for silacyclobutane (SCB) using HF/3-21G(d). Data taken from Ref. [27].
[d] Electron diffraction data (r_g) for vinyltrimethylsilane (VTMS) taken form Ref. [28].

Conclusion

Quantum chemical calculations using the MP2 method were performed on DMSCBene to obtain structural and vibrational data. With the aid of the *ab initio* methods, the first normal coordinate analysis was performed on this molecule. The vibrational assignments were updated from those proposed from the Ar-IR spectrum of DMSCBene. Additionally, assignments were made with the aid of a low resolution mid-IR spectrum of the sample in the vapor phase. Overall, only two vibrational modes in the mid-IR region (4000 – 400 cm^{-1}) were not assigned. Comparison of the reported gas-phase mid IR spectrum with the predicted IR spectrum indicates the utility of *ab initio* calculations for vibrational analyses. It should be noted that the ring puckering mode for DMSCBene is actually a twisting motion about the C=C bond, rather than an enveloping motion of the ring puckering mode for DMSCBane (Chapter 1), but is still nonetheless an out-of-plane ring bending motion. Additionally, the ring puckering frequency is predicted higher (345 cm^{-1}) than that of DMSCBane (253 cm^{-1}); but this frequency seems reasonable as it is consistent with the predicted ring puckering frequency at 306 cm^{-1} for cyclobutene,[26] and corresponds to experimental condensed phase Raman data[29,30] at 325 and 327 cm^{-1} respectively. Predicted structural parameters were also determined and reported for DMSCBene. The heavy-atom bond distance parameters from the *ab initio* results match very well with the ED data for an analogous molecule, vinyltrimethylsilane.

Future Work

Because very little spectroscopic, and no structural, data exist for DMSCBene, this presents many opportunities for studying this molecule in greater detail in order to further the study of silacyclobutane derivatives. Spectroscopically, a vibrational study using both IR and Raman spectroscopies of the molecule in different phases would be crucial to further confirm the accuracy

of the normal coordinate analyses in this work. Additionally, Far-IR (400 – 10 cm^{-1}) spectroscopic studies can be used to assign the ring puckering mode, the two torsional frequencies, and associated overtones with these vibrational modes. This information can then be used to determine the potential function governing the ring puckering normal mode, as well as the barrier to internal rotation of the methyl groups. Furthermore, a microwave study would be useful to obtain structural data and rotational constants for a number of isotopes so that adjusted r_0 structural parameters can be determined. Finally, a gas-phase electron diffraction study would be useful in order to confirm the validity and accuracy of the structural parameters predicted herein.

CHAPTER 3

MONITORING PHOSPHOENOLPYRUVATE BINDING TO RABBIT MUSCLE PYRUVATE KINASE USING INFRARED DIFFERENCE SPECTROSCOPY

Introduction

Pyruvate kinase (PYK) catalyzes the last step of the glycolytic pathway, where it transfers the phosphate group from phosphoenolpyruvate (PEP) to adenosine diphosphate (ADP) to produce pyruvate and adenosine triphosphate (ATP).

$$PEP + ADP \rightarrow Pyruvate + ATP$$

While the catalytic functionality is conserved in PYK isozymes, allosteric regulation amongst the PYK protein family can be altered by small variations or mutations in highly conserved areas of the protein.[31,32] Consequently this reason is why rabbit muscle pyruvate kinase (rM_1-PYK) is allosterically inhibited by L-phenylalanine (Phe) and human liver pyruvate kinase (hL-PYK) is inhibited by L-alanine (Ala). Using amino acid analogues to probe allosteric function, Fenton and co-workers have determined there are distinct chemical requirements (moieties) for protein binding versus magnitude of allosteric regulation for rM_1-PYK; requirements for binding and allosteric inhibition for hL-PYK, however, are the same.[31,32] A similar study of analogues of rM_1-PYK's substrate (PEP) indicated there are also separate chemical requirements (moieties) to elicit an allosteric response versus those necessary for binding.[33]

PEP has been previously investigated[34] where Rudbeck and coworkers initiated a computational and vibrational investigation into PEP's different ionization states. With the aid of frequency calculations from *ab initio* methods, the geometry and frequencies were calculated, using density function theory (DFT), with the B3LYP functional and 6-31G(d,p) basis set using

an implicit solvation model. The investigators were able to make vibrational assignments for fully ionized PEP^{3-} in H_2O. In total, they were able to identify and assign a total of 10 modes and used $^{13}C_{2,3}$ labeled PEP to aid in assignments. The same researchers then studied rM_1-PYK/PEP binding using reaction inducted infrared difference spectroscopy.[35] Using a custom-made dialysis accessory,[36] Kumar and Barth recorded infrared spectra while PEP was diffusing into the reservoir filled with rM_1-PYK. By recording spectra between 96 and 240 seconds after adding PEP to the dialysis accessory reservoir, the authors contended that PEP diffusing through the dialysis membrane into the sampling volume containing the ATR crystal and protein is primarily from bound PEP. The result of the study was that the authors reported shifts of 4 cm^{-1} or more to higher frequencies for both the CO_2^- antisymmetric stretch and CO_2^- symmetric stretch, as well as both PO_3^{2-} antisymmetric stretching modes. The results indicate the strengthening of the C-O bonds on the CO_2^- moiety. Other modes such as the bridging C-O stretch or PO_3^{2-} symmetric stretch saw decreases in frequency between 4 and 16 cm^{-1}. The authors concluded this IR study of PEP binding to rM_1-PYK by suggesting that, during binding, one of the carboxylate C-O bonds decreases in bond length whereas the bridging P-O bond weakens and consequently lengthens.

The focus of this present study was to analyze PEP binding to rM_1-PYK using a methodological approach involving infrared difference spectroscopy to address the following: 1) Is a standard attenuated total reflectance (ATR) FTIR setup sensitive enough to detect small frequency shifts due to changes in PEP when bound to rM_1-PYK? If so, which functional groups are affected when PEP is bound to the protein? 2) Will increasing rM_1-PYK's affinity for PEP by shifting to higher pH (9.0)[37] alter the frequency shifting? 3) Are frequency shifts for different concentrations of protein-bound versus free PEP statistically significant and/or reproducible? To address these questions, a vibrational analysis of PEP was performed to correctly identify

vibrational modes in an aqueous buffer solution. Using the vibrational assignments of PEP, triplicate spectra of free PEP and protein-bound PEP were recorded from 1800 – 800 cm^{-1}. Infrared (IR) difference spectroscopy was used to process the spectra and obtain vibrational frequencies for each replicate, the results of which are reported herein.

Materials and Methods

Materials

Tris(hydroxymethyl)aminomethane (Tris base), ethylenediaminetetraacetic (EDTA) disodium salt dihydrate, and potassium chloride (KCl) were all purchased from Fisher Scientific. Magnesium chloride ($MgCl_2$) was purchased from Sigma Aldrich. Phosphoenolpyruvic acid monopotassium salt (PEP) was purchased from Chem-Impex Int'l Inc. Lastly, rabbit muscle pyruvate kinase (rM_1-PYK) ammonium sulfate suspension was purchased from Roche Diagnostics GmbH.

Sample Preparations

The buffer solution used in the current study (50 mM Tris base, 10 mM $MgCl_2$, 0.1 mM EDTA, and 500 mM K^+) for both protein and PEP samples were prepared using the same assay conditions from a previous study on rM_1-PYK.[37] A 10x concentrated buffer solution was first prepared (500 mM Tris base, 100 mM $MgCl_2$, 1 mM EDTA) at room temperature and titrated to pH = 9.0 using 3 M HCl. The 10x buffer was diluted with water to achieve a 1x concentration. KCl was added during dilution to obtain the appropriate components and concentrations for the 1x dialysis buffer. For stock PEP solutions, room temperature 10x buffer was first used (and later diluted to 1x concentration) and titrated to pH = 9.0. The total K^+ concentration was carefully monitored to maintain $[K^+]$ = 500 mM and appropriate 1x dialysis buffer concentration. After titration and dilution, a solution of 160 mL stock PEP was obtained. The PEP stock solution was

then diluted with dialysis buffer to obtain the following solutions: 150 mM, 75 mM, 15 mM, and 7.5 mM PEP. The 7.5 mM and 15 mM PEP samples were prepared by adding 6 µL of 75 mM PEP or 150 mM PEP to a 0.6 mL microcentrifuge tube and subsequently diluted to 60 µL with dialysis buffer.

To prepare the rM_1-PYK samples, the ammonium sulfate suspension was centrifuged and pelletized via a microcentrifuge at room temperature (14000 RMP, 30 min). After pelletization, the supernatant was discarded and the pellet diluted in in a minimal amount of dialysis buffer. The solution was then dialyzed and desalted with four 250 mL exchanges of dialysis buffer over a two-hour period. After completion of the last dialysis buffer exchange, the solution was kept for analysis by FTIR and used for spectral subtraction. The protein solution was centrifuged once more (14000 RMP, 15 min) to remove any undissolved protein, thereby preventing protein aggregation which will lead to unwanted precipitation. This last step appeared to substantially increase the longevity (solubility) of the concentrated rM_1-PYK solution when stored at 4°C. The protein concentration was determined based on the absorbance at 280 nm using a Thermo Scientific NanoDrop One UV-Vis spectrophotometer. Using the experimentally determined extinction coefficient[38] of 29670 cm^{-1} M^{-1} (or 0.54 mL mg^{-1} cm^{-1}), the final stock protein concentration was determined to be 0.468 mM (or 25.7 mg/mL).

Because rM_1-PYK contains four binding sites, 7.5 mM and 15 mM PEP protein solutions were chosen so that the ratio of concentrations of PEP to all of rM_1-PYK's binding sites were 5:1 and 10:1 respectively. To minimize protein dilution, the 7.5 mM PEP + rM_1-PYK and 15 mM PEP + rM_1-PYK solutions were prepared in the following manner: 48 µL of stock rM_1-PYK solution was added to a 0.6 mL microcentrifuge tube, followed by an addition of either 5 µL of 75 mM PEP, or 150 mM PEP, and subsequently diluted to 60 µL with dialysis buffer. Additionally, a

separate diluted rM_1-PYK solution was prepared by diluting 48 µL of stock protein to 60 µL in total with dialysis buffer. All solutions were made at room temperature and were allowed to equilibrate for 20 to 30 minutes prior to collecting IR spectra. The protein concentration of these three samples were all expected to have the same concentration of 0.374 mM (or 20.6 mg/mL).

Experimental Details

All spectra were recorded using a Nicolet iS10 FTIR spectrometer, equipped with a DTGS detector, using a single bounce diamond attenuated total reflectance (ATR) crystal plate mounted on a Smart iTX optical base. The interferograms were recorded at a resolution of 4 cm^{-1} using a Happ-Genzel apodization function. All sample spectra (512 scans) were ratioed against a 1024 scan background of air. For both background and sample spectra, a cap was placed over the ATR crystal to minimize evaporation. For samples, a 10 µL drop was sufficient to cover the ATR crystal.

Prior to sample collection, CO_2 and water vapor were removed from the spectrometer by purging the system with dry nitrogen. The IR single-beam spectrum was continually monitored until the signal from water vapor was effectively removed and maintained a constant signal for at least 30 min. Depending on the relative humidity, purging could take three or more hours to achieve a constant baseline. Occasionally during sample collection, a small change in humidity within the spectrometer resulted in the appearance of positive or negative water vapor bands in the spectra. In this case, a sample spectrum of air (containing water vapor) was added or subtracted until visual inspection of the sample spectrum indicated water vapor was fully removed.

Computational Methods

To determine which functional groups from PEP contribute to protein-ligand binding, an accurate and thorough vibrational analysis is crucial. To build upon a previous vibrational analysis of PEP,[34] *ab initio* calculations were performed for fully ionized PEP in C_1 and C_s point group

symmetries using the Gaussian 09® program.[7] Because PEP is an anion with a net charge of negative 3, doubly diffuse functions were added to the usual 6-31G(d) basis set, using the MP2 method, to improve accuracy of predicted frequencies. The optimized geometry and the predicted force constants, dipole derivative, and polarizability derivative were subsequently used for a normal coordinate analysis. It should be noted that calculations performed for the C_s conformation of PEP yielded at least one imaginary frequency. Therefore, it is assumed the C_s symmetry form is a transition state of PEP, rather than a stable form. To obtain the C_1 form, all parameters (bond distances, bond angles, and dihedral angles) were relaxed to find the lowest energy structure. The optimized geometry of PEP is shown in Fig. 3.1. A comparison between the observed and calculated wavenumbers (Fig. 3.2), along with the calculated infrared intensities, Raman activities, depolarization ratios and potential energy distributions for PEP in the C_1 form are listed in Table 1. No scaling factors were applied to the predicted frequencies.

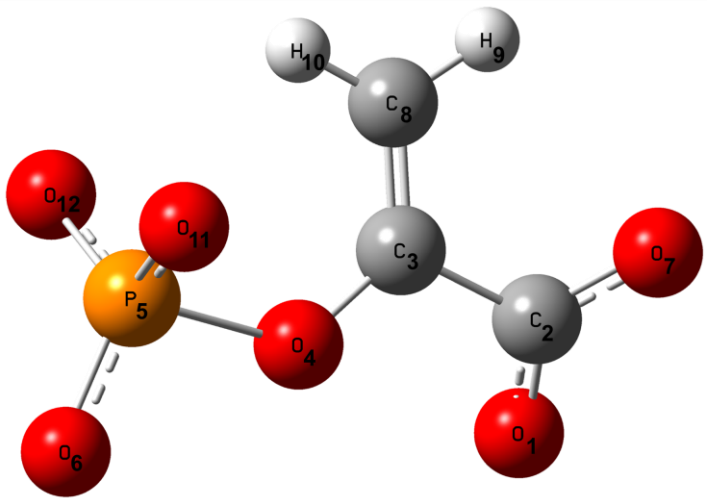

Figure 3.1. The calculated C_1 structure of PEP using MP2(full)/6-31++G(d).

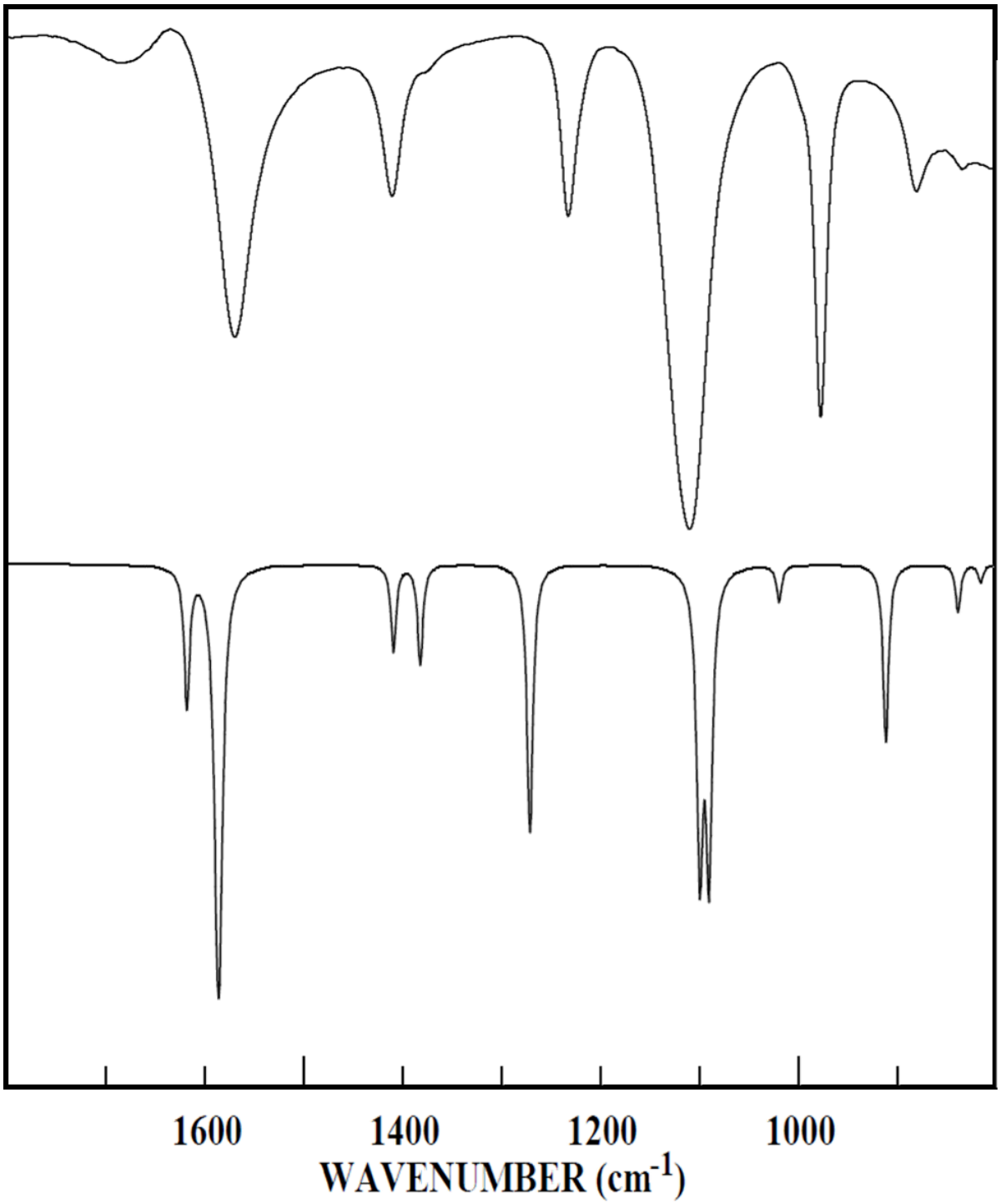

Figure 3.2. Comparison of predicted (bottom) and experimental (top) infrared spectra of PEP between 1800 – 800 cm^{-1}. The experimental spectrum consists of 150 mM PEP dissolved in dialysis buffer with the aqueous buffer subtracted from the original spectrum.

Table 3.1. Observed[a] and calculated[b] frequencies (cm^{-1}) for the C_1 conformation of phosphoenolpyruvate (PEP).

Vib. No.	Approximate Descriptions	ab initio	IR int.	Raman act.	dp ratio	IR Soln (cm^{-1})	P.E.D.[c]
ν_1	CH_2 antisymmetric stretch	3296	17	55.6	0.65	–	98 S_1
ν_2	CH_2 symmetric stretch	3189	18.3	102.2	0.35	–	98 S_2
ν_3	C=C stretch	1618	134.7	180.2	0.11	–	55 S_3, 18 S_5, 9 S_4
ν_4	CO_2^- antisymmetric stretch	1586	852.7	30.4	0.28	1567	83 S_4
ν_5	CH_2 deformation	1409	78.7	45.9	0.35	1407	72 S_5, 9 S_3
ν_6	CO_2^- symmetric stretch	1382	91.7	36.6	0.25	1373	38 S_6, 19 S_7, 16 S_{19}, 9 S_{10}
ν_7	C-O stretch	1271	316.9	4.6	0.63	1229	36 S_6, 21 S_7, 20 S_{10}
ν_8	α-PO_3^{2-} antisymmetric stretch	1099	417.3	11.1	0.70	1106	94 S_8
ν_9	β-PO_3^{2-} antisymmetric stretch	1090	423.5	2.6	0.74	1106	96 S_9
ν_{10}	CH_2 rock	1019	31.6	5.3	0.34	~995	50 S_{10}, 34 S_7
ν_{11}	PO_3^{2-} symmetric stretch	911	180.3	15.2	0.02	974	98 S_{11}
ν_{12}	CO_2^- deformation	838	41.3	30.6	0.03	877	33 S_{12}, 29 S_{19}, 16 S_6
ν_{13}	CO_2^- wag	815	15.2	6.6	0.41	830	70 S_{13}, 15 S_{22}
ν_{14}	CH_2 twist	738	4.7	3.9	0.75	–	73 S_{14}, 17 S_{22}
ν_{15}	C-C-O deformation	682	48	3.5	0.28	–	25 S_{15}, 22 S_{12}
ν_{16}	CH_2 wag	617	101.2	64.1	0.45	–	58 S_{16}, 16 S_{14}
ν_{17}	CO_2^- rock	608	75.8	25.3	0.46	–	28 S_{16}, 16 S_{26}, 12 S_{12}, 9 S_{17}
ν_{18}	PO_3^{2-} symmetric deformation	543	281.8	26.5	0.12	–	45 S_{18}, 17 S_{26}, 9 S_{17}
ν_{19}	C-C stretch	510	70	2.2	0.28	–	41 S_{18}, 13 S_{21}, 12 S_{19}
ν_{20}	β-PO_3^{2-} antisymmetric deformation	487	29.1	1	0.75	–	73 S_{20}, 18 S_{24}
ν_{21}	α-PO_3^{2-} antisymmetric deformation	470	12.1	1.7	0.67	–	65 S_{21}
ν_{22}	C=C(H_2) wag	391	3	2	0.18	–	23 S_{22}, 19 S_{23}, 11 S_{13}, 10 S_{17}
ν_{23}	C=C(H_2) rock	352	6.4	2.1	0.23	–	32 S_{23}, 28 S_{17}
ν_{24}	PO_3^{2-} wag	309	0.8	1.7	0.70	–	55 S_{24}, 13 S_{20}
ν_{25}	PO_3^{2-} rock	287	0.9	2.6	0.53	–	53 S_{25}, 10 S_{21}, 10 S_{17}
ν_{26}	O-P stretch	196	5.7	3.3	0.32	–	38 S_{26}, 27 S_{15}, 11 S_{27}
ν_{27}	C-O-P deformation	138	1.7	2.2	0.36	–	64 S_{27}, 20 S_{15}, 12 S_{25}
ν_{28}	C-C-O-P torsion	95	0.1	0.9	0.72	–	46 S_{30}, 39 S_{28}
ν_{29}	CO_2^- torsion	44	2.3	2.3	0.70	–	75 S_{29}, 25 S_{28}
ν_{30}	PO_3^{2-} torsion	30	1.7	1.2	0.75	–	49 S_{30}, 31 S_{28}, 19 S_{29}

[a] Observed experimental frequencies observed for 150 mM PEP dissolved in an aqueous tris buffer solution (pH=9.0).
[b] MP2(full)/6-31++G(d) *ab initio* calculations, infrared intensities (km/mol), Raman activities ($Å^4$/amu), depolarization ratios, and potential energy distributions (P.E.D.s).
[c] Contributions less than 9% are omitted.

Table 3.2. Symmetry coordinates of phosphoenolpyruvate (PEP).

Description	Symmetry Coordinate[a,b]
CH_2 antisymmetric stretch	$\mathbf{S_1} = \mathbf{r}_{8,9} - \mathbf{r}_{8,10}$
CH_2 symmetric stretch	$\mathbf{S_2} = \mathbf{r}_{8,9} + \mathbf{r}_{8,10}$
C=C stretch	$\mathbf{S_3} = \mathbf{R}_{3,8}$
CO_2^- antisymmetric stretch	$\mathbf{S_4} = \mathbf{R}_{2,1} - \mathbf{R}_{2,7}$
CH_2 deformation	$\mathbf{S_5} = 2\boldsymbol{\alpha}_{9,8,10} - \boldsymbol{\alpha}_{3,8,9} - \boldsymbol{\alpha}_{3,8,10}$
CO_2^- symmetric stretch	$\mathbf{S_6} = \mathbf{R}_{2,1} + \mathbf{R}_{2,7}$
C-O stretch	$\mathbf{S_7} = \mathbf{R}_{3,4}$
α-PO_3^{2-} antisymmetric stretch	$\mathbf{S_8} = 2\mathbf{R}_{5,6} - \mathbf{R}_{5,11} - \mathbf{R}_{5,12}$
β-PO_3^{2-} antisymmetric stretch	$\mathbf{S_9} = \mathbf{R}_{5,11} - \mathbf{R}_{5,12}$
CH_2 rock	$\mathbf{S_{10}} = \boldsymbol{\alpha}_{3,8,9} - \boldsymbol{\alpha}_{3,8,10}$
PO_3^{2-} symmetric stretch	$\mathbf{S_{11}} = \mathbf{R}_{5,6} + \mathbf{R}_{5,11} + \mathbf{R}_{5,12}$
CO_2^- deformation	$\mathbf{S_{12}} = 2\boldsymbol{\theta}_{1,2,7} - \boldsymbol{\theta}_{1,2,3} - \boldsymbol{\theta}_{7,2,3}$
CO_2^- wag	$\mathbf{S_{13}} = \boldsymbol{\theta}_{1,2,7} + \boldsymbol{\theta}_{1,2,3} + \boldsymbol{\theta}_{7,2,3}$
CH_2 twist	$\mathbf{S_{14}} = \boldsymbol{\tau}_{9,8,3,4}$
C–C–O deformation	$\mathbf{S_{15}} = 2\boldsymbol{\theta}_{2,3,4} - \boldsymbol{\theta}_{8,3,2} - \boldsymbol{\theta}_{8,3,4}$
CH_2 wag	$\mathbf{S_{16}} = \boldsymbol{\alpha}_{9,8,10} + \boldsymbol{\alpha}_{3,8,9} + \boldsymbol{\alpha}_{3,8,10}$
CO_2^- rock	$\mathbf{S_{17}} = \boldsymbol{\theta}_{1,2,3} - \boldsymbol{\theta}_{7,2,3}$
PO_3^{2-} symmetric deformation	$\mathbf{S_{18}} = \boldsymbol{\phi}_{11,5,12} + \boldsymbol{\phi}_{6,5,11} + \boldsymbol{\phi}_{6,5,12} - \boldsymbol{\phi}_{6,5,4} - \boldsymbol{\phi}_{11,5,4} - \boldsymbol{\phi}_{12,5,4}$
C–C stretch	$\mathbf{S_{19}} = \mathbf{R}_{3,2}$
β-PO_3^{2-} antisymmetric deformation	$\mathbf{S_{20}} = \boldsymbol{\phi}_{6,5,11} - \boldsymbol{\phi}_{6,5,12}$
α-PO_3^{2-} antisymmetric deformation	$\mathbf{S_{21}} = 2\boldsymbol{\phi}_{11,5,12} - \boldsymbol{\phi}_{6,5,11} - \boldsymbol{\phi}_{6,5,12}$
C=C(H_2) wag	$\mathbf{S_{22}} = \boldsymbol{\theta}_{2,3,4} + \boldsymbol{\theta}_{8,3,2} + \boldsymbol{\theta}_{8,3,4}$
C=C(H_2) rock	$\mathbf{S_{23}} = \boldsymbol{\theta}_{8,3,2} - \boldsymbol{\theta}_{8,3,4}$
PO_3^{2-} wag	$\mathbf{S_{24}} = \boldsymbol{\phi}_{11,5,4} - \boldsymbol{\phi}_{12,5,4}$
PO_3^{2-} rock	$\mathbf{S_{25}} = 2\boldsymbol{\phi}_{6,5,4} - \boldsymbol{\phi}_{11,5,4} - \boldsymbol{\phi}_{12,5,4}$
O–P stretch	$\mathbf{S_{26}} = \mathbf{R}_{4,5}$
C–O–P deformation	$\mathbf{S_{27}} = \boldsymbol{\theta}_{3,4,5}$
C–C–O–P torsion	$\mathbf{S_{28}} = \boldsymbol{\tau}_{5,4,3,2}$
CO_2^- torsion	$\mathbf{S_{29}} = \boldsymbol{\tau}_{7,2,3,4}$
PO_3^{2-} torsion	$\mathbf{S_{30}} = \boldsymbol{\tau}_{3,4,5,6}$

[a] Not normalized.

[b] The subscripted numbers of the internal coordinates correspond to the atom numbering in Fig. 3.1 of PEP.

Results and Discussion

Vibrational Analysis of PEP in Buffer Solution

Accurate vibrational assignments of PEP are critical to this study as we are attempting to correlate frequency shifts to certain functional groups to determine which moieties are affected, and to what extent, when binding to rM_1-PYK. Because PEP belongs to the C_1 point group, its 30 vibrational modes possess only an identity symmetry element, thus all modes belong to the same "A" species. As a result, all 30 vibrational modes are IR and Raman active, with the intensities, activities, and depolarization ratios also varying between each vibrational mode. Assignments for PEP were made in a spectrum of 150 mM PEP dissolved in an aqueous dialysis buffer solution (see the "Sample Preparations" section for more details of buffer components) at pH = 9.0. The concentration was chosen to maximize signal from PEP to accurately identify bands, including shoulder bands that may not be readily present at weaker concentrations, and assign them to the corresponding vibrational modes and moieties. Because the signal from water in the dialysis buffer dominates the spectrum (see Figure 3.3), the only resolvable bands for PEP were between 1800 – 800 cm^{-1}, therefore limiting assignments to this region as well. The results of the analysis are reported herein and compared with a previous spectroscopic study[34] of PEP.

Predicted frequencies from the *ab initio* results (Table 3.1) indicate there are 11 IR-active vibrational modes between 1800 – 800 cm^{-1}. Furthermore, the six prominent bands in the PEP spectrum are well separated (>35 cm^{-1}) which is helpful when attempting to making accurate assignments. Comparison of the predicted spectrum to the experimental spectrum (Fig. 3.2) shows reasonable agreement between the theoretical and experimental results. In the previous two chapters, scaling factors were imposed on the predicted frequencies of the two

silacylcobutane derivatives to scale them down since the MP2(full) 6-31G(d) calculation consistently overestimates the vibrational frequencies. In the case of PEP, the predicted frequencies show varying levels of accuracy with some bands predicted higher, and others lower, in frequency. Consequently, scaling factors were not applied in this study.

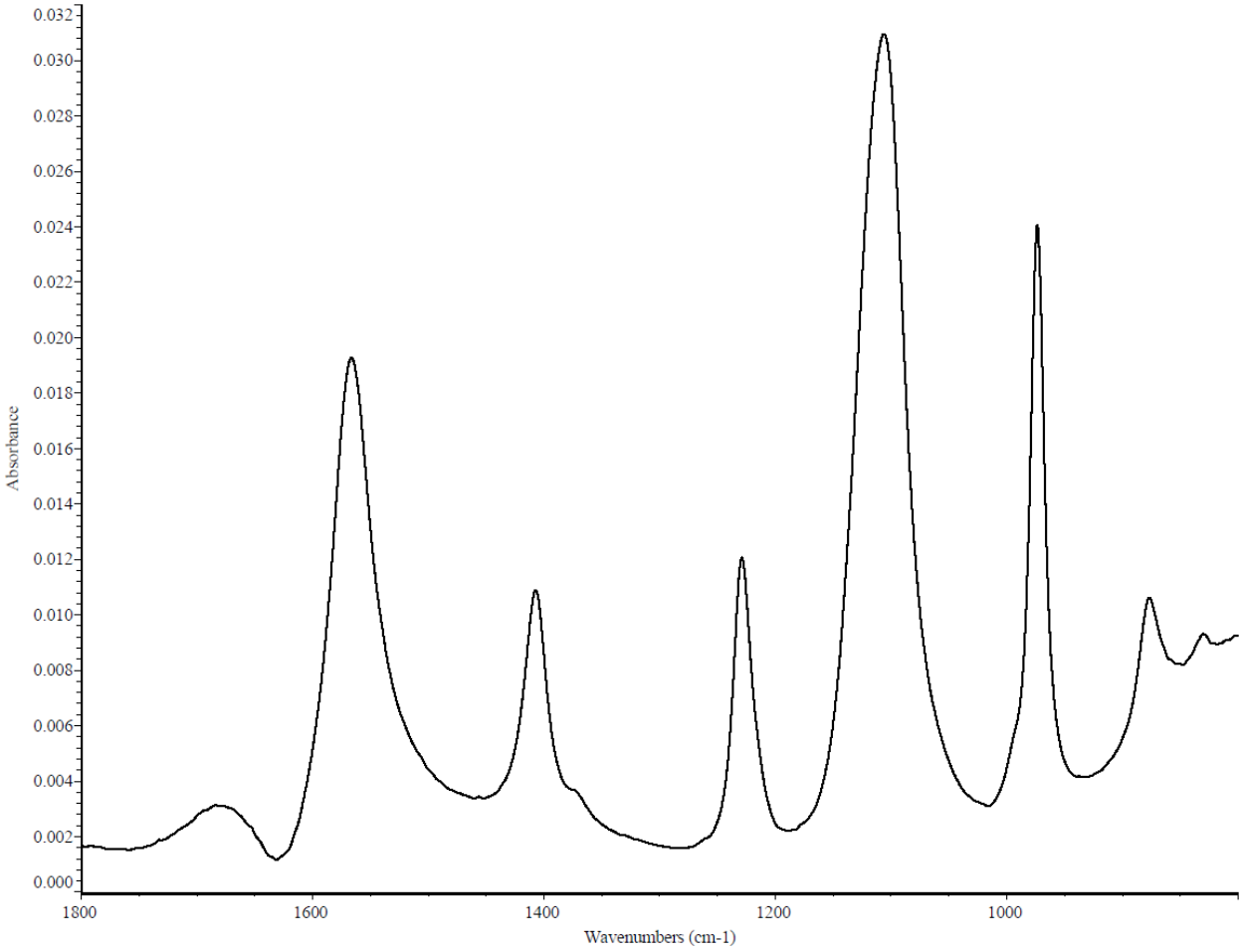

Figure 3.3. Dialysis buffer subtracted spectrum of 150 mM PEP.

Although the broad peak at 1680 cm^{-1} falls within the region where C=C stretches often occur, the C=C stretching mode (ν_3) was not assigned to this band. The band shape, mainly its broadness, indicates this is due to imperfect subtraction of water that partially shifted in the presence of 150 mM PEP. Additional evidence to support this assumption is indicated in the valley minimum at 1631 cm^{-1} that lies between the 1680 and 1567 cm^{-1} bands – which happens to fall close to the H–O–H bending mode of water at 1636 cm^{-1}. The peak at 1566 cm^{-1} was assigned to the CO_2^- antisymmetric stretching (ν_4) mode based on the predicted frequency and intensity, but likely contains the C=C stretching mode (ν_3) buried underneath the large-intensity band. This conclusion is supported by the previous analysis[34] of PEP where Rudbeck et al. reported a splitting of this band into two for ^{13}C labeled PEP at the α and β carbon positions. The medium intensity peak at 1407 cm^{-1} was assigned to the CH_2 deformation (ν_5) mode, with the shoulder band at 1373 cm^{-1} being assigned to the CO_2 symmetric stretching (ν_6) mode. This assignment seems to improve upon the previous vibrational analysis where the authors assigned both modes to the 1407 cm^{-1}, leaving the shoulder band unassigned. The C–O stretching (ν_7) mode was assigned to the medium intensity band at 1229 cm^{-1} and agrees with Rudbeck and coworkers, who reported a 15 cm^{-1} decrease in this band in the isotopologue of PEP. The highest intensity band in the spectrum at 1106 cm^{-1} was assigned to both the α and β PO_3^{2-} antisymmetric stretching (ν_8 & ν_9) modes which were predicted at 1099 and 1090 cm^{-1}, respectively. A weak shoulder band, which was also previously reported as a shoulder at ~980 cm^{-1}, was identified at ~995 cm^{-1} in the current study and was assigned to the CH_2 rocking (ν_{10}) mode, which was predicted to have a weak intensity. Subsequently, the PO_3^{2-} symmetric stretching (ν_{11}) mode was assigned to a sharp band with strong intensity at 974 cm^{-1}. The medium intensity band at 877 cm^{-1} was assigned to the CO_2^- deformation (ν_{12}), whereas

Rudbeck et al. assigned both the C–C stretching and CO_2^- deformation modes to this peak. Lastly, a very weak peak near the edge of the spectrum at 830 cm^{-1} was assigned to the CO_2^- wagging (ν_{13}) mode, which was predicted as a weak intensity peak at 815 cm^{-1}. In total, 10 of 11 possible vibrational modes in this region were assigned, including two new additional modes not previously assigned. The experimental frequencies are in good agreement with the *ab initio* predictions even with the sample dissolved in a buffer solution containing metal ions. Table 3.3 shows a comparison of the vibrational assignments from this work to the previous assignments of PEP. The predicted frequencies using gas-phase *ab initio* calculations in the current study produced similar results to the implicit solvation *ab initio* calculations used by Rudbeck et al., leading to nearly identical assignments in the PEP spectrum.

Table 3.3. Comparison of current and previous[34] vibrational assignments.

Assignments from this work	**IR Band (cm^{-1})**	**Previous Assignments**
CO_2^- antisymmetric stretch	1567	CO_2^- antisymmetric stretch
CH_2 deformation	1407	CH_2 deformation / CO_2^- symmetric stretch
CO_2^- symmetric stretch	1373	
C–O stretch	1229	C–O stretch
α-PO_3^{2-} antisymmetric stretch β-PO_3^{2-} antisymmetric stretch	1106	2x PO_3^{2-} antisymmetric stretches
CH_2 rock	~995	CH_2 rock (~980 cm^{-1})
PO_3^{2-} symmetric stretch	974	PO_3^{2-} symmetric stretch
CO_2^- deformation	877	C–C stretch / CO_2^-
CO_2^- wag	830	

Infrared Difference Spectra

When collecting an IR spectrum, a background is first collected, followed by data collection of the sample, which in turn, yields an IR spectrum. When measuring an IR spectrum in transmittance, the instrument ratios the amount of light passing through a sample (I) to the amount of incident light from a refence (I_0):

$$T = \frac{I}{I_0} \tag{3.1}$$

The problem with transmittance, however, is peak height and area do not follow Beer's law, or in other words, are not proportional to concentration.[39] Therefore, a transmittance spectrum must be converted to absorbance prior to spectral subtraction. The relationship between absorbance and transmittance is given by:

$$A = \log_{10} \frac{1}{T} = \log_{10} \frac{I_0}{I} \tag{3.2}$$

For simple mixtures, such as a single component dissolved in a solvent, it is standard practice, and relatively straight forward, to use pure solvent as a background. Upon data collection from the sample, the resulting spectrum should yield only the component (i.e., sample) and ideally no residual positive or negative bands from the solvent remain in the spectrum. An alternative approach to this method is to collect a spectrum of the solvent, separately from the sample dissolved in solvent, ratioing both against a common background (e.g., air). Then, once both spectra are converted to absorbance, one can manually subtract the solvent from the sample dissolved in solvent and ideally yield the exact same result as equation 3.2 above using the algorithm:

$$[\text{Sample} + \text{Solvent}] - [\text{Solvent}] = [\text{Sample}] \tag{3.3}$$

The result is called an infrared difference spectrum. It is important to note the algorithm above requires a linear response to concentration (Beer's law) and that the solvent concentration does not change when adding a sample to it.[39,40] This situation, however, is rarely, if ever, the case – what typically results is the signal from the solvent ($S_{solvent}$) is greater than the solvent signal with sample ($S_{solvent + sample}$) such that $S_{solvent} > S_{solvent + sample}$. In this situation, one cannot use equation 3.3 without residuals appearing in the spectrum. To effectively remove solvent sample from the spectrum, a subtraction factor must be applied to the solvent spectrum so that $S_{solvent} = S_{solvent + sample}$ and the same result can be achieved in equation 3.3. When applying a spectral subtraction factor to the refence spectrum, equation 3.3 takes on the form:

$$[\text{Sample} + \text{Solvent}] - k * [\text{Solvent}] = [\text{Sample}] \quad (3.4)$$

Where k is the subtraction factor the solvent spectrum is multiplied by to achieve full subtraction of the solvent, yielding the same result as equation 3.3. Typically, $k < 1$, however, when $k = 1$, equation 3.4 yields the same result as equation 3.3. Both equations require the sample and solvent to obey Beer's law – otherwise an imperfect subtraction will occur. Additionally, careful determination of the subtraction factor is necessary to remove, or zero, any solvent peaks present.

One of the more interesting aspects about equation 3.4 is that it can also be applied to multi-component spectra. For instance, in the case of a two component solution, one can apply equation 3.4 to remove one component (C#1) from a second one (C#2) in a mixture and vice-versa to achieve the desired IR difference spectrum:

$$[(C\#1) + (C\#2) + \text{Solvent}] - k * [\text{Solvent} + C(\#2)] = [C(\#1)]$$

or (3.5)

$$[(C\#1) + (C\#2) + \text{Solvent}] - k * [\text{Solvent} + C(\#1)] = [C(\#2)]$$

For equation 3.5, the subtraction factor for either scenario must be carefully applied such that the bands from both the solvent and the respective component are canceled out to achieve the desired component spectrum. In this situation, it is generally recommended, if possible, to collect an IR spectrum of each individual component (C#1 + Solvent, C#2 + Solvent, and Solvent), using the exact same reference spectrum (e.g., air). Then, the three components can be used as bench markers to determine if each component is properly subtracted from the IR difference spectrum. The subtraction factor-based approach has recently been applied to studying mineral components in soil[41] and protein-molecule interations.[42] In the current study, we attempt to use this approach to study protein-ligand binding where rM_1-PYK and PEP are the two components in a mixture.

PEP Spectra

For the PEP samples, three spectra were measured for each concentration of 7.5 mM and 15 mM PEP in buffer solution. All samples were made using the exact same dialysis buffer, therefore the buffer was subtracted from all PEP spectra using the algorithm described in equation 3.3. With the aid of the vibrational analysis of 150 mM PEP, the peak positions for both 7.5 mM and 15 mM solutions were determined and their standard deviations for each band given in Table 3.4. The averaged triplicate spectra for 7.5 mM and 15 mM PEP are shown in Fig 3.4. The buffer subtracted spectra of 7.5 mM, 15 mM, 75 mM, and 150 mM PEP concentrations are given in Fig. 3.5. The results in Table 3.4 show very small differences in

the averages of the frequencies between 7.5 mM and 15 mM PEP for all six listed vibrational frequencies.

Table 3.4. Triplicate averages and standard deviations of peak positions (in cm^{-1}) for 7.5 mM and 15 mM PEP.

Vibrational Mode	**7.5 mM PEP**		**15 mM PEP**	
	Avg	**SD**	**Avg**	**SD**
CO_2^- antisymmetric stretch	1568.50	0.13	1568.24	0.24
CH_2 deformation	1409.81	0.14	1408.14	0.85
CO_2^- symmetric stretch	1368.79	0.08	1369.89	1.12
C–O stretch	1229.43	0.36	1228.79	0.18
α & β-PO_3^{2-} antisymmetric stretches	1110.05	0.09	1108.34	1.28
PO_3^{2-} symmetric stretch	974.43	0.02	974.07	0.09

[a] Standard deviation = 1σ.

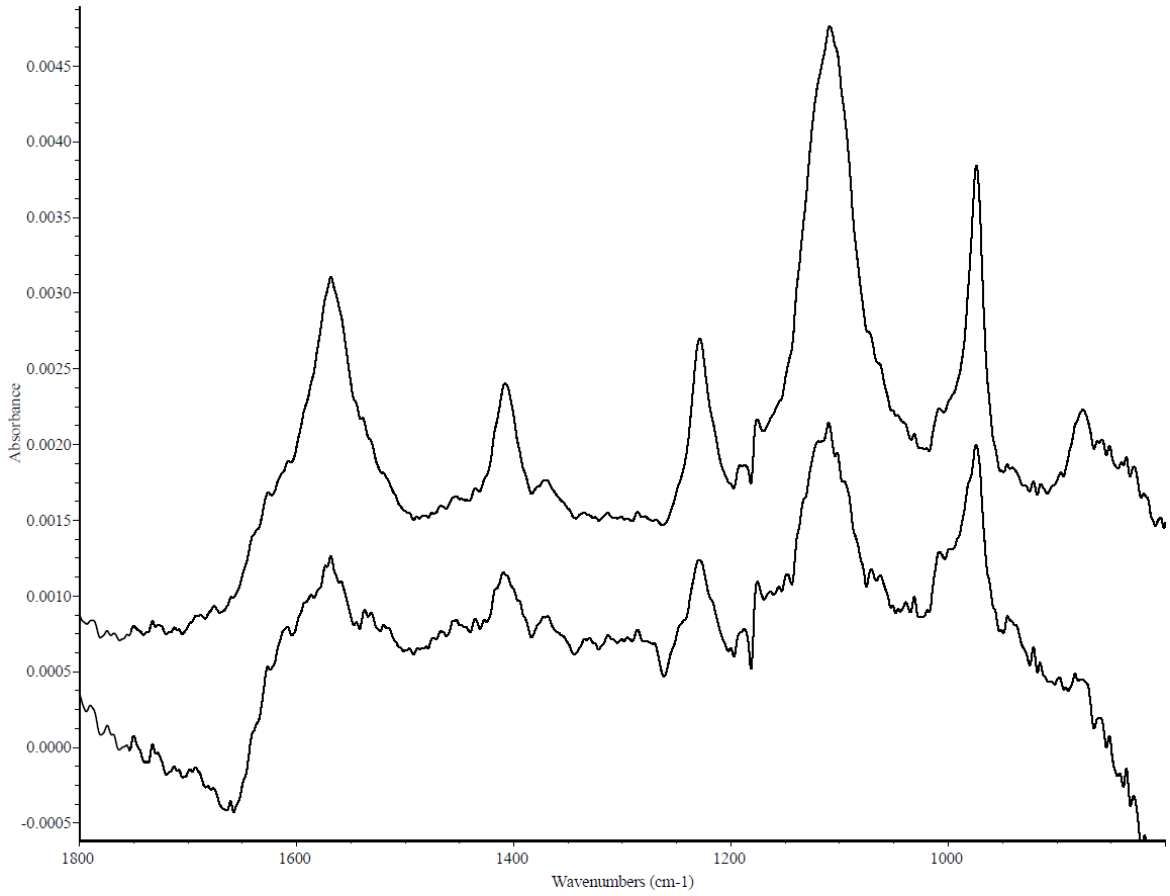

Figure 3.4. Comparison of the averaged triplicate spectra for 7.5 mM PEP (bottom) and 15 mM PEP (top).

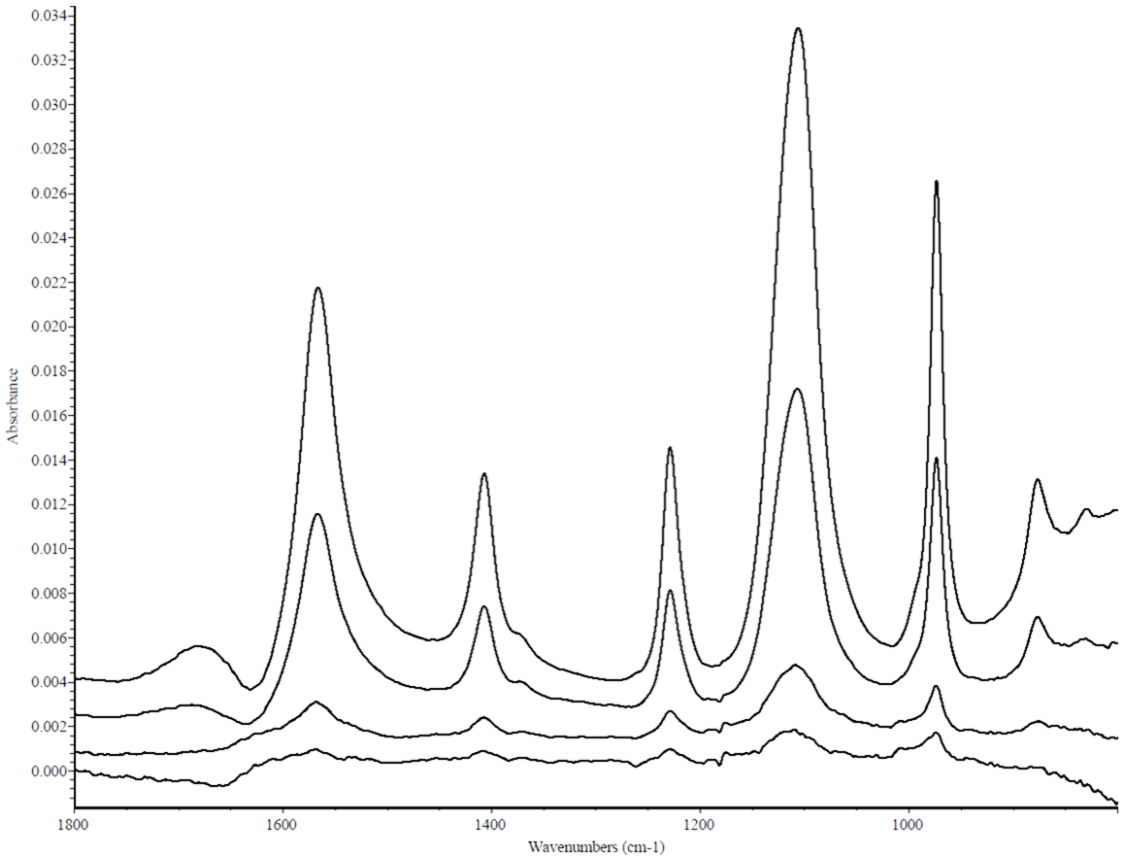

Figure 3.5. Spectra of PEP at concentrations from bottom to top: 7.5 mM, 15 mM, 75 mM, and 150 mM.

PEP + rM$_1$-PYK Spectra

Three spectra each were measured for rM$_1$-PYK, 7.5 mM PEP + rM$_1$-PYK, and 15 mM PEP + rM$_1$-PYK. Similar to the PEP solutions, the dialysis buffer was subtracted from all spectra using the algorithm described in equation 3.3. The averaged triplicate spectrum for rM$_1$-PYK is shown in Fig. 3.6. For both samples of 7.5 mM PEP + rM$_1$-PYK and 15 mM PEP + rM$_1$-PYK, the protein was subtracted using the algorithm in equation 3.5. To ensure the protein was consistently removed from the spectra, the subtraction factor was varied until the protein peak at ~1450 cm^{-1} was consistently and effectively subtracted from the spectrum. This

frequency was chosen specifically because it is isolated from water and PEP signals. The resulting IR difference spectra for 7.5 mM PEP + rM_1-PYK and 15 mM PEP + rM_1-PYK are shown in Fig. 3.7. The frequency averages and standard deviations of all four PEP solutions are provided in Table 3.5

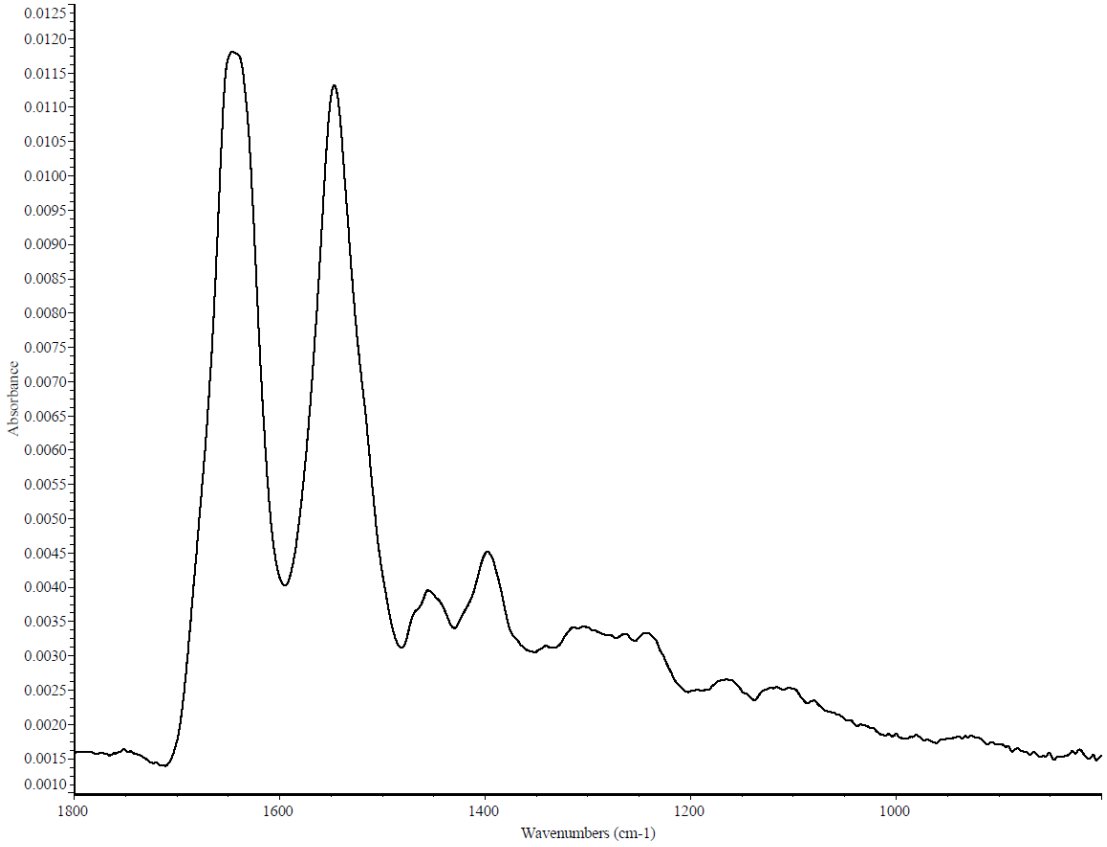

Figure 3.6. Spectrum of a triplicate-averaged and buffer-subtracted rM_1-PYK.

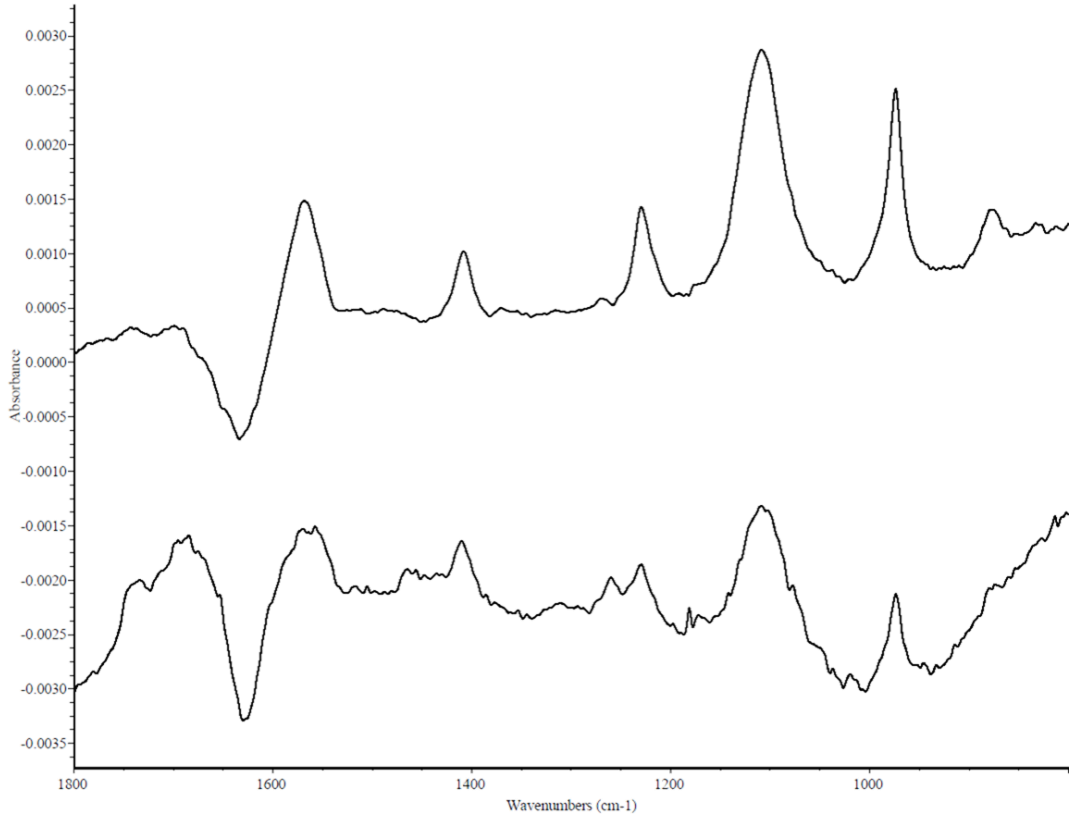

Figure 3.7. IR difference spectra of 7.5 mM PEP + rM_1-PYK (bottom) and 15 mM PEP + rM_1PYK (top).

Table 3.5. Triplicate averages and standard deviations[a] of peak positions (in cm^{-1}) for unbound and protein-bound PEP.

Vibrational Mode	**15 mM PEP**		**15 mM PEP + rM_1-PYK**		**7.5 mM PEP**		**7.5 mM PEP + rM_1-PYK**	
	Avg	**SD**	**Avg**	**SD**	**Avg**	**SD**	**Avg**	**SD**
CO_2^- antisymmetric stretch	1568.24	0.24	1567.01	2.99	1568.50	0.13	1571.37	0.50
CH_2 deformation	1408.14	0.85	1407.96	0.64	1409.81	0.14	1410.03	0.42
CO_2^- symmetric stretch	1369.89	1.12	1370.62	0.73	1368.79	0.08	1372.61	0.39
C–O stretch	1228.79	0.18	1229.59	0.18	1229.43	0.36	1229.58	0.25
α & β-PO_3^{2-} antisymmetric stretches	1108.34	1.28	1108.50	1.17	1110.05	0.09	1108.67	2.20
PO_3^{2-} symmetric stretch	974.07	0.09	973.82	0.11	974.43	0.02	973.62	0.24

[a] Standard deviations are reported as 1σ.

For free PEP, the frequencies do not appear to change drastically with concentration. The small variation in standard deviations (<1.3 cm^{-1}) for free PEP and protein-bound 7.5 mM PEP indicates frequencies for all six assigned vibrational modes are highly stable and thus are reproducible from one spectrum collection to another. For protein-bound PEP samples, the standard deviation appears to increase with increasing (15 mM) PEP concentration. It is possible that, at higher concentrations, signal from free PEP is dominating the spectrum, compared to protein-bound PEP samples with lower (7.5 mM) PEP concentrations. Nonetheless, the data in Table 3.5 indicates three vibrational modes with statistically significant frequency shifts when PEP is bound to rM_1-PYK. The following frequencies for 7.5 mM PEP spectra appear to shift upon binding to the protein: the antisymmetric CO_2^- stretch (Δ = +2.87 cm^{-1}), the symmetric CO_2^- stretch (Δ = +3.83 cm^{-1}), and the PO_3^{2-} symmetric stretch (Δ = -0.81cm^{-1}).

Conclusion

A normal coordinate analysis was performed for PEP, reporting predicted vibrational spectroscopic parameters for all 30 vibrational modes and assignments made between 1800 – 800 cm^{-1}. Replicates were recorded for different concentrations of free versus bound PEP to determine changes in frequencies. Standard deviations for each frequency were determined and compared to free versus protein-bound PEP in solution. Three frequencies of PEP were found to have statistically significant shifts, with respect to their standard deviations which, in turn, suggests the CO_2^- moiety is more affected from PEP binding to rM_1-PYK than the PO_3^{2-} moiety or bridging O–P bond. The results of this study indicate the following: 1) Replicates are necessary to determine standard deviations in vibrational frequencies to establish statistically significant shifts between free versus bound PEP. 2) A standard ATR-FTIR

accessory with a lower sensitivity detector (DTGS compared to HgCdTe) is capable of detecting frequency shifts in free versus protein-bound PEP. 3) Subtraction factors applied to IR difference spectra are necessary to ensure proper subtraction and removal of any unshifted protein from a sample spectrum.

Future Work

There are many possibilities to add on to the current work to study PEP/rM_1-PYK binding, as well as its allosteric regulation, using FTIR spectroscopy. First, increasing the number of replicates measured would be useful in determining if the frequency shifts presented in this work are truly statistically significant, or even reproducible. One could carry this study even further by adjusting the ratio of PEP to the number of protein binding sites from 20:1 to 1:20 to measure the protein and PEP in response to PEP fully saturating rM_1-PYK's binding sites versus minimally saturating them.

Another study of interest would be to monitor binding of PEP analogs with the phosphate or carboxylate moiety removed. A previous attempt was made[33] to determine if the phosphate moiety of PEP was required for an allosteric response in rM_1-PYK. In this study, Urness et al. used PEP analogs without the phosphate moiety and found that the removal of the phosphate group reduced substrate affinity, whereas the removal of the carboxylate moiety diminished the ability to allosterically reduce Phe binding. Alternatively, the study on rM_1-PYK's allosteric effector, Phe, and its analogs, would provide new insights into how the effector binds to the protein in the allosteric site since it has been previously shown[37] that the aryl group is not required to initiate an allosteric response.

REFERENCES

(1) Durig, J. R.; Compton, D. A. C.; Johnson-Streusand, M. Spectra and Structure of Silicon Containing Compounds. Part XI. Infrared and Raman Spectra of 1,1-Dimethyl-1-Silacyclobutane. *J. Mol. Struct.* **1979**, *56*, 175–190.

(2) Laane, J. Vibrational Spectra and Normal-Coordinate Analyses of Silacyclobutanes. *Spectrochim. Acta Part A Mol. Spectrosc.* **1970**, *26* (3), 517–540.

(3) Shen, Q.; Apen, P. G.; Hilderbrandt, R. L. The Molecular Structures of 1,1-Dimethylsilacyclobutane and 1,1,3,3-Tetramethyl-1,3-Disilacyclobutane as Determined by Gas-Phase Electron Diffraction. *J. Mol. Struct.* **1991**, *246* (3–4), 229–236.

(4) Philen, D. L.; Chao, T. H.; Laane, J. Vibrational Analyses of Silacyclopentanes. *J. Mol. Struct.* **1973**, *16* (3), 417–431.

(5) Novikov, V. P.; Tarasenko, S. A.; Samdal, S.; Quang Shen; Vilkov, L. V. The Molecular Structure and the Puckering Potential Function of 1,1-Dimethylsilacyclobutane Determined by Gas Electron Diffraction and Relaxation Constraints from Ab Initio Calculations. *J. Mol. Struct.* **1999**, *477* (1–3), 71–89.

(6) Hirota, E.; Ohashi, N.; Kawashima, Y.; Usami, T. Fourier Transform Microwave Spectroscopy of 1,1-Dimethylsilacyclobutane. Interplay of Two Types of Large-Amplitude Motions: Two-Top Internal Rotation and Ring Puckering. *J. Mol. Spectrosc.* **2004**, *228* (2 SPEC. ISS.), 258–278.

(7) Frisch, M. J.; Trucks, G. W.; Schlegel, H. B.; Scuseria, G. E.; Robb, M. A.; Cheeseman, J. R.; Scalmani, G.; Barone, V.; Mennucci, B.; Petersson, G. A.; Nakatsuji, H.; Caricato, M.; Li, X.; Hratchian, H. P.; Izmaylov, A. F.; Bloino, J.; Zheng, G.; Sonnenberg, J. L.; Hada, M.; Ehara, M.; Toyota, K.; Fukuda, R.; Hasegawa, J.; Ishida, M.; Nakajima, T.; Honda, Y.; Kitao, O.; Nakai, H.; Vreven, T.; Montgomery Jr., J. A.; Peralta, J. E.; Ogliaro, F.; Bearpark, M.; Heyd, J. J.; Brothers, E.; Kudin, K. N.; Staroverov, V. N.; Kobayashi, R.; Normand, J.; Raghavachari, K.; Rendell, A.; Burant, J. C.; Iyengar, S. S.; Tomasi, J.; M., C.; Rega, N.; Millam, J. M.; Klene, M.; Knox, J. E.; Cross, J. B.; Bakken, V.; Adamo, C.; Jaramillo, J.; Gomperts, R.; Stratmann, R. E.; Yazyev, O.; Austin, A. J.; Cammi, R.; Pomelli, C.; Ochterski, J. W.; Martin, R. L.; Morokuma, K.; Zakrzewski, V. G.; Voth, G. A.; Salvador, P.; Dannenberg, J. J.; Dapprich, S.; Daniels, A. D.; Farkas, O.; Foresman, J. B.; Ortiz, J. V.; Cioslowski, J.; Fox, D. J. Gaussian 09, Revision D.01. Gaussian, Inc.: Wallingford, CT 2009.

(8) Pulay, P. Ab Initio Calculation of Force Constants and Equilibrium Geometries in Polyatomic Molecules. *Mol. Phys.* **1969**, *17* (2), 197–204.

(9) Møller, C.; Plesset, M. S. Note on an Approximation Treatment for Many-Electron Systems. *Phys. Rev.* **1934**, *46* (7), 618–622.

(10) Guirgis, G. A.; Zhu, X.; Yu, Z.; Durig, J. R. Raman and Infrared Spectra, Conformational Stability, Normal Coordinate Analysis, Vibrational Assignment, and Ab Initio Calculations of 3,3-Difluorobutene. *J. Phys. Chem. A* **2000**, *104* (19), 4383–4393.

(11) Frisch, M. J.; Yamaguchi, Y.; Gaw, J. F.; Schaefer, H. F.; Binkley, J. S. Analytic Raman Intensities from Molecular Electronic Wave Functions. *J. Chem. Phys.* **1986**, *84* (1), 531–532.

(12) Amos, R. D. Calculation of Polarizability Derivatives Using Analytic Gradient Methods. *Chem. Phys. Lett.* **1986**, *124* (4), 376–381.

(13) Polavarapu, P. L. Ab Initio Vibrational Raman and Raman Optical Activity Spectra. *J. Phys. Chem.* **1990**, *94* (21), 8106–8112.

(14) Chantry, G. W. *Chapter 2*, 1st ed.; Anderson, A., Ed.; New York, 1971.

(15) Al-Saadi, A. A.; Laane, J. Structure, Vibrational Spectra, and DFT and Ab Initio Calculations of Silacyclobutanes. *Organometallics* **2008**, *27* (14), 3435–3443.

(16) van der Veken, B. J.; Herrebout, W. A.; Durig, D. T.; Zhao, W.; Durig, J. R. Conformational Stability of 3-Fluoropropene in Rare Gas Solutions from Temperature-Dependent FT-IR Spectra and Ab Initio Calculations. *J. Phys. Chem. A* **1999**, *103* (13), 1976–1985.

(17) Durig, J. R.; Ng, K. W.; Zheng, C.; Shen, S. Comparison of Ab Initio MP2/6-311+G(d,p) Predicted Carbon–Hydrogen Bond Distances with Experimentally Determined r0 (C–H) Distances. *Struct. Chem.* **2004**, *15* (2), 149–157.

(18) McKean, D. C. New Light on the Stretching Vibrations, Lengths and Strengths of CH, SiH and GeH Bonds. *J. Mol. Struct.* **1984**, *113*, 251–266.

(19) Durig, J. R.; Jin, Y.; Zhen, P.; Gounev, T. K.; Guirgis, G. A. Infrared and Raman Spectra, Conformational Stability, Normal Coordinate Analysis, Ab Initio Calculations, and Vibrational Assignment of 1-Methylsilacyclobutane. *J. Mol. Struct.* **1999**, *477* (1–3), 31–47.

(20) Durig, J. R.; Gounev, T. K.; Zhen, P.; Guirgis, G. A. Infrared, and Raman Spectra, Conformational Stability, Normal Coordinate Analysis, Ab Initio Calculations, and Vibrational Assignment of 1-Chlorosilacyclobutane. *J. Mol. Struct. THEOCHEM* **2000**, *500* (1–3), 275–291.

(21) Gounev, T. K.; Guirgis, G. A.; Zhen, P.; Durig, J. R. Spectra and Structure of Small Ring Compounds. LXVII Vibrational Spectra, Variable Temperature FT-IR Spectra of Krypton Solutions, Conformational Stability and Ab Initio Calculations of 1-Bromosilacyclobutane. *Spectrochim. Acta Part A Mol. Biomol. Spectrosc.* **2000**, *56* (13), 2563–2579.

(22) Guirgis, G. A.; Gounev, T. K.; Zhen, P.; Durig, J. R. Infrared and Raman Spectra, Conformational Stability, Normal Coordinate Analysis, Ab Initio Calculations, and Vibrational Assignment of 1-Fluoro-1-Methylsilacyclobutane. *Spectrochim. Acta Part A Mol. Biomol. Spectrosc.* **1999**, *55* (14), 2753–2770.

(23) Gounev, T. K.; Guirgis, G. A.; Mohamed, T. A.; Zhen, P.; Durig, J. R. Raman and Infrared Spectra, Conformational Stability, Normal Coordinate Analysis,Ab Initio Calculations and Vibrational Assignment of 1-Chloro-1-Methylsilacyclobutane. *J. Raman Spectrosc.* **1999**, *30* (5), 399–411.

(24) Korolev, V. A.; Mal'tsev, A. K.; Nefedov, O. M. A Matrix IR Study of the Pyrolysis of Dimethyldiallylsilane and 1,1-Dimethylsila-2-Cyclobutene and the Low-Temperature Stabilization of 1,1-Dimethyl-1-Sila-1,3-Butadiene. *Bull. Acad. Sci. USSR Div. Chem. Sci.* **1985**, *34* (3), 651–654.

(25) Whitehead, K. G. Preparation and Vibrational Spectra of Novel Ring Compounds and Computer-Assisted Identification of FT-IR Spectra, Mississippi State University, 1980.

(26) Wiberg, K. B.; Rosenberg, R. E. Infrared Intensities: Cyclobutene. A Normal-Coordinate Analysis and Comparison with Cyclopropene. *J. Phys. Chem.* **1992**, *96* (21), 8282–8292.

(27) Boatz, J. A.; Gordon, M. S. Theoretical Studies of Silabicyclobutanes and Silacyclobutenes, CnSi4-NH6 (n = 0-4). *J. Phys. Chem.* **1988**, *92* (11), 3037–3042.

(28) Page, E. M.; Rice, D. A.; Walsh, R.; Hagen, K. Determination of the Molecular Structure of (CH3)3SiCH:CH2 by Gas-Phase Electron Diffraction and Ab Initio Methods. *J. Mol. Struct.* **1997**, *403* (3), 199–206.

(29) Lord, R. C.; Rea, D. G. The Vibrational Spectra and Structure of Cyclobutene and Cyclobutene-d61. *J. Am. Chem. Soc.* **1957**, *79* (10), 2401–2406.

(30) Aleksanyan, V. T.; Garkusha, O. G. Analysis of the Vibrational Spectra of Cyclobutene. *Bull. Acad. Sci. USSR Div. Chem. Sci.* **1976**, *25* (10), 2079–2083.

(31) Pendergrass, D. C.; Williams, R.; Blair, J. B.; Fenton, A. W. Mining for Allosteric Information: Natural Mutations and Positional Sequence Conservation in Pyruvate Kinase. *IUBMB Life* **2006**, *58* (1), 31–38.

(32) Alontaga, A. Y.; Fenton, A. W. Effector Analogues Detect Varied Allosteric Roles for Conserved Protein-Effector Interactions in Pyruvate Kinase Isozymes. *Biochemistry* **2011**, *50* (11), 1934–1939.

(33) Urness, J. M.; Clapp, K. M.; Timmons, J. C.; Bai, X.; Chandrasoma, N.; Buszek, K. R.; Fenton, A. W. Distinguishing the Chemical Moiety of Phosphoenolpyruvate That Contributes to Allostery in Muscle Pyruvate Kinase. *Biochemistry* **2013**, *52* (1), 1–3.

(34) Rudbeck, M. E.; Kumar, S.; Mroginski, M. A.; Lill, S. O. N.; Blomberg, M. R. A.; Barth, A. Infrared Spectrum of Phosphoenol Pyruvate: Computational and Experimental Studies Maria. *J. Phys. Chem. A* **2009**, *113*, 2935–2942.

(35) Kumar, S.; Barth, A. Phosphoenolpyruvate and Mg2+ Binding to Pyruvate Kinase Monitored by Infrared Spectroscopy. *Biophys. J.* **2010**, *98* (9), 1931–1940.

(36) Krasteva, M.; Kumar, S.; Barth, A. A Dialysis Accessory for Attenuated Total Reflection Infrared Spectroscopy. *J. Spectrosc.* **2006**, *20* (3), 89–94.

(37) Williams, R.; Holyoak, T.; McDonald, G.; Gui, C.; Fenton, A. W. Differentiating a Ligand's Chemical Requirements for Allosteric Interactions from Those for Protein Binding. Phenylalanine Inhibition of Pyruvate Kinase. *Biochemistry* **2006**, *45* (17), 5421–5429.

(38) Prasannan, C. B.; Villar, M. T.; Artigues, A.; Fenton, A. W. Identification of Regions of Rabbit Muscle Pyruvate Kinase Important for Allosteric Regulation by Phenylalanine, Detected by H/D Exchange Mass Spectrometry. *Biochemistry* **2013**, *52* (11), 1998–2006.

(39) Smith, B. C. *Fundamentals of Fourier Transform Infrared Spectroscopy, Second Edition*; 2011.

(40) Smith, B. C. Spectral Subtraction. *Spectrosc. (Santa Monica)* **2021**, *36* (5).

(41) Margenot, A. J.; Calderón, F. J.; Parikh, S. J. Limitations and Potential of Spectral Subtractions in Fourier-Transform Infrared Spectroscopy of Soil Samples. *Soil Sci. Soc. Am. J.* **2016**, *80* (1), 10–26.

(42) Lorenz-Fonfria, V. A. Infrared Difference Spectroscopy of Proteins: From Bands to Bonds. *Chem. Rev.* **2020**, *120* (7).

VITA

Reid Ethan Brenner was born August 8, 1990 in Warren, Michigan. He graduated in 2008 from Camdenton High School in Camdenton, Missouri. He subsequently attended the University of Missouri-Kansas City (UMKC) and graduated in 2012 with a Bachelor of Science degree in Physics, with departmental honors (*cum laude*). During his junior and senior years, Reid conducted undergraduate research in physics. His first foray into research was as a volunteer in the lab of Prof. Anthony Caruso, where he assisted in determining work functions of various materials using X-ray photoelectron spectroscopy (XPS). Reid later worked as an undergraduate research assistant in the lab of Prof. Michael Kruger where he assisted in experiments involving condensed matter physics.

Reid continued his education in physics, staying on as a Master's student in the Kruger lab. His research focused on determining yield strengths of metal foils under high pressures and temperatures. He successfully defended his thesis titled: "THE YIELD STRENGTH OF MOLYBDENUM UNDER PRESSURE AND TEMPERATURE" in 2014. During this time, Reid developed an interest in chemistry and spectroscopy while assisting Prof. James R. Durig in his experiments. Reid decided to pursue his Ph.D. in chemistry and moved to the Durig lab as a graduate research assistant in the summer of 2014 to begin his training. During the next academic year, he took additional coursework at UMKC to earn the equivalent of a Bachelor of Science degree in chemistry, and officially graduated in 2015 with his Master of Science Degree in physics.

Reid formally enrolled in the interdisciplinary Ph.D. program at UMKC in Fall of 2015, continuing his research in physical chemistry in the field of molecular spectroscopy under his advisor, Prof. James R. Durig. Upon Prof. Durig's retirement in 2016, Reid joined the research lab of Prof. Kathleen Kilway, continuing his research in molecular spectroscopy under the guidance of Prof. Charles J. Wurrey. During his tenure as a Ph.D. student, Reid was a two-time recipient of the Mr. & Mrs. Fong Wu Cheng Scholarship (2017 and 2018) for demonstration of ability in chemical research. Additionally, he has co-authored papers published in several different journals. Reid has presented his

work at the American Chemical Society Midwest Regional Meeting, American Chemical Society National Meeting & Exposition, and SciX Conference. Reid has also held leadership roles, serving as secretary, vice president, and president of the Chemistry Graduate Student Association at UMKC.

Publications:

Menuey, E. M.; Zhou, J.; Tian, S.; **Brenner, R. E**.; Ren, Z.; Hua, D. H.; Kilway, K. V.; Moteki, S. A. Chirality-Driven Self-Assembly: Application toward Renewable/Exchangeable Resin-Immobilized Catalysts. *Org. Biomol. Chem.* **2022**. Accepted.

Jabri, A.; Marshall, F. E.; Tonks, W. R. N.; **Brenner, R. E.**; Gillcrist, D. J.; Wurrey, C. J.; Kleiner, I.; Guirgis, G. A.; Grubbs, G. S. The Conformational Landscape, Internal Rotation, and Structure of 1,3,5-Trisilapentane Using Broadband Rotational Spectroscopy and Quantum Chemical Calculations. *J. Phys. Chem. A* **2020**, *124* (19).

Guirgis, G. A.; Sawant, D. K.; **Brenner, R. E.**; Deodhar, B. S.; Seifert, N. A.; Geboes, Y.; Pate, B. H.; Herrebout, W. A.; Hickman, D. V.; Durig, J. R. Microwave, r_0 Structural Parameters, Conformational Stability, and Vibrational Assignment of (Chloromethyl)Fluorosilane. *J. Phys. Chem. A* **2015**, *119* (47).

Deodhar, B. S.; **Brenner, R. E.**; Sawant, D. K.; Guirgis, G. A.; Geboes, Y.; Herrebout, W. A.; Durig, J. R. Vibrational Assignments and Conformer Stability Determination of Cyclobutyldichlorosilane by Variable Temperature Raman Spectra in Krypton Solution. *Vib. Spectrosc.* **2015**, *81*.

Deodhar, B. S.; **Brenner, R. E.**; Klaassen, J. J.; Tubergen, M. J.; Durig, J. R. Microwave, Structural, Conformational, Vibrational Studies and Ab Initio Calculations of Fluoroacetyl Chloride. *Spectrochim. Acta - Part A Mol. Biomol. Spectrosc.* **2015**, *148*.

Presentations:

Brenner, R. E.; Wurrey, C. J.; Fenton, A. W.; Vibrational frequency shifts of phosphoenolpyruvate upon binding to allosterically regulated pyruvate kinase. Poster session presented at: 257th ACS National Meeting & Exposition, March 31-April 4, 2019; Orlando, FL.

Brenner, R. E.; Wurrey, C. J.; Fenton, A. W.; Infrared spectra of phosphoenolpyruvate in aqueous solutions: Vibrational frequency shifts of functional groups due to presence of metal ions. Poster session presented at ACS Midwest Regional Meeting; 2017 Oct 18 – 20, Lawrence, KS.

Brenner, R. E.; Deodhar, B. S.; Sawant, D. K.; Guirgis, G. A.; Geboes, Y.; Herrebout, W. A.; Durig, J. R. Vibrational assignments and conformer stability determination of cyclobutyldichlorosilane by variable temperature Raman spectra in krypton solution. Poster session presented at SciX 2016; 2016 Sept 18 – 23, Minneapolis, MN.